Journal of Research

of the

U.S. National Bureau of Standards

JANUARY 1953

VOLUME 50 NUMBER 1

U. S. DEPARTMENT OF COMMERCE
Charles Sawyer, Secretary
NATIONAL BUREAU OF STANDARDS
A. V. Astin, Director

JANUARY • 1953
VOLUME • 50
NUMBER • 1

JOURNAL OF RESEARCH

of the

NATIONAL BUREAU OF STANDARDS

PERIODICALS OF THE NATIONAL BUREAU OF STANDARDS

The National Bureau of Standards is engaged in fundamental and applied research in physics, chemistry, mathematics, and engineering. Projects are conducted in fifteen fields: electricity, optics and metrology, heat and power, atomic and radiation physics, chemistry, mechanics, organic and fibrous materials, metallurgy, mineral products, building technology, applied mathematics, electronics, ordnance development, radio propagation, and missile development. The Bureau has custody of the national standards of measurement and conducts research leading to the improvement of scientific and engineering standards and of techniques and methods of measurement. Testing methods and instruments are developed; physical constants and properties of materials are determined; and technical processes are investigated.

JOURNAL OF RESEARCH

Internationally known as a leading scientific periodical, the Journal presents research papers by authorities in the specialized fields of physics, mathematics, chemistry, and engineering. Complete details of the work are presented, including laboratory data, experimental procedures, and theoretical and mathematical analyses. Each of the monthly issues averages 85 two-column pages; illustrated. Annual subscription: domestic, $5.50; foreign, $6.75.

TECHNICAL NEWS BULLETIN

Summaries of current research at the National Bureau of Standards are published each month in the Technical News Bulletin. The articles are brief, with emphasis on the results of research, chosen on the basis of their scientific or technologic importance. Lists of all Bureau publications during the preceding month are given, including Research Papers, Handbooks, Applied Mathematics Series, Building Materials and Structures Reports, and Circulars. Each issue contains 12 or more two-column pages; illustrated. Annual subscription: domestic, $1.00; foreign, $1.35.

BASIC RADIO PROPAGATION PREDICTIONS

The Predictions provide the information necessary for calculating the best frequencies for communication between any two points in the world at any time during the given month. The data are important to all users of long-range radio communications and navigation, including broadcasting, airline, steamship, and wireless services, as well as to investigators of radio propagation and ionosphere. Each issue, covering a period of one month, is released three months in advance and contains 16 large pages, including pertinent charts, drawings, and tables. Annual subscription: domestic, $1.00; foreign, $1.25.

Order all publications from the Superintendent of Documents
U. S. Government Printing Office, Washington 25, D. C.

The printing of this publication has been approved by the Director of the Bureau of the Budget, April 9, 1953

Journal of Research of the National Bureau of Standards Vol. 50, No. 1, January 1953 Research Paper 2380

The Sixth Series in the Spectrum of Atomic Hydrogen[1,2]

Curtis J. Humphreys

The first member of the sixth series ($6h\ ^2H^\circ - 7i\ ^2I$) in the spectrum of atomic hydrogen has been observed at 12.37μ, in agreement with the predicted position. Other newly observed lines include the second line of the Pfund series and the third, fourth, and fifth lines of the Brackett series. The source was a water-cooled discharge tube drawing 640 milliamperes at 5,000 volts. The tube was fitted with a KBr lens, which served also as a window for end-on observation. An atomic-hydrogen discharge was maintained by admitting water vapor through a Hopfield leak and pumping continuously. A conventional dispersing and recording system was used, consisting of a Perkin-Elmer model 12 spectrometer with a d-c breaker amplifier and Speedomax recorder. Relative-intensity measurements are included.

1. Introduction

The last new series to be discovered in the spectrum of atomic hydrogen was reported by Pfund[3] in 1924. This series originates in transitions to the fifth orbit from those of greater quantum number. This had been preceded 2 years earlier by the discovery by Brackett[4] of the series originating in transitions to the fourth orbit. Both of these contributions followed closely and probably received considerable impetus from the spectacular experiments of Wood,[5] in which he succeeded in exciting exceptionally long Balmer series in hydrogen discharges. This spectrum was of unusual purity, and, because of the striking contrast between the brilliant lines and dark background between, was called the "black discharge." Brackett inferred correctly that the excitation conditions favoring the "black discharge" were prerequisite to the production of series resulting from transitions to levels higher than the second or third. This conclusion depends on the fact that the length of series and the appearing of series having a high level as the final state are both dependent on the density of population of the more highly excited states.

The extension of the hydrogen spectrum farther into the infrared region to include additional series predicted by theory has long constituted a challenge. This has become increasingly insistent when one considers that in more than a quarter of a century of intensive infrared activity, marked by spectacular developments in observing techniques, there has been no further infrared extension of the hydrogen spectrum. A review of the present state of our knowledge of this spectrum will be followed by a discussion of the experimental conditions required for the excitation of higher series and utilized in the current experiments. Of the many compilations of hydrogen data, one of the most satisfactory is that given by Grotrian.[6] The Paschen series was observed, in the range of photography, as far as the eighth member by Poetker.[7] Brackett observed only two members of his series, and Pfund found only the first member of the series bearing his name. Table 1 is introduced to point out the locations of the first two members of known and predicted series. The latter include all entries below Pfund-α. Predicted positions of the higher members of infrared series, including and beyond that of Brackett, are given by Swensson.[8]

TABLE 1. *Locations of the various hydrogen series according to the series formula* $\nu = R\left(\frac{1}{n_1^2} - \frac{1}{n_2^2}\right)$

Series	n_1	n_2	λ	ν
			Å	cm^{-1}
Lyman	1	2	1215.68 (vac)	82258.31
		3	1025.73 (vac)	97491.36
Balmer	2	3	6562.79 (air)	15233.22
		4	4861.33 (air)	20564.79
Paschen	3	4	18751.1	5331.58
		5	12818.1	7799.33
Brackett	4	5	40511.4	2467.77
		6	26251.3	3808.29
Pfund	5	6	74577.6	1340.52
		7	46524.7	2148.81
6	6	7	123684	808.29
		8	75091.5	1332.89
7	7	8	190569	524.60
		9	113057	884.27

Results of a new investigation presented and discussed here include observation of the first member of an entirely new series, $6h\ ^2H^\circ - 7i\ ^2I$, a second member of the Pfund series, and three additional members of the Brackett series beyond the two originally reported.

2. Experiments

The method of exciting the hydrogen spectrum adopted in these experiments was similar to that employed by earlier observers mentioned in the references, consisting of a high-current Geissler discharge. Modifications were introduced to meet the special requirements of the observations, the most important of which was the necessity for using a transparent window on the discharge tube to permit emergence of energy associted with the first line of the new series at 12.37 μ. All reported observations of the hydrogen spectrum emphasize the difficulty of maintaining an atomic spectrum because of the tendency of hydrogen atoms to associate

[1] Curtis J. Humphreys, J. Opt. Soc. Am. **42**, 432 (1952).
[2] Presented at the Symposium on Molecular Structure and Spectroscopy, Ohio State University, 1952.
[3] A. H. Pfund, J. Opt. Soc. Am. **91**, 193 (1924).
[4] F. S. Brackett, Astrophys. J. **56**, 154 (1922).
[5] R. W. Wood, Proc. Roy. Soc. (London) [A] **97**, 455 (1920); Phil. Mag. **42**, 729 (1921).
[6] W. Grotrian, Handbuch der Astrophysik, Kap. 5, Gesetzmässigkeiten in der Serienspektren, p. 475 (Springer, Berlin, 1930).
[7] A. H. Poetker, Phys. Rev. **30**, 418 (1927).
[8] J. W. Swensson, Prédictions de raies atomiques dans l'infrarouge, extrait des Mémoires in-8° de la Société Royale des Sciences de Liége, quatrième série, XI, fasc. I (Louvain, 1951).

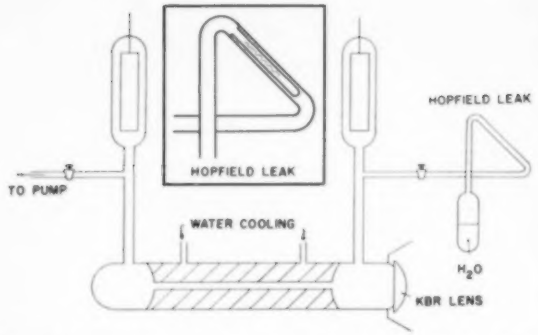

FIGURE 1. *Schematic design of source tube and Hopfield leak.*

to form H^2 molecules, with the attendant development of the many-line molecular spectrum. This association is favored in the vicinity of the electrodes and is probably caused by a catalytic action by the metal. Wood's successful excitation of a pure atomic-hydrogen discharge apparently resulted from two features of his technique: (1) construction of an extremely long tube, of which only the central portion was used for end-on observation through a thinly-blown bend, and (2) provision for continuous change of the hydrogen supply, accomplished by connecting a constantly operating exhaust pump to the system, and at the same time admitting hydrogen through a capillary tube drawn to a fineness determined by experiment to give the optimum pressure.

More recent investigations have pointed to the advantage of using moist hydrogen. This is made obvious by the appearing of the intense Balmer series in a vacuum system when the last traces of moisture are being pumped out. This condition favoring the atomic spectrum is probably caused by liberation of hydrogen in the atomic state upon dissociation of the water molecule. Arnulf and Dunoyer[9] described the design of a tube for producing atomic-hydrogen discharges of high intensity, featuring a side tube containing gypsum and from which small amounts of moisture could be liberated into the system by heating.

For the current series of experiments, several tubes were built and tried out, all of which had the advantageous features established by earlier investigators to the extent permitted by the practical requirements of the work. The desirable characteristics included provision for cooling, associated with ability to withstand steady high currents, satisfactory attachment of a suitable transparent window, and geometric design to provide a region of maximum intensity and to permit illumination of large-aperture optics. The tube used in obtaining the reported data is illustrated schematically in figure 1. The principal differences between this and other preliminary designs is in the size of the central discharge tube. The improved intensity resulting from a relatively small capillary, approximately 4 mm in diameter, more than makes up for the small size of the image projected onto the slit of the spectrometer. The really unique feature of the source operation was the manner of admitting hydrogen. Because the use of wet hydrogen has been demonstrated to be advantageous, the idea of introducing pure water vapor suggested itself. This proved to be successful and also made the replenishment of hydrogen extremely simple. As indicated, a small tube of distilled water was attached to the source through a Hopfield leak. This leak, illustrated in figure 1, consists of a crack generated in the small blind-end tube sealed inside the figure-4 shaped tube with a ring seal. The opening of the crack is controlled by a clamp at the crossover point of the tubing. In practice, the rate of vapor flow was increased somewhat by mounting a radiant heater near the water supply. The lens of KBr on the end of the tube was used in the final version, replacing a flat window. This is one of the lenses supplied for a Perkin-Elmer model 21 spectrometer, which had not been installed owing to prevailing low humidity. Actually, the lens made possible a considerable increase in the amount of energy that could be admitted to the optical system. In addition to the water cooling the tube was wrapped in cotton, over which a continuous stream of water flowed. The best development of higher series was found to be realized when the tube was operated at the lowest pressure for which a steady discharge could be maintained.

All other components in the setup were conventional commercially available pieces of apparatus. The source of power was a 2½-kva transformer. The output voltage was rated at 5,000. The transformer was slightly overloaded at the maximum source current of 630 ma. A variable-voltage autotransformer of 40-amp capacity was used to control the power supply.

A Perkin-Elmer model 12 spectrometer with a rock-salt prism was used as the dispersing system, modified only by removal of the housing over the source optics to permit advantageous placement of the source, and attachment of a simple motor-driven gear train for scanning. In the later phases of the work, an improvised housing was mounted so as to enclose the end of the light source and projecting system to permit filling the entire optical path with oil-pumped nitrogen for the purpose of eliminating water vapor. For the preliminary experiments a Hornig thermopile, as used in the early Perkin-Elmer models, was used. This was later replaced by one of the fast-response a-c couples in current production. A d-c system was used throughout the experiments for amplifying and recording the voltage output. This consisted of a Liston-Folb breaker amplifier and a Speedomax recorder. All of the visible components are readily identifiable in figure 2.

It is apparent that the experimental setup does not differ markedly from that used by previous observers, particularly in regard to operating characteristics of the source and specifications of the dispersing system. The use of an amplifying and recording system does, however, provide a margin of sensitivity that could not be matched in the older

[9] A. Arnulf and L. Dunoyer, Rev. Optique **9**, 510 (1930).

FIGURE 2. *Layout of apparatus.*

point-by-point observations with a galvanometer.

The observation of the first line of the sixth series was accomplished after considerable preliminary experimentation to achieve optimum conditions, including optical adjustment to obtain maximum signal strength, choice of the most suitable component ratings in the improvised filtering circuit placed between the amplifier and recorder, and selection of the most satisfactory amplifier gain. The replacement of the window with a lens and the substitution of the a-c thermopile were made after observation of the new line had been confirmed by several records. These changes resulted in a marked improvement in signal strength, making it possible to reduce the slit width from 1.7 mm, necessary to obtain the first indications of the line, to 0.5 mm, the settings used to obtain the records reproduced in figures 3 and 4.

Most of the records were run with a gain such that a 0.1-μv signal gave a deflection of from 30 to 40 percent of full scale on the chart. The profiles shown in reproduction of actual records appear rather broad. This is mainly because available speed-changing gears did not permit selection of optimum ratio of scanning speed to record-chart speed. Of course, the slit widths that necessarily had to be used were much too great to permit development of true profiles. The wavelength calibration of the spectrometer was accomplished by using well-known emission and absorption sources, including a mercury lamp, atmospheric carbon dioxide and water vapor, and a polystyrene film. The determination of the wavelength of the new line is not to be regarded as precise, because fairly broad absorption bands were used for calibration in the 12-μ region. It is precise enough for certain identification, but the numerical wavelength listed is the calculated value. As an extra precaution, to make sure that the new line was genuine, records were run with a CaF_2 filter in front of the slit to eliminate all radiant energy of wavelength greater than 12 including the new line, and with a scattering filter to remove all energy of wavelengths shorter than about 6.5 μ and to permit the new line to pass.

3. Discussion

Figures 3 and 4 are reproductions of records of the first line of the new series, selected from a large number of similar records. The scale of ordinates shown on each figure is to show the relation of deflection to chart width, one division being equivalent to five scale divisions on the chart. Figure 3 represents a considerable improvement over the record submitted with a recent letter,[10] but was obtained by using a similar program of observation, namely, to record the new line and the Pfund line under the same conditions in order to compare intensities. Figure 4 shows the best record obtained to date.

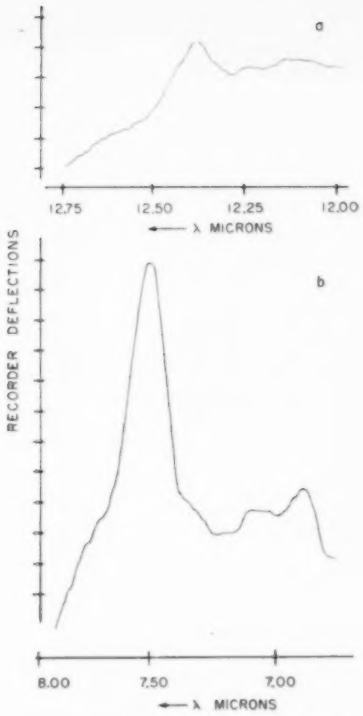

FIGURE 3. *First, or α, lines of (a) sixth series and (b) Pfund series, in the infrared under identical conditions (slit 0.5 mm., signal 0.1-μv full scale on recorder chart).*

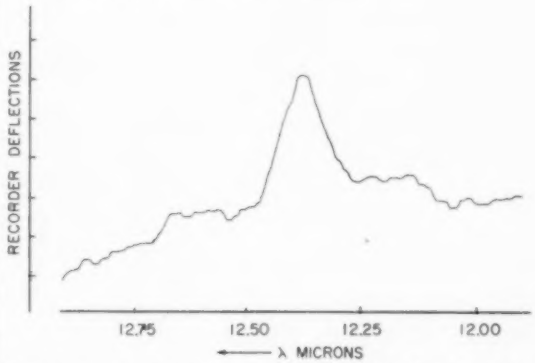

FIGURE 4. *First, or α, line of sixth series, in infrared, observed under optimum conditions (slit 0.5 mm).*

[10] J. Opt. Soc. Am. **42**, 432 (1952).

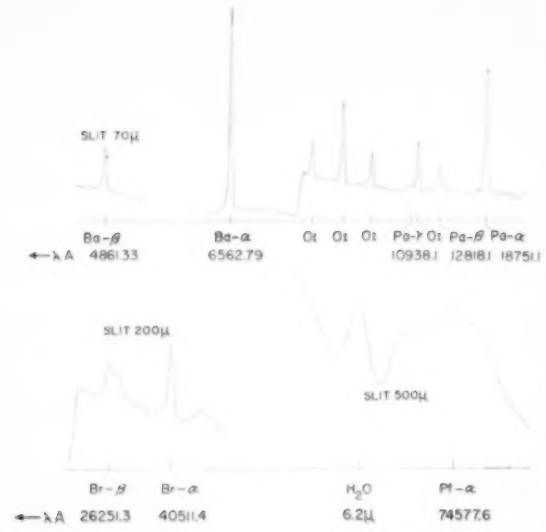

FIGURE 5. *Record covering interval from Balmer-β to Pfund-α.*

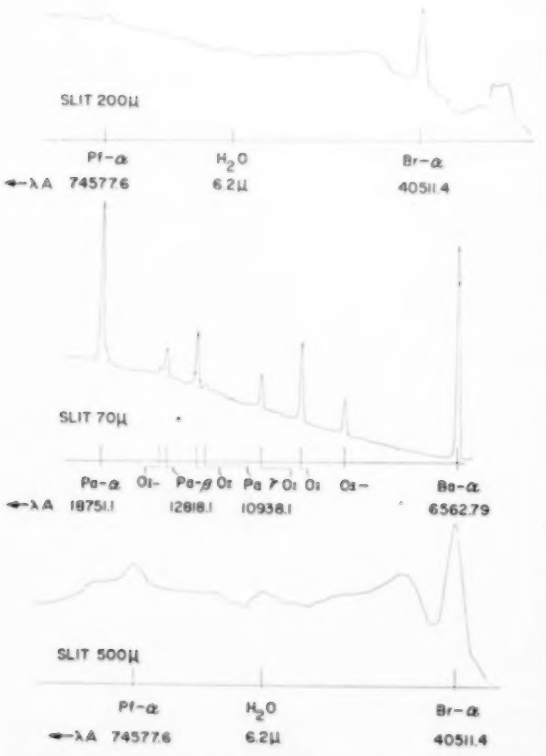

FIGURE 6. *Records covering interval from Balmer-β to Pfund-α, showing effect of removal of water vapor from optical path.*

Although the observation of the sixth series of hydrogen was the principal experimental objective, additional records were obtained for the purpose of extending known series and obtaining intensity comparisons within and between series. The entire spectral range available with the rock-salt prism installation was covered. This range extended from below Balmer-β to somewhat beyond the new line of the sixth series. Survey records described in the appropriate captions are reproduced in figures 5 and 6.

Figure 5 shows the entire region from Balmer-β to Pfund-α, with some featureless sections removed. At the top is shown the first two members of the Balmer series, illustrating the intensity decrement. This is followed, after adjustment for drift, by a record of the region from Balmer-α to Paschen-α. Three members of the latter series may be picked out, with a fourth probably distinguishable from noise. The other profiles are unresolved multiplets of O I. The lower section covers the region including Brackett-α and Pfund-α. The slit width was increased from 70 to 200 μ after traversing Paschen-α, and the recording was again interrupted to widen the slit to 500-μ and adjust the zero after passing Brackett-α. The recording was made without any attempt to remove H_2O vapor from the path, and the curve shows the characteristic profile of the 6.2-μ water-vapor band with a slit too wide to reveal rotational structure.

Figure 6, representing a record run in the opposite direction, covers the same features. There is slightly less noise because of the fact that the a-c thermopile of greater sensitivity was used, permitting operation on lower gain settings for the same slit openings. This run was made with dry nitrogen in the spectrometer and in the improvised housing enclosing the source optics. The 6.2-μ water-vapor band can hardly be seen. The upper and middle sections are part of a continuous run. The lower section illustrates the condition of partial removal of water vapor.

Table 1 shows that Pfund-β is located at wavelength 4.65 μ. On the basis of decrements found in other series, it is expected to be about one-sixth to one-seventh as intense as Pfund-α and about 2 percent of Brackett-α. Observation of Pfund-β under conditions of the earlier experiments (Brackett, Pfund) was quite hopeless because of inadequate sensitivity, coupled with the fact that it would have been completely masked in the wide-slit image of Brackett-α at 4.0 μ. Figure 7 shows the results of a very limited amount of work with a PbTe cell. The Pfund-β line can clearly be seen to the left of Brackett-α with intensity close to that estimated. In the lower curve the same line is shown with increased amplifier gain. In this case overloading prevented a satisfactory representation of the profile of Brackett-α. A difficulty of observing with a telluride cell in this region is that the maximum of temperature radiation from the tube comes at about 5 μ. The telluride detector is very sensitive to this continuous background. The trouble was overcome by greatly diminishing the power input to the source at some sacrifice of signal strength.

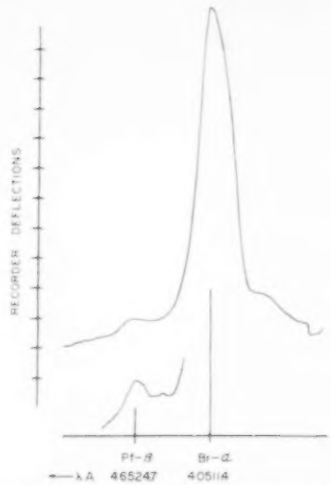

FIGURE 7. *Records showing Pfund-β and Brackett-α, as observed with a PbTe detector (slit 400 μ).*

The fact that all of the Brackett series beyond the first member lies in the wavelength region of maximum sensitivity of lead-sulfide photoconductive cells made the exploration of this series beyond the second member, as observed by Brackett, appear promising. Figure 8 shows the development of this series as observed with a PbS detector. Brackett-α is not included, being out of the range of sensitivity. The β- and γ-lines are well developed. Paschen-α, falling just between Brackett-δ and Brackett-ε, partly overlaps these lines with the scale of dispersion inherent in the system. It is certain that they could be clearly separated with a high-resolution spectrometer. As in the other records shown, the lines not identifiable with the hydrogen spectrum originate in O I, as would be expected when water vapor is dissociated in the source. In the lower record Paschen-α and its companion on the short wave side are attenuated by using a different gain setting. The upper short section displaced vertically only is a subsequent run without attenuation, starting just beyond but not including Paschen-α.

A final record, figure 9, is inserted to show the development of the Paschen series under the experimental conditions described and with a PbS detector. The series may be traced to six members. Poetker photographed it up to and including the eighth member. It appears certain that better results could be obtained with a grating instrument because of the possibility of separating weak hydrogen and oxygen lines by utilizing both higher dispersion and greater resolving power. The stronger lines, including Paschen-α were attenuated. The gain setting was changed in some instances after the profiles had started to develop, or before the background level was reached. This is the explanation of the sharp pips adjacent to some profiles.

The work on hydrogen to date is to be regarded as preliminary to more detailed investigation, which will include precise evaluation of intensities, search

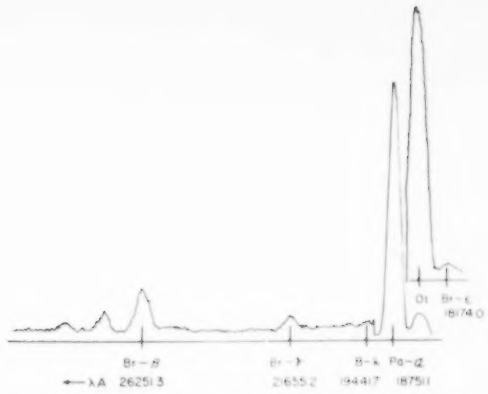

FIGURE 8. *Records showing the higher members of the Brackett series as observed with a PbS cell (slit 50 μ).*

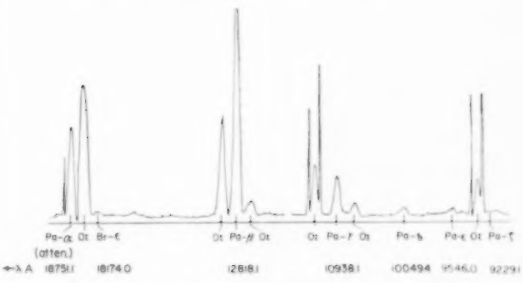

FIGURE 9. *Record of Paschen series observed with a PbS cell (slit 50 μ).*

for new series, extension of known series, and determination of excitation conditions required for maximum development of infrared series. The study of the excitation of the hydrogen emission spectrum is of great astrophysical interest in its relation to the theoretical explanation of the long Balmer series with small intensity decrement that occur in the solar chromosphere, stars with extensive gaseous envelopes, and planetary nebulas. A brief discussion of this matter with pertinent reference material is given by Kiess and Humphreys [11] in a report on the intensities in the flash spectrum observed at the solar eclipse of 1940. Correlation of astrophysical with laboratory data is needed. Brackett [12] regarded the hydrogen spectrum produced in his laboratory source as arising to a large extent from inelastic collision without ionization. He offered an explanation that was supported by the unexpectedly high ratio of the intensity of Paschen-α to Balmer-α, this reaching 4 to 3 in Brackett's experiments. This ratio was not attained in these experiments, the maximum Paschen-α to Balmer-α being 4 to 5, but even this is surprising, considering the behaviour of the other series.

The most significant information for the inter-

[11] C. C. Kiess and C. J. Humphreys, Nat. Geographic Soc., Contributed Tech. Papers, Solar Eclipse Ser. 2, p. 53 (1942).
[12] F. S. Brackett, Astrophys. J. 56, 154 (1922).

pretation of excitation conditions responsible for any observed hydrogen spectrum is to be found in intensity relationships, including decrement ratios within a series and intercomparisons between different series. Radiometric measurements with a thermopile readily lend themselves to intensity determinations owing to the essentially nonselective character of this detector. Table 2 gives a summary of the relative intensities of several hydrogen lines as estimated from the observations. Except for instances where photoconductive cell observations were made within relatively narrow wavelength intervals, as, for instance, the region from Brackett-β to Brackett-ϵ, these intensity comparisons are based on thermopile observations and should be reasonably precise, subject to some corrections, including those for reflection and scattering by the optical parts. These corrections, which vary with wavelengths have not been made in the preparation of this report. The exit slit was imaged within the boundaries of the receiver for all slit widths used.

Over a year ago E. U. Condon suggested to the author that it would be of great interest to intercompare intensities of hydrogen lines originating in a common upper state. Such intercomparison of course provides data for evaluating relative probabilities of transition to various lower states. The data of table 2 may be used to provide such information.

TABLE 2. *Observed relative intensities of hydrogen lines*

Line	λ	Relative intensity
	Å	
Balmer-β	4861.33	150
Balmer-α	6562.79	1000
Paschen-δ	10049.4	6
Paschen-γ	10938.1	28
Paschen-β	12818.1	140
Paschen-α	18751.1	700
Brackett-γ	21655.2	13
Brackett-β	26251.3	40
Brackett-α	40511.4	120
Pfund-β	46524.7	3
Pfund-α	74577.6	20
Sixth series-α	123684	3

For instance, the first line of the sixth series, Pfund-β, Brackett-γ, and Paschen-δ, all originate in a common upper level. The table shows that these intensities fall within the same order of magnitude. Mechanical limitations of the spectrometer prevented extending this array to Balmer-ϵ. This intercomparison is pointed out as a very sketchy beginning of something that should be carried out more precisely and in greater detail.

In conclusion, the author acknowledges with thanks the valuable help of L. G. Mundie and A. J. Cussen in all phases of the experimental work.

CORONA, CALIF., September 3, 1952.

Journal of Research of the National Bureau of Standards Vol. 50, No. 1, January 1953 Research Paper 2381

National Bureau of Standards Mobile Low-level Sounding System

P. D. Lowell, W. Hakkarinen, and D. L. Randall

The National Bureau of Standards Mobile Low-level Sounding System is a combination of an improved wiredsonde and an Army SCM–1A mobile weather station. Its purpose is to measure temperature and moisture distributions and their associated gradients and heights from near the ground up to a maximum height of 2,000 feet over different types of terrain. The system has six distinguishing features: 1. Balloon-level heights can be determined at all times during a flight by data recorded at the ground level by an electric altimeter. 2. Humidity data recorded with this system, which is energized with 60-cycles-per-second alternating current, are reliable for longer periods of time than those obtained by direct-current sounding systems. 3. The system can be operated from within the heated truck body and is suitable for use in dense fog, at night, or during very cold weather. 4. The air-borne unit is of lighter construction because switching and ventilating of the circuit measuring elements are done by a gravity motor instead of a battery-driven motor. 5. The system provides a condition of radio silence during operation. 6. The system is designed to operate into recorders requiring up to 500 microamperes of direct current. The intelligence from the system can therefore be recorded directly on the equipment in a standard radiosonde receptor installation.

1. Definition and Purpose of Equipment

The mobile low-level sounding system is a modification of that originally designed by P. D. Lowell and W. Hakkarinen for the Navy Department, Bureau of Ships, in combination with an Army SCM–1A Mobile Meteorological Station [1].[1] Its purpose is to measure temperature and moisture distributions and their associated gradients and heights from near the ground up to 2,000 ft over different types of terrain.

For tropospheric radio-wave propagation measurements, it is desirable to know the vertical gradients of temperature and humidity causing the curvature of transmitted radio energy. Booker [2] has calculated refractive-index gradients in terms of temperature and moisture gradients for a well-mixed layer of air having, at its top, a temperature of 50° F, a specific humidity of 6.7 g/kg, and a pressure of 1,015 mb. For this layer the critical values that would produce refraction equal to the curvature of the earth are (1) a specific humidity gradient of 0.5 (g/kg)/100 ft, and (2) a temperature gradient of −5.2° F/100 ft.

Sharp atmospheric refractive-index changes are those that occur in a distance of the order of a wavelength. For radio communication using 100-Mc transmission, this requires measuring the gradients for layers as thin as 10 ft, as well as those for thicker layers. Table 1 provides a comparison of the salient features of various meteorological sounding systems in existence prior to the development of the NBS equipment.

Low-level wiredsonde measuring systems are an attempt to combine the mobility and height of the radiosonde measuring system with the fine-grained measurements possible in the tower system. Meteorological sensing elements are supported by a tethered kite, balloon, or kytoon, and the height of the instruments is controlled by reeling the tethered cable in or out. Under calm conditions the balloon height can be regulated to stay at one particular level and the temperature and moisture values of that level studied in detail. The time-lag difficulty of the sensing elements is not so great a handicap in this system as in the radiosonde system because the elements can remain at a given level until they are in equilibrium with the environment.

TABLE 1. *Comparison of various meteorological sounding systems*

System	Elements measured	Sensitivity to features of air layer structure	Features of system
Radiosonde (Weather Bureau type).	Pressure, temperature, humidity.	Coarse-grained structure.	Ceiling 12 to 18 km, rapid rate of ascent, 50% recording of elements, time lags.
Tower.....	Refractive index, altitude, temperature, humidity, and wind.	Fine-grained structure.	Ceiling 50 to 150 m, continuous record, wide selection of measurements, restricted location.
Wiredsonde..	Altitude, temperature, humidity.	Medium-grained structure.	Ceiling [illegible] to [illegible] m, equilibrium of sensing elements with environment, uncertainty of heights.

2. Components

Low-level wiredsonde observations are made with equipment originally designed by P. D. Lowell and W. Hakkarinen. This system consists of an air-borne unit, a three-conductor cable, a cable-length controlling reel, an electronic panel, and a recorder. The air-borne unit, which measures pressure, temperature, and humidity, is connected by the three-conductor cable, through a slip-ring contacts on the cable reel to the electronic panel and recorder.

[1] Figures in brackets indicate the literature references at the end of this paper.

FIGURE 1. *Low-level sounding truck.*

Figure 1 shows a mobile adaptation of the system described herein.

Air-borne-unit support. The air-borne unit is supported by a pair of kytoons or a combination of several N–4 balloons in combination with a 7-ft kite. With the latter combination, it is possible to secure any desired height by adding more balloons, but the combination is not so stable as the arrangement of two kytoons tied side by side in a horizontal plane. The kytoon combination has a free lift of 4 lb in dead calm.

Air-borne unit. The air-borne unit (figs. 2, 3, 4) consists of a gravity motor, an aluminum tube that houses the regular radiosonde temperature and humidity elements, and the pressure-element container clamped to the side of the aluminum tube. At the upper end of the tube, a blower driven by the gravity motor draws air through the tube and expels

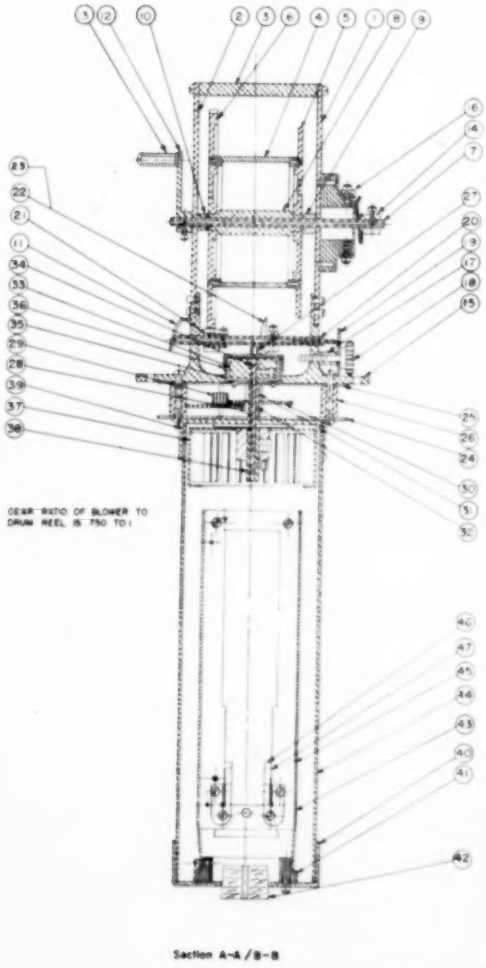

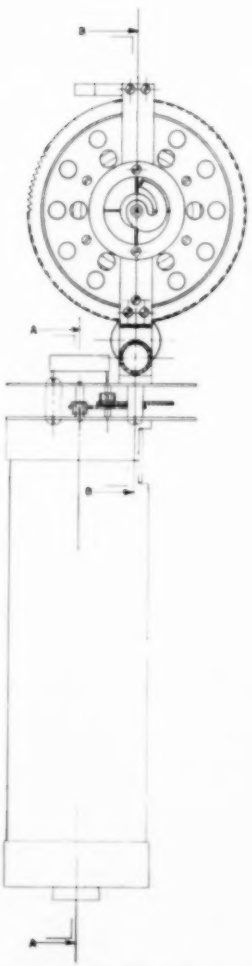

PIECE NO	NUMBER REQ'D	DESCRIPTION	MATERIAL
47	1	CONTACT SPRING	BRASS
46	1	CONTACT BACK	BRASS
45	1	SUPPORT	BAKELITE
44	1	CAN	[illegible] TUBING
43	1	SHIELD	ALUMINUM
42	1	PLUG	#2 RUBBER CORK
41	1	SUPPORT RING	POLYSTYRENE
40	1	LOWER CAP	ALUMINUM
39	1	UPPER CAP	ALUMINUM
38	1	BUSHING	STEEL
37	1	2" BLOWER	TORRINGTON OR EQUAL
36	1	CASE CAP	ALUMINUM
35	1	GOVERNOR CASE	ALUMINUM
34	2	GOVERNOR SHOES	WOOD
33	1	GOVERNOR	ALUMINUM
32	1	SHAFT	STEEL
31	1	COLLAR	BRASS
30	2	STAMPED CLOCK GEAR	BRASS
29	1	PINION	STEEL
28	1	PINION	STEEL
27	1	SHAFT	STEEL
26	4	PLATE SPACER	ALUMINUM
25	1	TOP GEAR PLATE	BRASS
24	1	BOTTOM GEAR PLATE	BRASS
23	1	PINION	BOSTON GEAR #8479 OR EQUAL (BRASS)
22	1	BEVEL GEAR	BOSTON GEAR #8479 OR EQUAL (BRASS)
21	1	PINION	STEEL
20	1	AXLE	STEEL
19	1	THRUST PLATE	COPPER
18	1	SET SCREW	BRASS
17	1	SLEEVE	BRASS
16	1	CONTACT	[illegible] BRASS
15	1	SPACER	ALUMINUM
14	1	CONTACT ROTOR	COPPER & BRASS
13	1	CRANK HANDLE	ALUMINUM
12	1	CRANK	ALUMINUM
11	1	SPRING	COPPER
10	1	COLLAR	STEEL
9	1	COLLAR	BRASS
8	1	BUSHING	ALUMINUM
7	1	AXLE	STEEL
6	1	SPUR GEAR	ALUMINUM
5	1	REEL END	ALUMINUM
4	1	REEL SPACER	ALUMINUM
3	1	END	ALUMINUM
2	1	SIDE BAR	ALUMINUM
1	1	SIDE BAR	ALUMINUM

FIGURE 2. *Gravity-motor assembly drawing.*

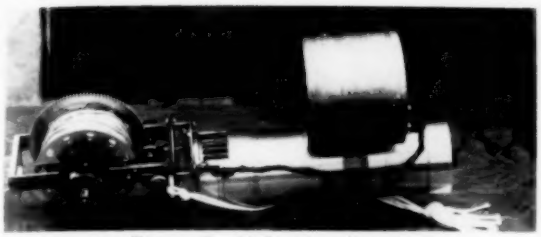

FIGURE 3. *Air-borne equipment.*

it through a vent in the side of the blower housing. The gravity motor also switches the pressure, temperature, humidity, and external reference elements into the ground measuring circuit. This motor is driven by the weight of the tethering line and the air-borne instruments suspended from the supporting balloon. A 40-ft length of nylon cord is wound around the drum of the gravity motor and attached to the balloon. The governor on the motor is set so that a tension of 4 lb in the nylon cord drives the blower at about 1,000 rpm and changes the contacts on the commutator switch approximately every 7 sec. The governor is effective in making the blower speed vary directly as the square root of the tension in the cord. A possible application of this relationship is to make gross measurements of the wind speed at the balloon level with respect to the ground. In actual flight tests, it requires about 35 min for the 40-ft length of cord to become unwound.

The pressure element consists of a beryllium-copper pressure capsule mounted on a rigid cast-aluminum rectangular frame. The pressure capsule is fastened to the bottom inside center of the frame by a screw connection made through its base. A Mu-metal bar is centered through its face and soldered to the stem of the pressure capsule. This bar completes a magnetic circuit in a U-shaped Mu-metal core, the flux of which is controlled by a coil of about 9,850 turns of No. 40 copper wire. The U-shaped portion of the magnetic circuit is mounted on a duralumin support and is spring-hinged to the cast-aluminum frame near the coil. The air-gap distance between the Mu-metal bar and the U-shaped magnet is adjusted by two controls—a coarse-threaded machine screw and a finely threaded shaft. These adjustment screws exert pressure against the top and extreme end of the duralumin core support opposite the spring hinge. A thumb wheel on the end of the fine-adjustment shaft is used to make the final settings of the air gap between the Mu-metal plate held by the pressure-capsule stem and the U-shaped core. This thumb wheel is turned against a tight friction bearing for close setting. These two adjustment controls are operated from the top of the aluminum casting. The aluminum casting fits snugly in the pressure-element housing, which is suspended during flight so as to minimize the effects of centrifugal force on the pressure capsule and the Mu-metal plate as the instruments swing about on the line.

The slightest expansion of the pressure capsule

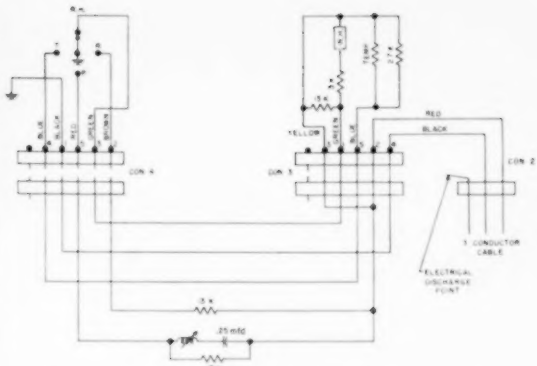

FIGURE 4. *Wiring diagram of Air-borne equipment.*

with increasing altitude changes the reluctance through the above-described high-permeability magnetic circuit by increasing the air gap over part of the circuit path. Magnetic flux through the high-permeability core and the variable air gap is induced by the above-mentioned coil of wire, which is energized by 60-c/s alternating current. Thus, the pressure cell, through the variable air gap in the magnetic circuit, controls the number of lines of magnetic intensity passing through the core of the coil and hence the inductive impedance of the coil as a function of pressure.

Temperature element. The temperature element consists of two radiosonde-type thermistors connected in parallel. These thermistors require 4.4 sec to indicate 63 percent of a sudden temperature change at a ventilation speed of 800 ft/min. The length of one of these rod thermistors is about 1.5 in., and its diameter is 0.052 in. These thermistors are mounted on a rectangular Bakelite frame that slides through the open end of an aluminum supporting tube. The opposite end of this tube is fitted with an aluminum cap that holds the tube rigidly in the larger 2½-in.-diameter aluminum tube of the air-borne unit. Ventilating holes are provided in the cap and in the end of the internal tube near the cap support. The connecting leads from the frame that supports the thermistors and humidity strip in the internal tube are brought out of the ventilating hole in the cap to a plug receptacle in the top of the pressure-capsule container.

Humidity element [4]. The humidity element is the radiosonde strip hygrometer. This element consists of two spaced conductors supported along the edges of a thin, narrow piece of nonhygroscopic dielectric material. The strip and conductors are covered with a film of polyvinyl alcohol containing lithium chloride.

Three-conductor cable. The three-conductor cable that connects the air-borne unit to the reel, the electronic panel, and to the recorder is made of No. 30 aluminum wire wrapped around a central nylon strength member. The cable is enclosed in a waterproof nylon cover and has a resistance of 1 megohm/1,000 ft between conductors and a resist-

233150—53——2

ance of 30 ohms/1,000 ft along the conductors. The weight of the cable is 2 lb/1,000 ft and its tensile strength is 100 lb.

Ground pulley. An omni-directional pulley is provided to allow the cable to rise from the ground in any direction (see fig. 5). This pulley is necessary to protect the tethering cable and is usually placed about 100 ft from the truck in a space free from ground obstructions.

Cable-length control. The length of the three-conductor cable is regulated by a motor-driven reel. Slip-ring contacts on the axle of the reel connect the air-borne instruments electrically to the electronic panel. A reversible variable-speed transmission drives the reel shaft through a 30-to-1 worm gear and allows the reel speed to be controlled to a maximum of 60 rpm in either direction. This arrangement eliminates any sudden jerks on the cable, provided that only the transmission is used to start, stop, and reverse the direction of the reel. An automatic-spacing mechanism (level winder) distributes the cable in even layers.

Electronic panel. The electronic panel (fig. 6) contains an electron-tube circuit that expresses the impedances of pressure, temperature, humidity, and reference elements in terms of direct-current values. The sensing elements are switched into one arm of a voltage-divider network in the grid circuit of a 6SJ7 tube in a manner so as to prevent the grid current from passing through the sensing elements. The transformer windings for the plate and grid voltages to the 6SJ7 tube are connected to make these supply voltages 180 degrees out of phase with each other. Thus, with the minimum value of impedance to be measured in the sensing circuit, the bias on the grid is essentially at cut-off for the low plate and screen voltages employed. The entire panel is supplied from a well-regulated source of 60-c/s power.

Four precision resistor units, two of 1,500 ohms each and two of 3,000 ohms each (R6, R7, R8, and R8A), connected in series can be inserted in the circuit by S2 and S5 for calibrating the plate current meter deflections. The recorder-division deflections are 90.0, 68.0, 45.0, and 6.2, respectively, on a 100-unit full-range chart. These values are obtained by adjusting R3, R12, and R2. R2 is set to the middle of its range for these calibration-current values. R3 is a voltage divider for selecting the desired grid potential and is adjusted in conjunction with R12 (voltage divider for the screen potential) so that tubes having a fairly large variation in transconductance can be used to provide the calibration-current values. Thus the circuit is not critical as to the selection of tubes or to the normal aging effects of them. Having set R3 and R12 to get the desired readings, it is generally only necessary to slightly adjust R2 to set the recorder pen on the reference readings. With 2,000 ft of the three-conductor cable, or the circuit compensated for this length of cable, the external reference in the air borne unit is 79.0 on the recorder scale.

The rectified plate current indicated on the recorder is determined by both the amplitude of the grid-cathode voltage and the phase relationship of that voltage with respect to the instantaneous plate and screen grid voltages. For this reason, the circuit can measure high resistances in the sensing positions at the end of 2,000 ft of cable, although it appears that the shunt capacitative reactance of the cable, approximately 35,000 ohms, would limit the maximum measurable resistance.

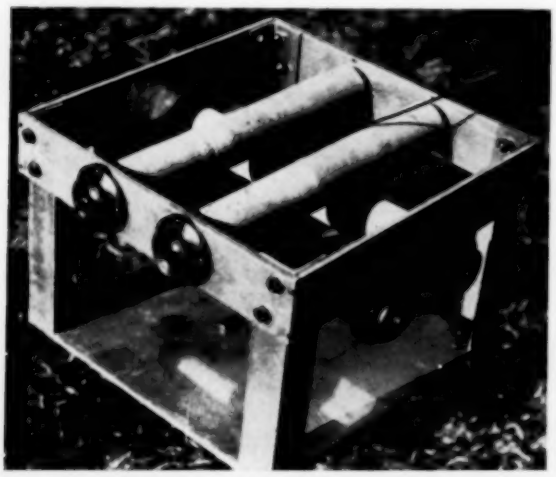

FIGURE 5. *Balloon tethering pulley.*

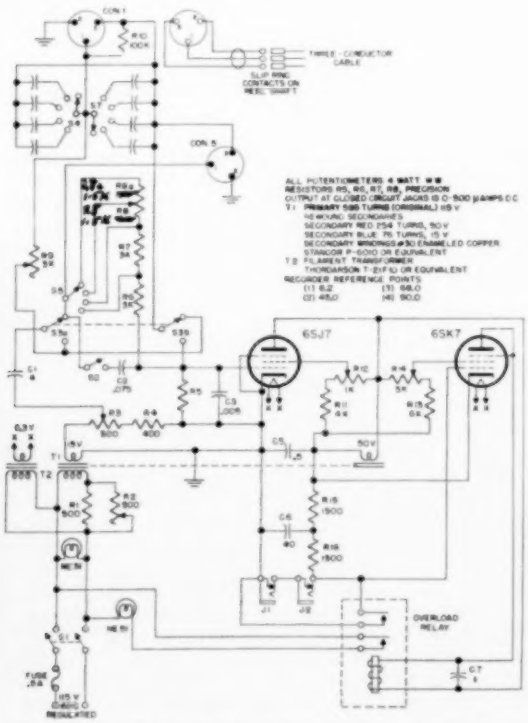

FIGURE 6. *Schematic diagram of the electronic panel.*

The shunt resistors in parallel with the sensing elements are used to limit the measured resistance between 1,500 and 10,000 ohms. This is necessary in order to get sufficient sensitivity in measuring high humidities, which cause the humidity element to have a resistance of about 1,800 ohms.

The third wire of the cable is grounded to prevent static charges due to the earth's potential gradient or charged air currents from causing disturbing fluctuations in the measurements. It also serves, in conjunction with its static-discharge point, as a means to keep cloud-induced charges in the cable from building up to lightning-discharge proportions.

The microammeter and the recorder, connected to J1 and J2, respectively, are protected against excessive current by a fast-acting, overload relay circuit. The relay in the plate circuit of the 6SK7 tube places a direct short across J1 and J2 and also operates an overload indicator light when the plate current of the 6SJ7 tube becomes excessive. The grid bias of the relay control tube is determined by the plate current of the 6SJ7 flowing through resistors R15 and R16. The screen grid voltage on the relay control tube is set by an adjustment of R14 so that the relay closes when more than 700 μa flow through J1 and J2.

Three calibrations are required for operation of the panel with the equipment: the first determines the tube sensitivity, the second locates the reference points for a full 2,000-ft length of cable inserted between connectors 1 and 5, and the third is performed to obtain these reference points in case of cable breakage.

1. *Tube-sensitivity calibration.* Switches S3A and S3B are set in the internal circuit, or up, position. Switch S2 is closed, placing C2, which simulates the capacity of the cable, in the circuit. The recorder-deflection reference positions 90.0, 68.0, 45.0, and 6.2 are obtained when R6, R7, R8, and R8A are in the circuit. These recorder-deflection values should be repeatable when a constant 115-v current is used to operate the panel. In the case 6SJ7 tube is changed or becomes aged, R2 and R12 are jointly adjusted until the above reference positions are obtained.

2. *Full-length-cable calibration.* Insert the 2,000-ft length of cable for which the panel is designed between connectors 1 and 5. Put S3A and S3B in the external, or down, position and open S2. Set R9 and S4 and S7 in the minimum position. Insert R6, R7, R8, R8A, and conductor 1 by means of switch S5 between C1 and R5. Without changing R2 or R12 the recorder-reference positions should be approximately the same as those found for the tube-sensitivity calibration. These values should be recorded and referred to for future calibration.

3. *Shortened length of cable calibration.* Measure the resistance of one conductor of the rejected broken piece of cable, and with an ohmmeter, adjust R9 to a position of twice this value. Insert the shortened length of cable between connectors 1 and 5. Put S3A and S3B in the external or down position with S2 open. Insert R6, R7, R8, R8A, R9, and conductor 1 into the circuit between C1 and R5 by the switch S5. Without changing R2 or R12, adjust S4 and S7 to reproduce the recorded calibration positions obtained in step 2.

CALIBRATION CHAMBER:

4. Ventilation in the chamber is provided under all conditions of pressure by a set of 7-in. fan blades that are driven through a mercury-seal, pressure-tight bearing at the bottom of chamber. The bearing shaft is coupled through a flexible rubber hose to a 600-rpm motor. The construction of the mercury-seal bearing is shown in figure 7.

The humidity box (fig. 8) fits inside the pressure calibration chamber. The mounting frame for the temperature and humidity elements is enclosed in this box. A ring, the same size as the tube on which this frame fits in the airborne unit, holds the temperature and humidity elements about an inch over a tray containing a saturated salt solution (see table 2). A small, motor-driven, centrifugal blower draws air from over the salt solution and blows it onto the bulbs of dry- and wet-bulb thermometers, and thence into the thermistor humidity-strip support. The walls and bottom of the calibration box are made of aluminum, but the top is made of Lucite. The motor is mounted on the outside of the box and is magnetically coupled to drive the ventilating fan.

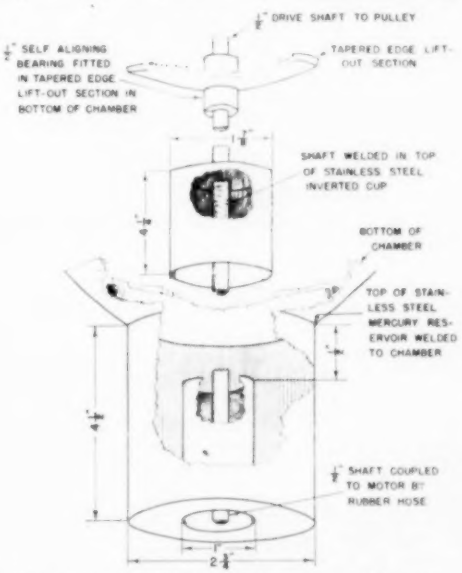
DRIVE SHAFT TO PULLEY
SELF ALIGNING BEARING FITTED IN TAPERED EDGE LIFT-OUT SECTION IN BOTTOM OF CHAMBER
TAPERED EDGE LIFT-OUT SECTION
SHAFT WELDED IN TOP OF STAINLESS STEEL INVERTED CUP
BOTTOM OF CHAMBER
TOP OF STAINLESS STEEL MERCURY RESERVOIR WELDED TO CHAMBER
SHAFT COUPLED TO MOTOR BY RUBBER HOSE

FIGURE 7. *Exploded view of mercury-seal bearing.*

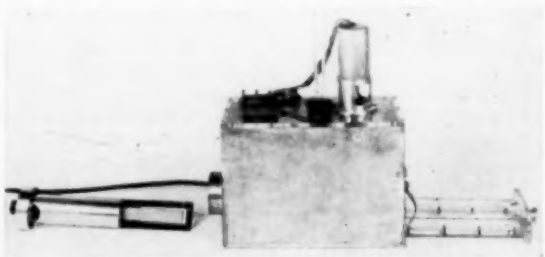

FIGURE 8. *Humidity calibration box.*

TABLE 2. *Standard humidity salt brines*

Chemical	Relative humidity at 20° C.
	Percent
Potassium nitrate, (KNO_3)	95
Sodium chloride, (NaCl)	75
Magnesium nitrate, ($Mg(NO_3)_2 \cdot 6H_2O$)	53
Magnesium chloride, ($MgCl_2 \cdot 6H_2O$)	32
Lithium chloride, (LiCl)	12

The dry- and wet-bulb thermometers are supported through a rubber stopper that plugs into this top. These thermometers are used as a standard measurement of temperature and humidity for the atmosphere of the humidity box.

3. Calibration Procedures

3.1. Pressure

The altimeter element registers the absolute pressure at the level of the air-borne equipment and is used to measure the difference in pressure between that level and the ground. A calibration curve for measuring these differences is constructed from data obtained by calibrating the altimeter in the sealed multipurpose calibration chamber against a precision aneroid barometer.

The air-borne unit is installed in the multipurpose calibration chamber and electrically connected to the three-conductor cable that leads to the reel, electronic panel, and recorder. The altimeter is then adjusted until the recorder reads 70, corresponding to the ambient or station pressure. Simultaneous readings are then taken of recorder deflection and aneroid-barometer pressures for 3 cycles over the range of 1,010 to 950 mb at 5-mb intervals.

The calibrations were made so that the difference in the recorder deflections between consecutive 5-mb intervals in the same cycle were obtained over three pressure levels. These sets of recorder-division differences were averaged and used with the corresponding pressure differences. The data given in table 3 were used to construct a calibration curve of pressure differences versus recorder-deflection difference (fig. 9).

TABLE 3. *Departures from the mean of the individual recorder-division difference for the indicated pressure levels, as shown by the calibration curve*

mb.	1,005	1,000	995	990	985	980	975	970	965	960
mb.	0.1	0.1	0.1	0.2	0.1	0.1	0.2	0.2	0.2	0.2

This curve was considered to hold for all 50-mb intervals from the station pressure (say from 1,020 to 970 or from 1,010 to 960) because (1) the altimeter when at the surface was always set to give a recorder deflection of 70, regardless of the station pressure; (2) these beryllium-copper capsules had linear pressure-expansion curves with a premissible 1-mb deviation, as specified by the manufacturer; and (3) the pressure, recorder-division calibration curve was not effected by temperature changes, as determined by test.

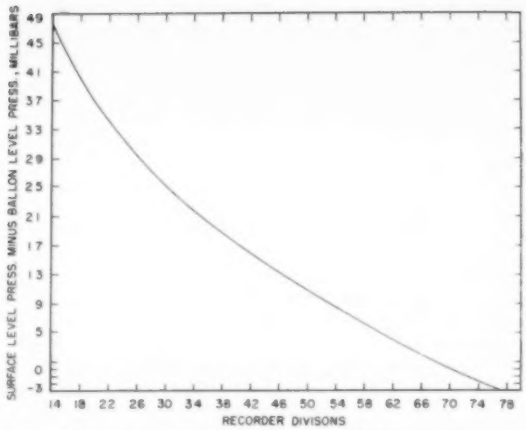

FIGURE 9. *Pressure calibration of the recorder.*

As a check on this linearity, a beryllium-copper capsule similar to that used in the altimeter was mounted in a bell jar so that it expanded against the level arm of a dial gage, which was calibrated to read ten-thousandths of an inch and from which it was possible to estimate values of half a ten-thousandth of an inch. A sensitive aneroid barometer, calibrated to ½-mb intervals, was used to measure the pressure inside the evacuated bell jar. Simultaneous readings of the barometer deflection and the capsule expansion were then made every 5 mb over the pressure range 995 to 940 mb. A straight line, fitted to the 10 readings thus obtained, showed that the expansion of the capsule was linear insofar as it was possible to measure it.

3.2. Temperature

The temperature element is a rod thermistor of the type used in the radiosonde. A convenient way to calibrate this thermistor is to use a Wheatstone bridge, a temperature-controlled oil bath, and an accurate mercurial thermometer. Because the change in temperature of the oil bath takes place very slowly, the Wheatstone bridge can be set for balance at a given resistance position and the temperature read on the thermometer exactly at the time the bridge comes to balance.

Sixty-eight evenly spaced readings were made in this fashion for two complete cycles over the range from 0° to 40° C. The temperature values were plotted to hundredths and the resistance values to the nearest ohm, and a smooth curve drawn to fit the greatest number of points. The departures from the curve in degrees centigrade were tabulated from the 68 points, and the average was found to be 0.07 deg C.

The temperature-versus-resistance calibration curve holds throughout the life of a particular thermistor. It is necessary to calibrate each thermistor used in the air-borne unit in this fashion (fig. 10).

To calibrate the recorder, a decade resistance box was connected in place of the rod thermistor in the

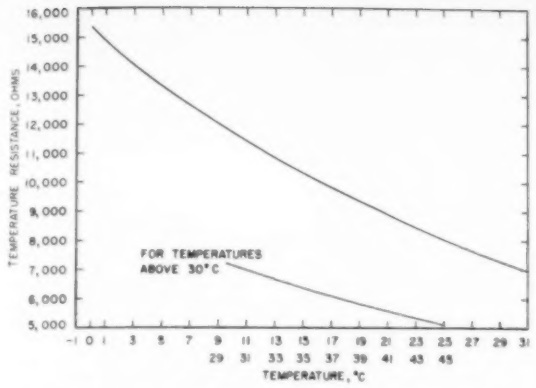

FIGURE 10. *Temperature versus resistance calibration.*

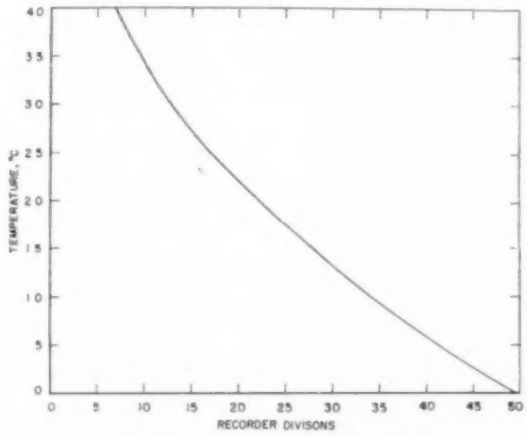

FIGURE 11. *Temperature calibration of the recorder.*

air-borne circuit, and a curve of resistance-versus-recorder division was constructed. The temperature versus-resistance calibration curve is used with a resistance-versus-recorder-division curve to construct a direct-reading temperature-versus-recorder-division curve (fig. 11).

3.3. Humidity

The humidity element is the standard strip hygrometer used in the radiosonde. The resistance of this element is both a function of temperature and of humidity. The hygrometer is placed in the previously described calibration compartment. The metal walls of the box are coated with a thin oil film so that condensation will be retarded on these surfaces. The box is cooled to the lowest temperature at which observations are to be taken, and a tray containing a saturated salt solution is inserted. After humidity equilibrium has been reached, simultaneous readings are taken of the resistance of the hygrometer strip and of the wet- and dry-bulb thermometers. The 60-cycle a-c resistance values of the strip are read from the dials of the

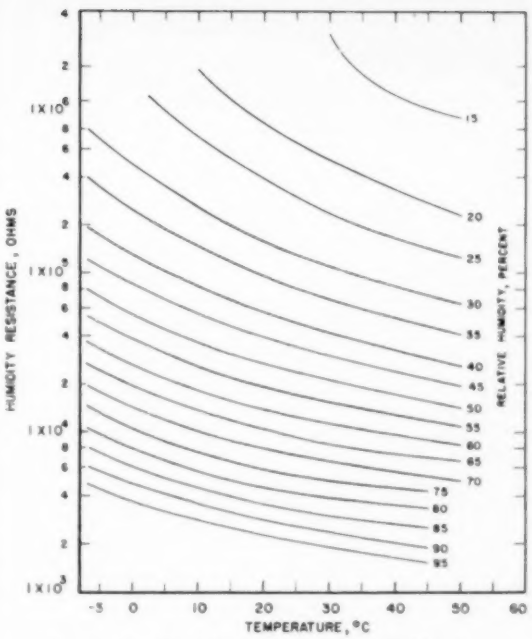

FIGURE 12. *Humidity versus resistance calibration.*

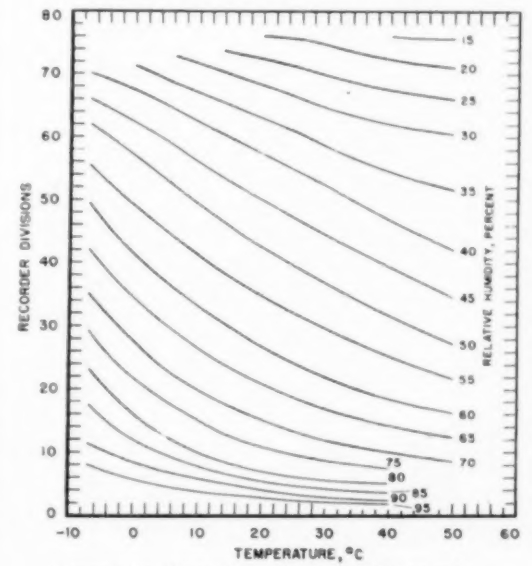

FIGURE 13. *Humidity calibration of the recorder.*

Wheatstone bridge, and the humidity percentages are computed from the dry- and wet-bulb temperatures. This procedure is followed for humidity atmospheres of 12, 32, 53, 75, and 95 percent.

Forty-six points were thus plotted. These values were compared with another, much more extensive, 60-cycle a-c calibration of the strip hygrometer

made by another laboratory. These data covered a range from $-10°$ to $+40°$ C. for humidities from 5 to 95 percent. The logarithims of the resistances were plotted against the temperatures. Curved diagonal lines were drawn across the chart for every five relative-humidity units (fig. 12). Figure 13 is a calibration chart showing relative-humidity-versus-recorder divisions.

4. Flight Computations

Two types of computations, height and refractivity, are made from the data recorded during a low-level sounding flight. Each revolution of the balloon-borne gravity-motor commutator gives an indication of a value of pressure, temperature, and humidity on the recorder trace in the truck for a particular point in space. The revolutions of the commutator are numbered on the recorder chart, and these numbers are used to identify the point data taken during a sounding. In an ordinary 40-min flight there are about 320 such points. The refractivity and height are worked out and tabulated for each of these positions. These points are then plotted on a graph with refractivity values as abscissas and height as ordinates. The work involved in the construction of this graph is simplified by the use of altitude charts. The formulas for these charts follow.

Altitude-computation charts formula. Three altitude-computation charts were prepared to cover the range from 928 to 1,050 mb. One of these charts is shown in figure 14. The charts are based on the formula [6, 7].

$$H = 67.403\ T'_M\ (\log 1{,}050 - \log P).$$

H is the altitude, in meters, above the 1,050-mb surface; T'_M is the mean virtual temperature of the layer whose height is measured and is equal to $T_M[1+0.376(e/p)_M]$, in which $(e/p)_M$ is the mean value of the ratio of the water-vapor pressure to the actual pressure throughout the layer, T_M is the actual mean temperature of the layer whose height is measured, and P is the pressure at the level of the surface whose height is measured above the 1,050-mb surface. A table of logarithms to the base 10 is used for substituting these pressure values in the formula.

In practice, over the short height intervals (less than 650 m) for which these charts are designed, it is sufficient to use the mean of the balloon-level and surface-level temperature for T'_M.

Refractive-index computation formula. The refractivity of the air, N, is computed from the temperature, pressure, and humidity measurements by use of the following formula [10]

$$N \equiv (n-1)10^6 = \frac{77.6}{T}\left(p + 4810\,\frac{e}{T}\right) = \frac{77.6p}{T} + \frac{3.73\times 10^5 e_s(RH)}{T^2},$$

where p is the total pressure in millibars, T is the absolute temperature in degrees Kelvin, e is the partial pressure of water vapor in millibars, e_s is the saturation vapor pressure in millibars, n is the refractive index of the air, and (RH) is the relative himidity in percent. A special slide rule for this computation has been developed by Weintraub [11].

Illustrative examples of flight computations. Figure 15 is a reproduction of a portion of a low-level sounding flight started at 11:50 a. m. on August 31, 1950. As explained previously, the sequences of pressure, relative humidity, and temperature measurements are numbered and tabulated corresponding to the revolutions of the balloon-borne gravity motor (table 4). No corrections are applied to the deflec-

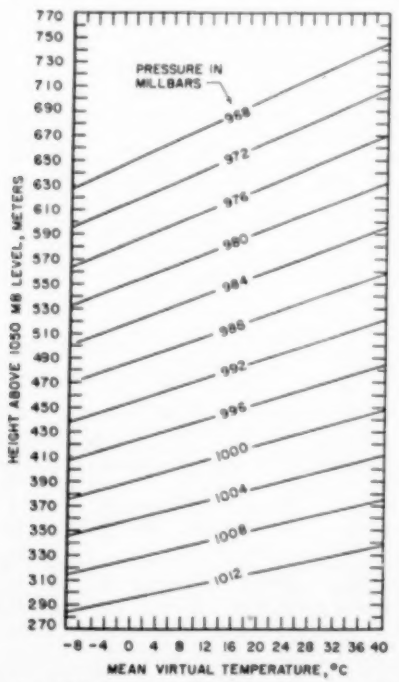

FIGURE 14. *Altitude computation chart (968 to 1,012 mb.).*

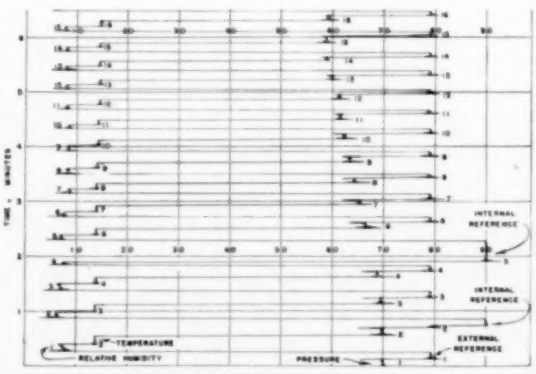

FIGURE 15. *Flight-record sample.*

TABLE 4. *Low-level sounding recorder data for the beginning of a flight started at 11:50 a. m.*

Commutator revolution	Temperature		Humidity		Pressure		Height above surface	Refractivity, N
	Recorder division	Degrees centigrade	Recorder division	Percent	Recorder division	Delta P above 1006.8 mb		
1			7.5	77	70.0	0	0	
2	13.8	28.6	6.3	77	69.8	.1	.8	387
3	13.8	28.6	7.0	78	69.6	.2	1.6	388
4	13.9	28.5	7.5	77	68.8	.6	5.3	386
5			7.3	78				
6	14.0	28.4	7.6	77	66.5	1.8	15.6	386
7	14.0	28.4	8.7	75	65.2	2.4	20.9	384
8	14.1	28.2	8.5	76	64.3	2.9	25.4	383
9	14.2	28.1	8.6	76	63.4	3.4	29.8	381
10	14.2	28.1	8.5	76	62.5	3.8	33.3	382
11	14.3	27.8	8.2	77	61.5	4.4	38.6	381
12	14.6	27.8	8.2	77	61.5	4.4	38.6	381
13	14.6	27.8	8.1	77	60.0	5.2	45.0	381
14	14.7	27.8	8.2	77	58.8	5.8	50.0	381

tions because the external reference position remains fixed.

The calibration curves (figs. 9, 11, 13) are used to obtain the temperature, humidity, and pressure values, respectively. The height of the balloon level above the surface is found by using the altitude-computation chart (fig. 14), and the corresponding refractivity value, N, is determined by use of the refractivity formula given above.

Sample balloon-height computation for balloon flight contact No. 14. Given: balloon-level pressure of 1,001.0 mb, surface-level pressure of 1,006.8 mb, and mean temperature, $(28.6+27.6)/2$, or 28.1° C.

Figure 14 gives the height of the balloon above the 1,050-mb surface for a mean temperature of 28.1° C as 421 m and the height of the ground above the 1,050-mb surface for the same mean temperature as 371 m. The height of the balloon above the ground is $421-371=50$ m.

Sample refractivity computation for balloon-flight contact No. 14. Given: Pressure at balloon level is 1,001.0 mb, temperature at balloon level is 27.5° C$=27.5+273=300.5°$ K, relative humidity at balloon level is 77 percent, the saturation vapor pressure is 36.71 mb [12].

$$N=\frac{77.6\times 1001.0}{300.5}+\frac{3.73\times 10^5\times 36.71\times 77}{300.5^2}=375.3.$$

5. Results of Checks and Flight Tests

The humidity and pressure (altitude) calibrations of the system were checked under field-test or calibration-chamber conditions. It was not believed necessary to perform a calibration-chamber check on the temperature calibration of the system because comparisons between the mercurial thermometer and air-borne unit in a well-ventilated instrument shelter showed little difference between two readings, that is, the values checked within $\pm\frac{1}{2}$ deg C. The variation in temperatures read from two mercurial thermometers suspended under similar conditions in the shelter was also of this order of magnitude.

Humidity. The humidity check consisted of 101 comparisons of strip-hygrometer and dry- and wet-bulb humidity values in the humidity compartment of the multipurpose calibration chamber. Five separate hygrometer strips were used in making these comparisons; the hygrometer strips were taken from a production lot that met a manufacturing tolerance of ±5-percent relative humidity when used in a radiosonde. No attempt was made to establish a lock-in or check point for any strip in order to get the greatest accuracy from it. The greatest deviation between the observed values was 5 percent. The exposure life of the first strip was 26 hr; the second, 72 hr; the third, 20 hr; the fourth, 4 hr; and the fifth strip was still good after 3 hr. The first three strips were used for measurements about 6 hr at the beginning of the test and then for about 1 hr at the end. The fourth and fifth strips were used continuously. It is generally believed that the life of a humidity strip is about 1 hr, but with the use of 60-c/s current in the measuring circuit, the life was extended considerably.

The strip hygrometer was placed in an airtight compartment that provided an approximately constant humidity atmosphere. The temperature of this compartment was varied by applying heat or cold to the multipurpose chamber, and the humidity varied by changing the salt solutions in the compartment. The range of humidity covered was from 20 to 94 percent at controlled temperatures of from −5° to +45° C. The standard deviation of the humidities indicated by the calibration system as compared to the dry- and wet-bulb humidity was 2.2 percent.

Altitude. An extensive test consisting of 40 observations comparing heights measured by the balloon-borne altimeter of the low-level sounding system and those found by double theodolite triangulation was made. For these results, over the range from 0 to 137 m, the combined standard deviations of the two systems was 3.5 percent.[2] This value was obtained by taking the standard deviation of all 40 of the individual ratios formed by corresponding pairs of height values about unity.

The heights used for checking the altimeter values were measured by two theodolites stationed at the ends of a level 100-m base line. The tethering pulley of the balloon cable was placed 50 m to the leeward side of the midpoint of the base line. Balloon heights were computed from the altimeter data and by each of the theodolites. The mean of the theodolite heights for each point was compared with the corresponding altimeter value by forming the ratio of altimeter height to mean theodolite height. The standard deviation of these ratio values from unity was computed (table 5).

The check of the altimeter by the double-theodolite method also afforded an opportunity to compare balloon heights determined by the length-of-cable-elevation-angle (h_C), and the double-theodolite-triangulation (h_T) methods. For this test the tethering

[2] The error of measurement appeared to be proportional to height, so that at 100 m the error of the combined system is ±3.5 m. The error for either system would be, of course, less than this. The separation of the errors due to each of the methods was tried, but the results were not satisfactory.

pulley to the balloon was located at one of the theodolite stations. Table 6 shows the results of such a comparison.

Although these data are not extensive enough for reliable statistical analysis, the following conclusions seem obvious: (1) The height by length-of-cable method is always the same or greater than that by the double-theodolite method. (2) The variation in height determinations between the two systems is greater at low than at high average surface-wind speeds. This is important to remember because sharp temperature and moisture stratification occurs at low wind speeds.

TABLE 5. *Comparison of balloon heights measured by the theodolites and the altimeter*

Number of observation	h by theodolite α	h by theodolite β	$\frac{h_\alpha+h_\beta}{2}$	h by altimeter
	m	m	m	m
1	58.8	59.6	59	58
2	59.0	54.9	57	55
3	53.9	57.4	56	53
4	50.8	50.6	51	52
5	50.5	48.4	49	54
6	52.1	52.7	52	53
7	53.6	53.4	54	55
8	58.8	57.8	58	60
9	55.5	56.4	56	54
10	56.9	57.6	57	57
11	78.3	77.3	78	75
12	79.2	79.2	79	77
13	81.1	81.0	81	77
14	82.5	82.0	82	79
15	79.3	78.8	79	78
16	80.1	77.6	79	78
17	87.9	87.4	88	87
18	81.2	81.4	81	82
19	76.2	78.2	77	79
20	83.5	83.1	83	80
21	113.6	113.2	113	110
22	107.9	110.6	109	112
23	108.0	108.7	108	108
24	105.6	102.8	104	104
25	106.3	105.5	106	104
26	103.9	103.8	104	104
27	109.1	110.2	110	110
28	111.2	109.8	110	108
29	120.9	113.4	117	110
30	114.2	114.6	114	110
31	131.0	129.3	130	125
32	131.5	133.9	133	128
33	125.2	127.0	126	130
34	131.4	131.1	131	134
35	130.2	133.6	132	134
36	134.5	134.6	135	133
37	132.5	129.9	131	131
38	127.8	130.5	129	133
39	137.1	136.4	137	131
40	135.7	135.4	136	132

TABLE 6. *Comparison of balloon heights*

Soundings taken at Sterling, Va.

June 9, 1950, 1:30 to 2:30 p. m. Average surface wind speed, 9 mph				June 15, 1950, 12:30 to 2:30 p. m. Average wind speed (surface), 15 mph		
h_T	h_C	Delta h	Delta h *	h_T	h_C	Delta h
Cable length 91 m				Cable length 152 m		
77	84	7	11	115	119	4
83	89	6	10	128	132	4
76	78	2	3	129	138	9
67	70	3	5	118	122	4
78	79	1	2	139	142	3
				116	120	4
				117	120	3
				127	130	3
				123	128	5
				123	128	5
Cable length 152 m						
51	81	30	.....			
109	116	6	.....			
126	126	0	.....			
73	83	10	.....			
87	100	13	.....			

* Weighted by the ratio 152/91 for comparison with 152-m cable length.

6. Status and Future Improvements

The National Bureau of Standards low-level sounding system in its present state of development is a usable system. The altimeter is designed to be accurate within ± 50 ft, or less, up to heights of 2,000 ft. This accuracy can be easily met, and, up to heights of 600 ft, double this accuracy can be obtained. The double-theodolite altimeter tests show that at a height of 328 ft the combined error of both systems is ± 11 ft and that this error is proportional to the height. This means that the error of the altimeter itself is less than ± 11 ft. With care and critical adjustment, the altimeter can be initially set to record surface pressure within $\pm 1/10$ mb. Within the first 200 ft above the ground, elevation changes of 6 ft are readily detectable.

The possibilities of future improvement of this system are numerous. It appears that the sensitivity of the system can be further increased by amplifying the grid-circuit signal. This will permit decreasing the current flowing through the sensing elements and make it possible to use quicker responding temperature elements, such as a bead thermistor, which has a 1-sec time lag in zero ventilation. The life of the strip hygrometer for high humidity values should also be further increased by using this decreased current.

The following are some of the other possible applications of this system: (1) To detect the density of fog or smoke by photometric means. A photronic-type photocell can be used as a sensing element so that illumination values from total darkness to bright sunlight can be measured over the full range of the recorder scale. (2) To measure wind speed relative to the ground. The switching rate of the gravity motor is a function of line tension as controlled by the force of the wind on the system. (3) To investigate static charges in the lower atmosphere. The use of an electron tube in the panel measuring circuit makes it possible to measure potentials as a function of heights and charged air currents. The effects of these potentials interfered with the measurement of pressure, temperature, and humidity by the system before one of the conductors of the cable was grounded.

In preparing this report, the authors are indebted to many people for assistance and information, but particular acknowledgment is due E. E. King, W. W. Warren, and Leo L. Hughes, for their valuable suggestions and faithful services.

7. References

[1] Mobile Meteorological Station SCM–1, War Department Technical Manual TM 11–2409 (March 29, 1945).

[2] H. G. Booker, Some problems in radio meteorology, Quart. J. Roy. Meteorol. Soc. **74,** 331–332 (July–October 1948).

[3] Manual of radiosonde observations (WBAN) Circular P, U. S. Dept. of Commerce, Weather Bureau.

[4] F. W. Dunmore, An electronic hygrometer and its applications to radio meteorography, J. of Research of NBS **20** (June 1935), RP1102.

[5] Arnold Wexler and W. G. Brombacher, Methods of measuring humidity and Testing Hygrometers, NBS Circular 512 (1951).

[6] Pressure-Altitude Chart (1050–800 mb), U. S. Weather Bureau Form (WB Form 1154A) U. S. Dept. of Commerce, Weather Bureau.

[7] D. L. Randall and M. Shulkin, CRPL 2–1, U. S. Dept of Commerce, NBS, Survey of meteorological instruments used in tropospheric progagation investigations.

[8] M. Shulkin, CRPL 2–2, U. S. Dept. of Commerce, NBS, Average radio ray refraction.

[9] Propagation of radio waves, Summary Technical Report of NDRC, CP **3.**

[10] Ernest K. Smith, Jr. and Stanley Weintraub, The Constants in the equation for atmospheric refractive index at radio frequencies, J. Research NBS **50,** (1953) RP.

[11] Stanley Weintraub, Slide rule for the computation of the radio refractive index of air, NBS Report (in preparation).

[12] Smithsonian Meteorological Tables, p. 351–53 (1951).

WASHINGTON, June 1951.

Journal of Research of the National Bureau of Standards Vol. 50, No. 1, January 1953 Research Paper 2382

A Simple Calculation of Dielectric Loss from Dielectric Dispersion for Polar Polymers

Paul Ehrlich

For polar polymers undergoing orientation polarization it is possible to calculate dielectric losses from dielectric constant data by use of a single approximation already familiar from its application to mechanical properties, if this approximation is applied to the real part of the dielectric constant only and if data over a sufficiently wide frequency range are available. Data obtained at frequencies from 10^2 to 10^5 cycles per second for Butvar and for a copolymer of styrene and methyl methacrylate are analyzed and it is found that observed and calculated values of the dielectric losses agree within 10 percent or better.

Equations relating the real and the imaginary parts of the dielectric constant have been given, but are not in general use because the equations involved are cumbersome [1, 2, 3].[1] Workers interested in the mechanical behavior of high polymers have shown how the real and the imaginary parts of the modulus of rigidity are related through a distribution function [4] and how this function can be obtained by an approximation method from the real part of the modulus [5, 6] and from both real and imaginary parts [7]. It will be shown how the dielectric loss can be calculated from dielectric constant data by an analogous approximation method.

The Debye equations [8], generalized for a distribution of capacitance elements with resistance elements in parallel [9], each with its characteristic relaxation time, mathematically equivalent to a mechanical retardation time, are

$$\epsilon' - \epsilon_\infty = \int_0^\infty \frac{y(\tau)\,d\tau}{1+\omega^2\tau^2} \tag{1a}$$

$$\epsilon'' = \int_0^\infty \frac{\omega\tau\, y(\tau)\,d\tau}{1+\omega^2\tau^2}, \tag{1b}$$

where ϵ', ϵ'' are the real and the imaginary parts of the dielectric constant, ω is the angular frequency, τ is the relaxation time and $y(\tau)$ is the distribution of relaxation times. For mathematical convenience, we define $y(\tau)d\tau = Y(\ln\tau)d\ln\tau$. The cut-off approximation [5, 6, 7] assuming the integrands in (1a), (1b) to vanish for $\omega\tau > 1$ and to reduce to their numerators for $\omega\tau \leq 1$ gives

$$\epsilon' - \epsilon_\infty = \int_{-\infty}^{\ln\frac{1}{\omega}} Y(\ln\tau)\,d\ln\tau \tag{2a}$$

$$\epsilon'' = \int_{-\infty}^{\ln\frac{1}{\omega}} \omega\tau\, Y(\ln\tau)\,d\ln\tau. \tag{2b}$$

(2a) gives agreement with (1a) well within the graphical error involved in the calculations, whereas values of ϵ'' calculated from (2b) are generally 30 to 40 percent low when compared to those obtained from (1b). We therefore use the approximation (2a) only, obtaining

$$Y\left(\ln\frac{1}{\omega}\right) = -\frac{d\epsilon'}{d\ln\omega} \tag{3}$$

by differentiation of (2a) with respect to the upper limit and carry out this operation graphically. The exact eq (1b) is then used to obtain ϵ''[2] by a graphical integration for each value of ω. The integration is done graphically, because even the most widely applicable equations that have been suggested for $y(\tau)$ on semiempirical grounds [2, 10] and that might have been expected to represent the results cited do not fit the data over the entire frequency range and because, if the curve for $Y(\ln\tau)$ is approximated in sections by simple analytical expressions, integration often becomes impossible.

Data are presented over a wide frequency range, including either side of the absorption maximum, for Butvar (polyvinylbutyral) [11], a material which, for an unplasticized polymer, has a fairly sharp dispersion and for SM-2, a copolymer with a broad dispersion made from 49-mole-percent styrene and 51-mole-percent methyl methacrylate; both polymers having negligible d-c conductivity (tables 1 and 2). In each case the calculated values of ϵ'', which can be obtained for points at least one decade interior

TABLE 1. *Electrical properties of Butvar* [1]

Frequency	ϵ'	ϵ''	Y	$-\log\tau$	ϵ'' (calculated)
c/s					
10^2	3.415	0.0238	0.0130	2.80	.....
4×10^2	3.394	.0271	.0152	3.40	.....
10^3	3.382	.0301	.0200	3.80	0.032
3×10^3	3.364	.0367	.0243	4.275	.041
10^4	3.336	.0550	.0317	4.80	.056
3×10^4	3.307	.0788	.0433	5.275	.073
10^5	3.253	.104	.062	5.80	.094
3×10^5	3.170	.110	.073	6.275	.107
10^6	3.075	.111	.078	6.80	.114
3×10^6	2.988	.101	.073	7.275	.111
10^7	2.915	.092	.063	7.80	.099
4×10^7	2.83	.079	.059	8.40	.....
10^8	2.77	.072	.053	8.80	.....

[1] Data were obtained on a 3-terminal Schering bridge at frequencies of 10^2 to 10^5 c/s and by resonance methods from 10^5 to 10^8 c/s.

[1] Figures in brackets indicate the literature references at the end of this paper

[2] J. D. Ferry and E. R. Fitzgerald (reported before the American Physical Society in March 1952 at Columbus, Ohio) have also made similar calculations, but use the cut-off approximation for both real and imaginary parts and then apply a second approximation requiring a certain analytical formulation of their distribution function.

TABLE 2. *Electrical properties of copolymer SM–2* [1]

Frequency	ϵ'	ϵ''	Y'	$-\log \tau$	ϵ'' (calculated)
c/s					
10^2	3.090	0.0667	0.0443	2.80	
10^3	2.990	.0705	.0417	3.80	0.068
10^4	2.898	.0681	.0329	4.80	.064
10^5	2.818	.0605	.0360	5.80	.058
10^6	2.740	.0504	.0393	6.80	.046
10^7	2.679	.0400	.0217	7.80	

[1] Data were obtained on a three-terminal Schering bridge at frequencies of 10^2 to 10^5 c/s and by resonance methods from 10^5 to 10^8 c/s.

to the frequency limits, agree within 10 percent or better with the experimental ones, a discrepancy that can be accounted for by the graphical error. This suggests that the method described is applicable to polar polymers in the region in which they undergo orientation polarization, if the dispersion range is wide. It should be possible to deal with nonpolymeric materials in the same way, provided their electrical behavior meets these requirements.

The author has profited from discussions with R. S. Marvin and R. G. Breckenridge.

[1] B. Gross, Phys. Rev. **59,** 748 (1941).
[2] R. M. Fuoss and J. G. Kirkwood, J. Am. Chem. Soc. **63,** 385 (1941).
[3] J. R. McDonald, J. Chem. Phys. **20,** 1107 (1952).
[4] T. Alfrey Jr., Mechanical behavior of high polymers (Interscience Publishers, New York, N. Y., 1948).
[5] D. G. Ivey, B. A. Mrowca, E. Guth, J. Applied Phys. **20,** 486 (1949).
[6] A. W. Nolle, J. Polymer Sci. **5,** 1 (1950).
[7] J. D. Ferry, W. M. Sawyer, G. V. Browning, A. H. Groth, J. Applied Phys. **21,** 513 (1950).
[8] P. Debye, Polar molecules (Dover Publishers, New York, N. Y.).
[9] H. Fröhlich, Theory of dielectrics, p. 92 to 94 (Oxford Univ. Press, 1950).
[10] K. S. Cole and R. H. Cole, J. Chem. Phys. **9,** 341 (1941).
[11] A. H. Scott, J. H. Beardsley, P. Ehrlich, E. C. Bamberger and D. R. Tilley, Unpublished data, obtained in Divs. 1 and 14 of NBS under the supervision of A. H. Scott and J. L. Dalke.

WASHINGTON, May 20, 1952.

Journal of Research of the National Bureau of Standards Vol. 50, No. 1, January 1953 Research Paper 2383

Struve Function of Order Three-Halves[1]

The Struve functions of half-integral order appear, among other places, in radiation problems with spherical symmetry. They can be generated by recurrence:

$$H_{1/2}(x)=\left(\frac{2}{\pi x}\right)^{1/2}(1-\cos x)$$

$$H_{3/2}(x)=\left(\frac{x}{2\pi}\right)^{1/2}\left(1+\frac{2}{x^2}\right)-\left(\frac{2}{\pi x}\right)^{1/2}\left(\sin x+\frac{\cos x}{x}\right)$$

$$H_{\nu-1}(x)+H_{\nu+1}(x)=\frac{2\nu}{x}H_\nu(x)+\frac{(x/2)^\nu}{\Gamma(\nu+\frac{3}{2})\Gamma(\frac{1}{2})}.$$

It is often convenient to use instead of the $H_\nu(x)$ the function $h_\nu(x)$ defined by

$$h_\nu(x)=\left(\frac{2\pi}{x}\right)^{1/2}H_\nu(x).$$

These satisfy the recurrence relations

$$h_{1/2}(x)=\frac{2}{x}(1-\cos x),\quad h_{3/2}(x)=\left(1+\frac{2}{x^2}\right)-\frac{2}{x}\left(\sin x+\frac{\cos x}{x}\right)$$

$$h_{\nu-1}(x)+h_{\nu+1}(x)=\frac{2\nu}{x}h_\nu(x)+\frac{(\frac{1}{2}x)^{\nu-\frac{1}{2}}}{(\nu+\frac{1}{2})!}.$$

The calculation of the present table of $h_{3/2}(x)$ was suggested by E. W. Montroll. The fraction of energy scattered from a plane wave by a spherical obstacle when its wave transmission characteristics are not too different from those of the external medium is given by $h_{3/2}(x)$. The limiting behavior of $h_{3/2}(x)$ is given by

$$\lim_{x\to 0}h_{3/2}(x)=0,\qquad \lim_{x\to\infty}h_{3/2}(x)=1.$$

This function has been tabulated for $x=0(.02)15$ to 10 decimal places. The values are expected to be correct to within one unit of the last place. The table is also available on IBM cards.

Central differences, modified where necessary, have been provided. Modification has been indicated by the letter C printed after the number; the minus sign is printed after the number, and after the C in the case of a negative modified second difference. These unusual conventions were adopted so that the complete tabulation could be made mechanically.

To interpolate in this table to the full accuracy of ten decimals, it suffices to employ the Everett interpolation formula as far as the terms δ^2. Here the modified second central differences are to be employed in Everett's formula just as though they were not modified. Everett's formula is

$$f(x_0+ph)=pf(x_1)+qf(x_0)-\frac{p(1-p^2)}{6}\delta^2f(x_1)-\frac{q(1-q^2)}{6}\delta^2f(x_0),$$

where $x=x_0+ph$ is between x_0 and $x_1=x_0+h$, $q=1-p$, $\delta^2f(x_i)$ is the second central difference tabulated alongside $f(x_i)$, $i=0,1$, and here the tabular interval $h=0.02$. If one neglects the terms in δ^2, which is what is done in ordinary linear interpolation, an upper bound for the error is one-eighth of the second difference.

The entire computation of this table was done on the SEAC. The code employed subroutines for the sine and cosine functions. The actual calculation of the table by the SEAC and its transfer upon magnetic wire required only 15 minutes. This present copy of the table was prepared from the magnetic wire by the flexowriter.

This tabulation was used for the training of new staff. Three codes were prepared independently. The results of the three processes were compared and minor discrepancies due to different methods employed in the codes, were investigated and reconciled.

[1] The preparation of this table was done under the supervision of Ethel Marden by Kathryn Christoph, Anne Futterman, Renee Jasper, Sally Tsingou, and Bernard Urban, of the Bureau's Computation Laboratory.

x	$10^{10}h_{\frac{3}{2}}(x)$	$10^{10}\delta^2 h_{\frac{3}{2}}(x)$	x	$10^{10}h_{\frac{3}{2}}(x)$	$10^{10}\delta^2 h_{\frac{3}{2}}(x)$
0.00	0 00000 00000	2000054C	1.00	0 23645 34186	1373940C
.02	0 00009 99978	1999787C	.02	0 24545 14924	1350303C
.04	0 00039 99644	1998987C	.04	0 25458 45903	1326327C
.06	0 00089 98200	1997654C	.06	0 26385 03148	1302019C
.08	0 00159 94312	1995789C	.08	0 27324 62352	1277386C
.10	0 00249 86114	1993391C	.10	0 28276 98884	1252435C
.12	0 00359 71210	1990462C	.12	0 29241 87795	1227174C
.14	0 00489 46671	1987001C	.14	0 30219 03824	1201611C
.16	0 00639 09035	1983017C	.16	0 31208 31409	1175752C
.18	0 00808 54318	1978494C	.18	0 32209 14694	1149606C
.20	0 00997 77999	1973455C	.20	0 33221 57533	1123180C
.22	0 01206 75038	1967883C	.22	0 34245 23501	10964e8C
.24	0 01435 39863	1961790C	.24	0 35279 85903	1069520C
.26	0 01683 66362	1955176C	.26	0 36325 17775	1042302C
.28	0 01951 47982	1948041C	.28	0 37380 91909	1014836C
.30	0 02238 77528	1940389C	.30	0 38446 80832	987130C
.32	0 02545 47367	1932221C	.32	0 39522 56843	959193C
.34	0 02871 49333	1923540C	.34	0 40607 92006	931032C
.36	0 03216 74744	1914349C	.36	0 41702 58162	902656C
.38	0 03581 14411	1904649C	.38	0 42806 26935	874074C
.40	0 03964 58634	1894446C	.40	0 43918 69746	845292C
.42	0 04366 97211	1883740C	.42	0 45039 57e14	816322C
.44	0 04788 19437	1872537C	.44	0 46168 69171	787169C
.46	0 05228 14109	1860838C	.46	0 47305 53665	757844C
.48	0 05686 69552	1848648C	.48	0 48450 02973	728355C
.50	0 06163 73505	1835969C	.50	0 49601 30608	698711C
.52	0 06659 13361	1822806C	.52	0 50760 56927	668920C
.54	0 07172 75936	1809163C	.54	0 51926 02140	638990C
.56	0 07704 47556	1795044C	.56	0 53097 86370	608932C
.58	0 08254 14194	1780453C	.58	0 54275 79409	578753C
.60	0 08821 61170	1765395C	.60	0 55459 51230	548462C
.62	0 09406 73455	1749873C	.62	0 56648 71494	518069C
.64	0 10009 35529	1733894C	.64	0 57843 09810	487582C
.66	0 10629 31414	1717460C	.66	0 59042 35692	457009C
.68	0 11266 44676	1700578C	.68	0 60246 18570	426361C
.70	0 11920 58435	1683252C	.70	0 61454 27796	395646C
.72	0 12591 55364	1665487C	.72	0 62666 32658	364873C
.74	0 13279 17701	1647290C	.74	0 63882 02383	334050C
.76	0 13983 27250	1628664C	.76	0 65101 06151	303187C
.78	0 14703 65385	1609617C	.78	0 66323 13101	272293C
.80	0 15440 13060	1590153C	.80	0 67547 92340	241375
.82	0 16192 50813	1570278C	.82	0 68775 12954	210447
.84	0 16960 58769	1549998C	.84	0 70004 44014	179514
.86	0 17744 16651	1529320C	.86	0 71235 54583	148587
.88	0 18543 03780	1508249C	.88	0 72468 13750	117668C
.90	0 19356 99088	1486792C	.90	0 73701 90583	86775C
.92	0 20185 81118	1464955C	.92	0 74936 54197	55913C
.94	0 21029 28035	1442745C	.94	0 76171 73732	25091C
.96	0 21887 17629	1420168C	.96	0 77407 18368	56e1C-
.98	0 22759 27325	1397231C	.98	0 78642 57333	36385C-
1.00	0 23645 34186	1373940C	2.00	0 79877 59914	67042C-

x	$10^{10} h_{\frac{3}{2}}(x)$	$10^{10}\delta^2 h_{\frac{3}{2}}(x)$	x	$10^{10} h_{\frac{3}{2}}(x)$	$10^{10}\delta^2 h_{\frac{3}{2}}(x)$
2.00	0 79877 59914	67043C-	3.00	1 34814 05494	1335328C-
.02	0 81111 95467	97615C-	.02	1 35663 15764	1352308C-
.04	0 82345 33421	128102C-	.04	1 36498 72803	1368862C-
.06	0 83577 43239	158497C-	.06	1 37320 61560	1384985C-
.08	0 84807 94679	188789C-	.08	1 38128 65412	1400673C-
.10	0 86036 57300	218972C-	.10	1 38922 68672	1415924C-
.12	0 87263 00971	249035C-	.12	1 39702 56089	1430732C-
.14	0 88486 95631	278970C-	.14	1 40468 12856	1445095C-
.16	0 89708 11347	308769C-	.16	1 41219 24610	1459009C-
.18	0 90926 18319	338424C-	.18	1 41955 77439	1472471C-
.20	0 92140 86896	367926C-	.20	1 42677 57850	1485479C-
.22	0 93351 87577	397266C-	.22	1 43384 52927	1498029C-
.24	0 94558 91023	426437C-	.24	1 44076 50029	1510118C-
.26	0 95761 68065	455429C-	.26	1 44753 37098	1521745C-
.28	0 96959 89712	484236C-	.28	1 45415 02507	1532906C-
.30	0 98153 27153	512849C-	.30	1 46061 35097	1543599C-
.32	0 99341 51792	541259C-	.32	1 46692 24175	1553822C-
.34	1 00524 35206	569460C-	.34	1 47307 59518	1563574C-
.36	1 01701 49200	597442C-	.36	1 47907 31374	1572851C-
.38	1 02872 65793	625199C-	.38	1 48491 30466	1581654C-
.40	1 04037 57230	652722C-	.40	1 49059 47992	1589979C-
.42	1 05195 95989	680004C-	.42	1 49611 75628	1597826C-
.44	1 06347 54791	707037C-	.44	1 50148 05525	1605193C-
.46	1 07492 06602	733814C-	.46	1 50668 30318	1612080C-
.48	1 08629 24646	760327C-	.48	1 51172 43120	1618485C-
.50	1 09758 82417	786570C-	.50	1 51660 37525	1624408C-
.52	1 10880 53667	812534C-	.52	1 52132 07611	1629848C-
.54	1 11994 12435	838213C-	.54	1 52587 47939	1634804C-
.56	1 13099 33044	863600C-	.56	1 53026 53552	1639276C-
.58	1 14195 90108	888686C-	.58	1 53449 19978	1643264C-
.60	1 15283 58540	913469C-	.60	1 53855 43229	1646768C-
.62	1 16362 13561	937939C-	.62	1 54245 19400	1649789C-
.64	1 17431 30701	962086C-	.64	1 54618 46672	1652325C-
.66	1 18490 85614	985912C-	.66	1 54975 21308	1654378C-
.68	1 19540 55075	1009404C-	.68	1 55315 41654	1655949C-
.70	1 20580 14994	1032557C-	.70	1 55639 06140	1657037C-
.72	1 21609 42420	1055366C-	.72	1 55946 13678	1657644C-
.74	1 22628 14544	1077824C-	.74	1 56236 63659	1657772C-
.76	1 23636 08809	1099925C-	.76	1 56510 55958	1657420C-
.78	1 24633 03416	1121664C-	.78	1 56767 90924	1656590C-
.80	1 25618 76327	1143035C-	.80	1 57008 69387	1655284C-
.82	1 26593 06272	1164032C-	.82	1 57232 92653	1653504C-
.84	1 27555 72254	1184650C-	.84	1 57440 62503	1651251C-
.86	1 28506 53658	1204883C-	.86	1 57631 81188	1648526C-
.88	1 29445 30250	1224726C-	.88	1 57806 51432	1645333C-
.90	1 30371 82189	1244175C-	.90	1 57964 76430	1641673C-
.92	1 31285 90026	1263224C-	.92	1 58106 59840	1637548C-
.94	1 32187 34713	1281866C-	.94	1 58232 05786	1632962C-
.96	1 33075 97608	1300103C-	.96	1 58341 18856	1627915C-
.98	1 33951 60475	1317925C-	.98	1 58434 04094	1622413C-
3.00	1 34814 05494	1335328C-	4.00	1 58510 67003	1616456C-

x	$10^{10} h_{\frac{3}{2}}(x)$	$10^{10} \delta^2 h_{\frac{3}{2}}(x)$	x	$10^{10} h_{\frac{3}{2}}(x)$	$10^{10} \delta^2 h_{\frac{3}{2}}(x)$
4.00	1 58510 67003	1616456C-	5.00	1 44087 67350	838738C-
.02	1 58571 13539	1610048C-	.02	1 43503 58632	816160C-
.04	1 58615 50109	1603193C-	.04	1 42911 93783	793426C-
.06	1 58643 83569	1595893C-	.06	1 42312 05535	770543C-
.08	1 58656 21217	1588152C-	.08	1 41704 46771	747519C-
.10	1 58652 70793	1579973C-	.10	1 41089 40513	724362C-
.12	1 58633 40477	1571361C-	.12	1 40467 09916	701079C-
.14	1 58598 38879	1562318C-	.14	1 39837 78762	677678C-
.16	1 58547 75041	1552849C-	.16	1 39201 68950	654167C-
.18	1 58481 58432	1542959C-	.18	1 38559 05490	630554C-
.20	1 58399 98940	1532650C-	.20	1 37910 11493	606846C-
.22	1 58303 06875	1521927C-	.22	1 37255 10666	583051C-
.24	1 58190 92956	1510796C-	.24	1 36594 26801	559178C-
.26	1 58063 68320	1499259C-	.26	1 35927 83773	535232C-
.28	1 57921 44497	1487322C-	.28	1 35256 05523	511223C-
.30	1 57764 33424	1474990C-	.30	1 34579 16061	487159C-
.32	1 57592 47432	1462268C-	.32	1 33897 39448	463046C-
.34	1 57405 99242	1449160C-	.34	1 33210 99797	438894C-
.36	1 57205 01963	1435672C-	.36	1 32520 21258	414708C-
.38	1 56989 69081	1421809C-	.38	1 31825 28016	390495 -
.40	1 56760 14458	1407575C-	.40	1 31126 44278	366270 -
.42	1 56516 52327	1392978C-	.42	1 30423 94270	342035 -
.44	1 56259 97284	1378021C-	.44	1 29718 02227	317799 -
.46	1 55987 64285	1362711C-	.46	1 29006 90345	293569 -
.48	1 55702 68640	1347053C-	.48	1 28296 88974	269349C-
.50	1 55404 26004	1331054C-	.50	1 27582 16209	245153C-
.52	1 55092 52376	1314719C-	.52	1 26864 98286	220987C-
.54	1 54767 64089	1298054C-	.54	1 26145 59369	196857C-
.56	1 54429 77808	1281065C-	.56	1 25424 23587	172771C-
.58	1 54079 10520	1263759C-	.58	1 24701 15024	148738C-
.60	1 53715 79531	1246141C-	.60	1 23976 57713	124763C-
.62	1 53340 02456	1228219C-	.62	1 23250 75626	100856C-
.64	1 52951 97218	1209998C-	.64	1 22523 92670	77022C-
.66	1 52551 82036	1191484C-	.66	1 21796 32676	53271C-
.68	1 52139 75422	1172686C-	.68	1 21068 19396	29608C-
.70	1 51715 96174	1153609C-	.70	1 20339 76490	6041C-
.72	1 51280 63367	1134259C-	.72	1 19611 27524	17422C
.74	1 50833 96349	1114645C-	.74	1 18882 95960	40775C
.76	1 50376 14733	1094772C-	.76	1 18155 05150	64010C
.78	1 49907 38392	1074648C-	.78	1 17427 76326	87120C
.80	1 49427 87447	1054280C-	.80	1 16701 38599	110099C
.82	1 48937 82966	1033674C-	.82	1 15976 08945	132939C
.84	1 48437 43454	1012838C-	.84	1 15252 12204	155633C
.86	1 47926 91844	991779C-	.86	1 14529 71067	178175C
.88	1 47406 48495	970505C-	.88	1 13809 08077	200558C
.90	1 46876 34679	949022C-	.90	1 13090 45614	222776C
.92	1 46336 71879	927337C-	.92	1 12374 05896	244820C
.94	1 45787 81777	905460C-	.94	1 11660 10965	266687C
.96	1 45229 86250	883395C-	.96	1 10948 82686	288367C
.98	1 44663 07361	861152C-	.98	1 10240 42739	309856C
5.00	1 44087 67350	838738C-	6.00	1 09535 12613	331146C

x	$10^{10} h_{\frac{3}{2}}(x)$	$10^{10}\delta^2 h_{\frac{3}{2}}(x)$	x	$10^{10} h_{\frac{3}{2}}(x)$	$10^{10}\delta^2 h_{\frac{3}{2}}(x)$
6.00	1 09535 12613	331148C	7.00	0 82233 43492	1033118C
.02	1 08833 13598	352235C	.02	0 81909 33114	1038355C
.04	1 08134 66775	373111C	.04	0 81595 61022	1043213C
.06	1 07439 93026	393772C	.06	0 81292 32073	1047693C
.08	1 06749 13006	414210C	.08	0 80999 50747	1051794C
.10	1 06062 47158	434420C	.10	0 80717 21146	1055517C
.12	1 05380 15686	454397C	.12	0 80445 46992	1058862C
.14	1 04702 38566	474133C	.14	0 80184 31830	1061828C
.16	1 04029 35534	493625C	.16	0 79933 76027	1064417C
.18	1 03361 26082	512866C	.18	0 79693 88771	1066628C
.20	1 02698 29449	531852C	.20	0 79464 66075	1068464C
.22	1 02040 64619	550576C	.22	0 79246 11773	1069924C
.24	1 01388 50316	569033C	.24	0 79038 27327	1071009C
.26	1 00742 04997	587219C	.26	0 78841 13691	1071720C
.28	1 00101 46846	605129C	.28	0 78654 71966	1072059C
.30	0 99466 93772	622757C	.30	0 78479 02102	1072027C
.32	0 98838 63403	640099C	.32	0 78314 04198	1071625C
.34	0 98216 73080	657151C	.34	0 78159 77849	1070854C
.36	0 97601 39353	673907C	.36	0 78016 22288	1069717C
.38	0 96992 80478	690364C	.38	0 77883 38377	1068215C
.40	0 96391 11411	706516C	.40	0 77761 18613	1066350C
.42	0 95796 48804	722360C	.42	0 77649 67134	1064124C
.44	0 95209 03499	737892C	.44	0 77548 79712	1061539C
.46	0 94628 06027	753107C	.46	0 77458 53764	1058598C
.48	0 94056 56605	768003C	.48	0 77378 86349	1055309C
.50	0 93491 75125	782574C	.50	0 77309 74171	1051684C
.52	0 92934 76159	796818C	.52	0 77251 13563	1047765C
.54	0 92385 73951	810731C	.54	0 77203 00589	1043314C
.56	0 91844 82411	824309C	.56	0 77165 30546	1038627C
.58	0 91312 15118	837549C	.58	0 77137 99668	1033599C
.60	0 90787 85312	850449C	.60	0 77121 02026	1028233C
.62	0 90272 05891	863005C	.62	0 77114 32555	1022532C
.64	0 89764 89411	875214C	.64	0 77117 85556	1016500C
.66	0 89266 46061	887073C	.66	0 77131 54997	1010140C
.68	0 88776 93759	898580C	.68	0 77155 34516	1003455C
.70	0 88296 37952	909733C	.70	0 77189 17435	996449C
.72	0 87824 91812	920528C	.72	0 77232 96742	989125C
.74	0 87362 66134	930964C	.74	0 77286 65116	981487C
.76	0 86909 71352	941038C	.76	0 77350 14920	973539C
.78	0 86466 17542	950748C	.78	0 77423 38206	965285C
.80	0 86032 14413	960094C	.80	0 77506 26721	956729C
.82	0 85607 71310	969072C	.82	0 77598 71910	947874C
.84	0 85192 97210	977680C	.84	0 77700 64919	938726C
.86	0 84788 00723	985919C	.86	0 77811 96601	929288C
.88	0 84392 90087	993786C	.88	0 77932 57519	919565C
.90	0 84007 73168	1001280C	.90	0 78062 37951	909562C
.92	0 83632 57459	1008399C	.92	0 78201 27593	899282C
.94	0 83267 50082	1015144C	.94	0 78349 17068	888730C
.96	0 82912 57776	1021512C	.96	0 78505 94923	877912C
.98	0 82567 86916	1027504C	.98	0 78671 50642	866831C
7.00	0 82233 43492	1033118C	8.00	0 78845 73144	855493C

x	$10^{10} h_{\frac{3}{2}}(x)$	$10^{10} \delta^2 h_{\frac{3}{2}}(x)$	x	$10^{10} h_{\frac{3}{2}}(x)$	$10^{10} \delta^2 h_{\frac{3}{2}}(x)$
8.00	0 78845 73144	855493C	9.00	0 95560 65159	83205C
.02	0 79036 51092	843902C	.02	0 95985 71665	66289C
.04	0 79219 72897	832064C	.04	0 96411 44468	49420C
.06	0 79419 26722	819984C	.06	0 96837 66701	32605C
.08	0 79627 00456	807666C	.08	0 97264 21551	15849C
.10	0 79842 81873	795116C	.10	0 97690 92261	842C-
.12	0 80066 58336	782340C	.12	0 98117 62142	17462C-
.14	0 80298 17096	769342C	.14	0 98544 14575	34006C-
.16	0 80537 45159	756127C	.16	0 98970 33017	50467C-
.18	0 80784 29310	742702C	.18	0 99396 01009	66841C-
.20	0 81038 56126	729072C	.20	0 99821 02177	83121C-
.22	0 81300 11977	715242C	.22	1 00245 20242	99302C-
.24	0 81568 83035	701215C	.24	1 00668 39025	115379C-
.26	0 81844 55277	687006C	.26	1 01090 42448	131346C-
.28	0 82127 14491	672611C	.28	1 01511 14547	147198C-
.30	0 82416 46234	658039C	.30	1 01930 39470	162930C-
.32	0 82712 36084	643296C	.32	1 02348 01486	178536C-
.34	0 83014 69149	628387C	.34	1 02763 84990	194011C-
.36	0 83323 30572	613319C	.36	1 03177 74509	209350C-
.38	0 83638 05256	598097C	.38	1 03589 54703	224548C-
.40	0 83958 78069	582727C	.40	1 03999 10376	239600C-
.42	0 84285 33553	567216C	.42	1 04406 26477	254501C-
.44	0 84617 56228	551569C	.44	1 04810 88105	269247C-
.46	0 84955 30446	535792C	.46	1 05212 80516	283832C-
.48	0 85298 40437	519892C	.48	1 05611 89124	298252C-
.50	0 85646 70296	503873C	.50	1 06007 99513	312502C-
.52	0 86000 04008	487744C	.52	1 06400 97431	326577C-
.54	0 86358 25445	471509C	.54	1 06790 68805	340474C-
.56	0 86721 18372	455175C	.56	1 07176 99739	354187C-
.58	0 87088 66457	438747C	.58	1 07559 76521	367713C-
.60	0 87460 53274	422233C	.60	1 07933 85624	381047C-
.62	0 87836 62305	405638C	.62	1 08314 13716	394185C-
.64	0 88216 76967	388969C	.64	1 08685 47661	407123C-
.66	0 88600 80583	372231C	.66	1 09052 74519	419857C-
.68	0 88988 56417	355430C	.68	1 09415 81559	432383C-
.70	0 89379 87672	338574C	.70	1 09774 56256	444697C-
.72	0 89774 57492	321668C	.72	1 10128 86295	456795C-
.74	0 90172 48972	304719C	.74	1 10478 59579	468675C-
.76	0 90573 45163	287732C	.76	1 10823 64229	480332C-
.78	0 90977 29061	270713C	.78	1 11163 88589	491763C-
.80	0 91383 83708	253667	.80	1 11499 21228	502964C-
.82	0 91792 92001	236605	.82	1 11829 50947	513932C-
.84	0 92204 36899	219532	.84	1 12154 66777	524665C-
.86	0 92618 01329	202451	.86	1 12474 57986	535158C-
.88	0 93033 68210	185370	.88	1 12789 14082	545409C-
.90	0 93451 20461	168294	.90	1 13098 24814	555416C-
.92	0 93870 41007	151231	.92	1 13401 80176	565174C-
.94	0 94291 12783	134180C	.94	1 13699 70409	574683C-
.96	0 94713 18743	117157C	.96	1 13991 86006	583938C-
.98	0 95136 41866	100163C	.98	1 14278 17712	592938C-
9.00	0 95560 65159	83205C	10.00	1 14558 56528	601680C-

x	$10^{10} h_{\frac{3}{2}}(x)$	$10^{10}\delta^2 h_{\frac{3}{2}}(x)$	x	$10^{10} h_{\frac{3}{2}}(x)$	$10^{10}\delta^2 h_{\frac{3}{2}}(x)$
10.00	1 14556 56528	601680C-	11.00	1 19827 21745	687086C-
.02	1 14832 93711	610161C-	.02	1 19750 08839	681902C-
.04	1 15101 20782	618381C-	.04	1 19666 12873	676477C-
.06	1 15363 29521	626335C-	.06	1 19575 41074	670813C-
.08	1 15619 11973	634024C-	.08	1 19477 98507	664910C-
.10	1 15868 60452	641444C-	.10	1 19373 91073	658778C-
.12	1 16111 67536	648593C-	.12	1 19263 24905	652410C-
.14	1 16348 26077	655471C-	.14	1 19146 06369	645818C-
.16	1 16578 29196	662075C-	.16	1 19022 42057	639001C-
.18	1 16801 70793	668405C-	.18	1 18892 38764	631964C-
.20	1 17018 43034	674458C-	.20	1 18756 03583	624709C-
.22	1 17228 41369	680234C-	.22	1 18613 43722	617240C-
.24	1 17431 59520	685731C-	.24	1 18464 66655	609560C-
.26	1 17627 91992	690948C-	.26	1 18309 80067	601674C-
.28	1 17817 33568	695884C-	.28	1 18148 91841	593584C-
.30	1 17999 79312	700539C-	.30	1 17982 10068	585295C-
.32	1 18175 24568	704912C-	.32	1 17809 43037	576809C-
.34	1 18343 64964	709001C-	.34	1 17630 99232	568132C-
.36	1 18504 96411	712807C-	.36	1 17446 87330	559266C-
.38	1 18659 15103	716329C-	.38	1 17257 16196	550216C-
.40	1 18806 17518	719567C-	.40	1 17061 94879	540985C-
.42	1 18946 00418	722521C-	.42	1 16861 32610	531578C-
.44	1 19078 60849	725189C-	.44	1 16655 38795	521999C-
.46	1 19203 96144	727574C-	.46	1 16444 23011	512252C-
.48	1 19322 03917	729673C-	.48	1 16227 95005	502341C-
.50	1 19432 82069	731486C-	.50	1 16006 64688	492270C-
.52	1 19536 28786	733020C-	.52	1 15780 42129	482044C-
.54	1 19632 42534	734267C-	.54	1 15549 37553	471667C-
.56	1 19721 22068	735232C-	.56	1 15313 61337	461144C-
.58	1 19802 66421	735914C-	.58	1 15073 24004	450478C-
.60	1 19876 74913	736314C-	.60	1 14828 36218	439674C-
.62	1 19943 47142	736433C-	.62	1 14579 08787	428737C-
.64	1 20002 82990	736272C-	.64	1 14325 52633	417671C-
.66	1 20054 82617	735832C-	.66	1 14067 78336	406481C-
.68	1 20099 46464	735114C-	.68	1 13805 96579	395172C-
.70	1 20136 75248	734119C-	.70	1 13540 23171	383748C-
.72	1 20166 69964	732846C-	.72	1 13270 84036	372213C-
.74	1 20189 31881	731304C-	.74	1 12997 32707	360573C-
.76	1 20204 62546	729486C-	.76	1 12720 40884	348831C-
.78	1 20212 63774	727398C-	.78	1 12440 00127	336994C-
.80	1 20213 37653	725041C-	.80	1 12156 22454	325065C-
.82	1 20206 86541	722415C-	.82	1 11869 19730	313050C-
.84	1 20193 13062	719525C-	.84	1 11579 03972	300953C-
.86	1 20172 20107	716370C-	.86	1 11285 87274	288779C-
.88	1 20144 10830	712954C-	.88	1 10989 81512	276532C-
.90	1 20108 88648	709278C-	.90	1 10690 99529	264219C-
.92	1 20066 57235	705344C-	.92	1 10389 53639	251843C-
.94	1 20017 20525	701156C-	.94	1 10085 55617	239409C-
.96	1 19960 82705	696715C-	.96	1 09779 18196	226922C-
.98	1 19897 48216	692024C-	.98	1 09470 53861	214386C-
11.00	1 19827 21745	687086C-	12.00	1 09159 75147	201811C-

x	$10^{10} h_{\frac{3}{2}}(x)$	$10^{10}\delta^2 h_{\frac{3}{2}}(x)$	x	$10^{10} h_{\frac{3}{2}}(x)$	$10^{10}\delta^2 h_{\frac{3}{2}}(x)$
12.00	1 09159 75147	201811C-	13.00	0 93645 42218	378426C
.02	1 08846 94629	189195C-	.02	0 93387 66703	387180C
.04	1 08532 24922	176546C-	.04	0 93133 78336	395759C
.06	1 08215 75674	163869C-	.06	0 92883 85696	404162C
.08	1 07897 68560	151165 -	.08	0 92637 97185	412385C
.10	1 07578 07282	138447 -	.10	0 92396 21024	420425C
.12	1 07257 07557	125715 -	.12	0 92158 65256	428281C
.14	1 06934 82117	112974 -	.14	0 91925 37734	435949C
.16	1 06611 43702	100229 -	.16	0 91696 46126	443428C
.18	1 06287 05059	87485 -	.18	0 91471 97910	450714C
.20	1 05961 78930	74747 -	.20	0 91252 00373	457806C
.22	1 05635 78055	62018 -	.22	0 91036 60605	464701C
.24	1 05309 15162	49306 -	.24	0 90825 85503	471398C
.26	1 04982 02963	36608C-	.26	0 90619 81761	477894C
.28	1 04654 54151	23939C-	.28	0 90418 55877	484188C
.30	1 04326 81395	11299C-	.30	0 90222 14143	490277C
.32	1 03998 97334	1306C	.32	0 90030 62649	496161C
.34	1 03671 14572	13873C	.34	0 89844 07278	501836C
.36	1 03343 45674	26396C	.36	0 89662 53704	507302C
.38	1 03016 03164	38871C	.38	0 89486 07393	512557C
.40	1 02688 99515	51294C	.40	0 89314 73601	517600C
.42	1 02362 47150	63659C	.42	0 89148 57370	522430C
.44	1 02036 58432	75963C	.44	0 88987 63529	527044C
.46	1 01711 45665	88200C	.46	0 88831 96693	531442C
.48	1 01387 21084	100366C	.48	0 88681 61259	535623C
.50	1 01063 96856	112458C	.50	0 88536 61408	539586C
.52	1 00741 85072	124470C	.52	0 88397 01103	543330C
.54	1 00420 97742	136399C	.54	0 88262 84088	546854C
.56	1 00101 46794	148239C	.56	0 88134 13887	550158C
.58	0 99783 44069	159987C	.58	0 88010 93802	553240C
.60	0 99467 01313	171638C	.60	0 87893 26917	556100C
.62	0 99152 30176	183189C	.62	0 87781 16090	558738C
.64	0 98839 42210	194636C	.64	0 87674 63960	561153C
.66	0 98528 48860	205973C	.66	0 87573 72942	563345C
.68	0 98219 61461	217198C	.68	0 87478 45227	565313C
.70	0 97912 91240	228306C	.70	0 87388 82784	567058C
.72	0 97608 49302	239293C	.72	0 87304 87358	568580C
.74	0 97306 46634	250157C	.74	0 87226 60471	569878C
.76	0 97006 94100	260892C	.76	0 87154 03421	570953C
.78	0 96710 02433	271495C	.78	0 87087 17283	571804C
.80	0 96415 82235	281962C	.80	0 87026 02907	572433C
.82	0 96124 43975	292291C	.82	0 86970 60924	572839C
.84	0 95835 97975	302476C	.84	0 86920 91738	573022C
.86	0 95550 54431	312516C	.86	0 86876 95533	572985C
.88	0 95268 23373	322406C	.88	0 86838 72273	572726C
.90	0 94989 14692	332144C	.90	0 86806 21698	572247C
.92	0 94713 38127	341725C	.92	0 86779 43329	571545C
.94	0 94441 03257	351147C	.94	0 86758 36468	570631C
.96	0 94172 19504	360406C	.96	0 86743 00198	569496C
.98	0 93906 96126	369500C	.98	0 86733 33384	568144C
13.00	0 93645 42218	378426C	14.00	0 86729 34674	566576C

x	$10^{10} h_{\frac{3}{2}}(x)$	$10^{10}\delta^2 h_{\frac{3}{2}}(x)$
14.00	0 86729 34674	566576C
.02	0 86731 02501	564795C
.04	0 86738 35083	562799C
.06	0 86751 30426	560592C
.08	0 86769 86322	558175C
.10	0 86794 00356	555549C
.12	0 86823 69899	552715C
.14	0 86858 92119	549675C
.16	0 86899 63977	546431C
.18	0 86945 82229	542985C
.20	0 86997 43429	539339C
.22	0 87054 43932	535494C
.24	0 87116 79891	531452C
.26	0 87184 47267	527216C
.28	0 87257 41823	522787C
.30	0 87335 59132	518169C
.32	0 87418 94576	513363C
.34	0 87507 43347	508371C
.36	0 87601 00456	503196C
.38	0 87699 60727	497840C
.40	0 87803 18805	492306C
.42	0 87911 69157	486597C
.44	0 88025 06074	480714C
.46	0 88143 23674	474660C
.48	0 88266 15905	468442C
.50	0 88393 76548	462057C
.52	0 88525 99218	455511C
.54	0 88662 77371	448806C
.56	0 88804 04300	441945C
.58	0 88949 73147	434931C
.60	0 89099 76893	427768C
.62	0 89254 08390	420458C
.64	0 89412 60314	413005C
.66	0 89575 25217	405412C
.68	0 89741 95506	397681C
.70	0 89912 63452	389818C
.72	0 90087 21192	381824C
.74	0 90265 60732	373703C
.76	0 90447 73952	365459C
.78	0 90633 52609	357095C
.80	0 90822 88339	348615C
.82	0 91015 72663	340022C
.84	0 91211 96989	331320C
.86	0 91411 52615	322512C
.88	0 91614 30734	313602C
.90	0 91820 22438	304595C
.92	0 92029 18719	295493C
.94	0 92241 10476	286300C
.96	0 92455 88517	277020C
.98	0 92673 43562	267657C
15.00	0 92893 66250	258214C

WASHINGTON, October 21, 1952.

rnal of Research of the National Bureau of Standards Vol. 50, No. 1, January 1953 Research Paper 2384

Spectral Energy Distribution of the International Commission on Illumination Light Sources A, B, and C

Raymond Davis, Kasson S. Gibson, and Geraldine Walker Haupt

Standard light sources A, B, and C were adopted by the International Commission on Illumination (CIE) in 1931 for the colorimetry of materials. Source A is an incandescent lamp operated at 2,854° K. Sources B and C, representative of average noon sunlight and average daylight, respectively, are produced by passing radiant flux from source A through specified Davis-Gibson filters described in Bureau Miscellaneous Publication M114 (1931).

The CIE published relative energy data only from 370 to 720 mμ. The present paper gives data for these sources in the ultraviolet and extends the data in the red to 780 mμ. The new data were reported through the U. S. Secretariat Committee to the CIE at its 1951 meeting.

1. Introduction

In 1931 the International Commission on Illumination (Commission Internationale de l'Eclairage, CIE) recommended that three light sources, A, B, and C, be adopted for the general colorimetry of materials [1].[1] These were defined as: A, a gas-filled lamp at the color temperature of 2,848° K (c_2=14,350 micron degrees).[2] B, the same lamp used with a filter consisting of a layer, 1-cm thickness, of each of two solutions * * * contained in a double cell with colorless optical-glass plates. The compositions of the two solutions are specified in the resolution. C, the same lamp in combination with a second filter of the same type but with different composition, also specified in the recommendation.

Source A is intended to be typical of light from the gas-filled tungsten-filament incandescent lamp; source B is an approximate representation of noon sunlight; and source C is an approximate representation of average daylight (see fig. 1). The relative spectral-energy distributions for sources B and C are given in the CIE recommendations over the wavelength range from 370 to 720 mμ.

The two filters that, in combination with source A, comprise sources B and C are of the type designed by Davis and Gibson and described in detail in Bureau Miscellaneous Publication M114 [2]. They are two of a large number of such filters designed for the reproduction of the various phases of sunlight and daylight and the conversion of low to higher color temperatures. The particular filters used to obtain sources B and C are designated in [2] as 2,848° to 4,800° K and 2,848° to 6,500° K because they were designed to produce exactly the colors corresponding to 4,800° and 6,500° K, respectively, for the observer defined by the "Optical Society of America (OSA) excitations extrapolated". For the 1931 CIE standard observer [3, 4] and the modification of it tentatively proposed in 1951 [5], the colors produced are slightly too purple to match the colors of the black body at any temperature. The temperatures of the black body most similar to these colors (called correlated color temperatures) are as follows [6]:

Observer	Correlated color temperature				Departure from design color temperature	
	c_2=14,350		c_2=14,380			
	Source B	Source C	Source B	Source C	Source B	Source C
	°K	°K	°K	°K	μrd	μrd
OSA "Excitations."	4,800	6,500	4,810	6,514	0.0	0.0
1951 CIE tentative.	4,815	6,500	4,825	6,574	.7	1.4
1931 CIE standard.	4,860	6,726	4,870	6,740	2.6	5.4

From the indicated departures from the design color temperatures of 4,800° and 6,500° K, respectively, it will be noted that these designations are only approximate if the 1931 CIE standard observer is used to assess the colors. But if the tentative 1951 modified observer is used, the designations may be considered precise for ordinary observing conditions under which differences in reciprocal color

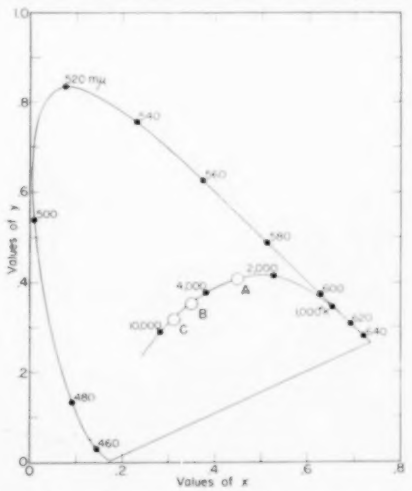

FIGURE 1. *Chromaticities of CIE light sources A, B, and C, together with spectrum locus and black-body locus, plotted on the 1931 CIE chromaticity diagram.*

Those unfamiliar with this chromaticity diagram will find it discussed in references [1, 3, 4, and 6].

[1] Figures in brackets indicate the literature references at the end of this paper.
[2] Equivalent to 2,854° K, with c_2=14,380 micron degrees.

temperature in the neighborhood of 1.0 μrd (micro-reciprocal-degree) are imperceptible.

Regardless of this, however, the spectral distributions of CIE light sources B and C define these sources in unambiguous terms, irrespective of observer or color temperature, and these distributions give approximately the colors of noon sunlight and average daylight.

It happened that charts illustrating these particular filters and the resulting spectral distributions were not given [2] among those chosen for illustration. The chart for the 2,848° to 4,800° K filter and source was later published [7] but that for the 2,848° to 6,500° K filter has not been published. Accordingly, as a matter of convenience, these are both reproduced in slightly revised form in the present paper, see figures 2 and 3. Hereafter the sources (and filters) will be designated as sources B and C (or filters B and C), as they were designated by the CIE in 1931.

Figures 1, 2, and 3 give considerable information about these filters and the resulting light sources. Many other details relating to the filters are given in the original publication [2].

In the (U. S.) Secretariat questionnaire and report prepared for the 1948 meetings of the CIE in Paris [8], the question of standard sources was raised anew, and the following question was asked:

"In view of the possible influence of ultraviolet irradiation on the colours of fluorescent samples, do you believe that the definition of standard illuminant A, B and C should be made more precise in regard to the ultraviolet?"

The authors of [2] offered to extend the data for sources B and C below 350 mμ if that seemed desirable.

Replies to the above question were received from several countries, and after discussion at the meetings the following recommendation was adopted [8]:

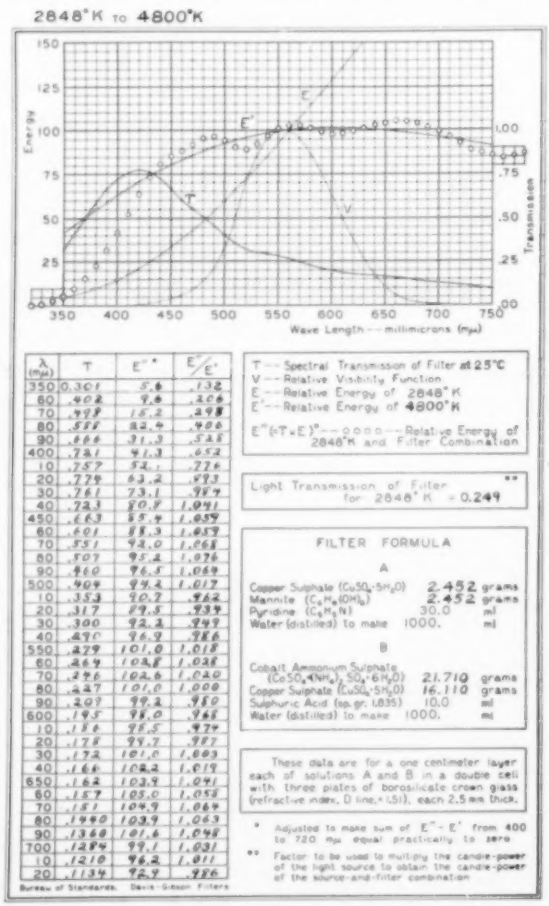

λ (mμ)	T	E''*	E/E'
350	0.301	5.6	.132
60	.402	9.6	.206
70	.478	15.2	.298
80	.551	22.9	.406
90	.606	31.3	.515
400	.781	41.3	.652
10	.757	52.	.776
20	.779	63.2	.873
30	.761	73.1	.957
40	.723	80.7	1.041
450	.663	85.9	1.059
60	.601	88.3	1.057
70	.551	92.0	1.068
80	.507	95.2	1.076
90	.460	96.5	1.069
500	.409	99.2	1.017
10	.353	90.7	.962
20	.317	89.5	.939
30	.300	92.2	.947
40	.290	96.9	.986
550	.279	101.0	1.018
60	.269	104.5	1.038
70	.256	106.6	1.060
80	.247	107.0	1.060
90	.209	99.2	.980
600	.195	98.0	.968
10	.186	98.5	.974
20	.178	99.7	.987
30	.172	101.0	1.003
40	.166	102.2	1.019
650	.162	103.9	1.041
60	.157	105.0	1.058
70	.151	104.9	1.069
80	.1490	103.9	1.063
90	.1360	101.6	1.048
700	.1284	99.1	1.031
10	.1210	96.2	1.011
20	.1139	92.9	.986

Bureau of Standards. Davis-Gibson Filters

T — Spectral Transmission of Filter at 25°C
V — Relative Visibility Function
E — Relative Energy of 2848° K
E' — Relative Energy of 4800° K
E''(=T×E)° — o o o o — Relative Energy of 2848° K and Filter Combination

Light Transmission of Filter for 2848° K = 0.249 **

FILTER FORMULA

A

Copper Sulphate ($CuSO_4 \cdot 5H_2O$)	2.452	grams
Mannite ($C_6H_8(OH)_6$)	2.452	grams
Pyridine (C_5H_5N)	30.0	ml
Water (distilled) to make	1000.	ml

B

Cobalt Ammonium Sulphate ($CoSO_4 \cdot (NH_4)_2SO_4 \cdot 6H_2O$)	21.710	grams
Copper Sulphate ($CuSO_4 \cdot 5H_2O$)	16.110	grams
Sulphuric Acid (sp.gr. 1.835)	10.0	ml
Water (distilled) to make	1000.	ml

These data are for a one centimeter layer each of solutions A and B in a double cell with three plates of borosilicate crown glass (refractive index, D line, = 1.51), each 2.5 mm thick.

* Adjusted to make sum of E'' - E' from 400 to 720 mμ equal practically to zero

** Factor to be used to multiply the candle-power of the light source to obtain the candle-power of the source-and-filter combination

FIGURE 2. *CIE light source B.*

Spectrophotometric data, and other information on this source and the filter used to obtain it. This chart is similar to the charts of reference [2] and [7]. Values below 350 and above 720 mμ are given in table 4.

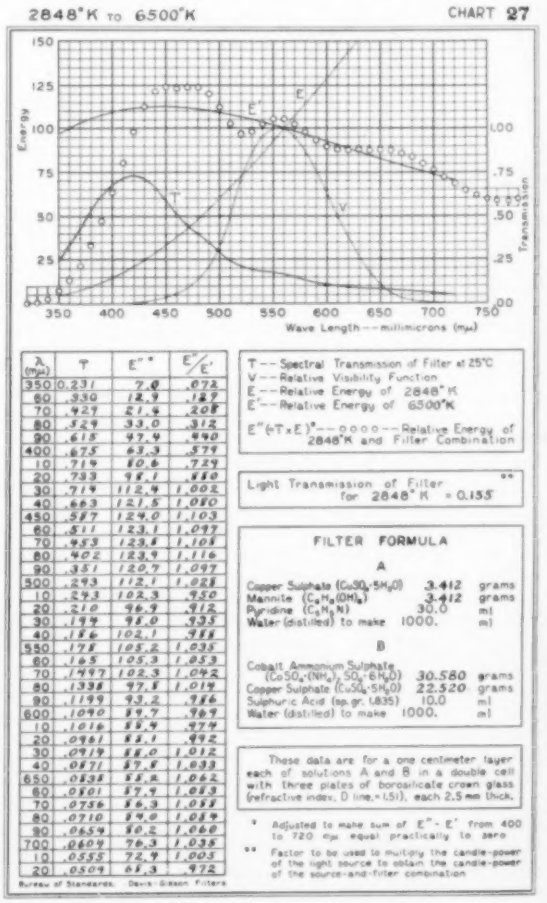

λ (mμ)	T	E''*	E/E'
350	0.231	7.0	.072
60	.330	12.9	.128
70	.427	21.4	.208
80	.529	33.0	.312
90	.615	47.4	.440
400	.675	62.3	.579
10	.719	80.6	.729
20	.733	98.1	.880
30	.719	112.9	1.002
40	.663	121.5	1.050
450	.587	124.0	1.103
60	.511	123.1	1.097
70	.453	123.8	1.105
80	.402	123.9	1.116
90	.351	120.7	1.097
500	.293	112.1	1.028
10	.243	102.3	.950
20	.210	96.9	.912
30	.199	98.0	.935
40	.186	102.1	.988
550	.178	105.2	1.035
60	.165	105.3	1.053
70	.1497	102.3	1.042
80	.1338	97.5	1.019
90	.1199	93.2	.986
600	.1090	89.7	.969
10	.1016	88.9	.974
20	.0961	89.1	.992
30	.0919	88.0	1.012
40	.0871	87.6	1.033
650	.0838	88.2	1.062
60	.0801	87.9	1.083
70	.0756	86.3	1.088
80	.0710	84.0	1.089
90	.0654	80.5	1.060
700	.0609	76.9	1.038
10	.0555	72.9	1.005
20	.0509	68.3	.972

Bureau of Standards. Davis-Gibson Filters

T — Spectral Transmission of Filter at 25°C
V — Relative Visibility Function
E — Relative Energy of 2848° K
E' — Relative Energy of 6500° K
E''(=T×E)° — o o o o — Relative Energy of 2848° K and Filter Combination

Light Transmission of Filter for 2848° K = 0.155 **

FILTER FORMULA

A

Copper Sulphate ($CuSO_4 \cdot 5H_2O$)	3.412	grams
Mannite ($C_6H_8(OH)_6$)	3.412	grams
Pyridine (C_5H_5N)	30.0	ml
Water (distilled) to make	1000.	ml

B

Cobalt Ammonium Sulphate ($CoSO_4 \cdot (NH_4)_2SO_4 \cdot 6H_2O$)	30.580	grams
Copper Sulphate ($CuSO_4 \cdot 5H_2O$)	22.520	grams
Sulphuric Acid (sp.gr. 1.835)	10.0	ml
Water (distilled) to make	1000.	ml

These data are for a one centimeter layer each of solutions A and B in a double cell with three plates of borosilicate crown glass (refractive index, D line, = 1.51), each 2.5 mm thick.

* Adjusted to make sum of E'' - E' from 400 to 720 mμ equal practically to zero

** Factor to be used to multiply the candle-power of the light source to obtain the candle-power of the source-and-filter combination

FIGURE 3. *CIE light source C.*

Spectrophotometric data and other information on this source and the filter used to obtain it. This chart is similar to those of reference [2]. Values below 370 and above 720 mμ are given in table 4.

"*Ultraviolet Content of Standard Illuminants.*—(a) It is recommended that the offer made through the United States Committee by Messrs. Davis and Gibson to determine the relative energy distributions for illuminants B and C below 370 mμ, including the spectral transmission factor of the cells, be accepted."

It was also recommended that the National Committees study the question of a standard source having relatively more ultraviolet energy than sources A, B, and C for the colorimetry of fluorescent materials.

In compliance with the first recommendation, the spectral transmittances of the B and C filters have been redetermined and extended in the ultraviolet, and these transmittances and the resulting spectral energy distributions were reported to the 1951 meetings of the Commission in Stockholm through the (U. S.) Secretariat Committee [9].

The present paper describes the measurements on which these new data are based, and gives the resulting values over the spectral range from 320 to 400 mμ. In addition, there are given some published and unpublished data for the long-wave end of the visible spectrum. In the charts of reference [2], as illustrated in figures 2 and 3 of the present paper, the data covered the visible range only to 720 mμ, this being the long-wave limit of the OSA excitations used in that work. However, the spectrophotometric data on the component filter parts had been determined to 750 mμ [2], so that extension of the transmission and energy data could readily be made.

When the CIE distributions defining the new standard observer were adopted, they were extended as far as 780 mμ [1]. At the request of Smith and Guild [3] values of relative energy for sources B and C were extended to 780 mμ. These values were published in table V, p. 102, of their paper. They were also published by Judd [4]. As the data entering into this extension of values have never been published, they are given in the present paper.

2. Spectrophotometric Measurements and Computations

The spectral transmittances of the filters (designated as spectral transmissions in [2]), given in figures 2 and 3 in the columns headed T were derived by computation from spectrophotometric measurements made on certain standard solutions, as explained in [2], including a study of Beer's law for the respective components over the range of concentrations of interest. This previous spectrophotometric work on the standard solutions was very extensive. It involved, for each standard component of the filter, measurements with several different solutions, at cell thicknesses from 1 to 10 cm and with three or four spectrophotometers. A detailed discussion of these measurements is given in [2]. All data were obtained at 25° C. Check measurements were also made on the complete filters.

No such elaborate series of measurements was considered necessary for the present purpose, which was primarily to extend the values of spectral transmittance and energy below 350 mμ, as far as there was significant transmittance. Because the filter cell contains three borosilicate glass plates of total thickness of about 7 mm, this transmittance could not in any case extend much below 300 mμ.

Two sets of solutions were prepared, one in February 1950 and one in January 1951. Spectrophotometric measurements were made on each set of solutions within 1 to 4 weeks from the date of preparation. In each case two methods of determining the filter transmittance were used: (1) The spectral transmittancies of the four standard filter components were measured and the transmittances of the B and C filters computed for the appropriate concentrations, as was done for all the filters of [2]. (2) direct measurements of spectral transmittance were made on B and C filters prepared in accordance with the specifications.

The Beckman quartz (DU) spectrophotometer was used for all the present measurements, with temperatures of filters and components kept at 25° C. The 1950 and 1951 measurements were equivalent in every respect, the repetition being made to obtain greater certainty in the results. The 1950–51 data presented are averages of the results obtained.

2.1. Standard Filter Components

These components are the A′, B'_1, and B'_2 solutions, and the double cell filled with distilled water. They are as follows [2]:

SOLUTION A′

Unfiltered, thickness 10.00 mm, temperature 25° C, having the composition:

Copper sulfate [3] ($CuSO_4 \cdot 5H_2O$)	g	3.000
Mannite ($C_6H_8(OH)_6$)	g	3.000
Pyridine [4] (C_5H_5N)	ml	30.0
Water (distilled) to make	ml	1,000

SOLUTION B'_1

Unfiltered, thickness 10.00 mm, temperature 25° C, having the composition:

Copper sulfate ($CuSO_4 \cdot 5H_2O$)	g	20.000
Sulfuric acid (specific gravity 1.835)	ml	10.0
Water (distilled) to make	ml	1,000

SOLUTION B'_2

Unfiltered, thickness 10.00 mm, temperature 25° C, having the composition: [5]

Cobalt ammonium sulfate [6] ($CoSO_4 \cdot (NH_4)_2SO_4 \cdot 6H_2O$)	g	14.481
Sulfuric acid (specific gravity 1.835)	ml	10.0
Water (distilled) to make	ml	1,000

[3] Chemical analysis showed the copper sulfate to have 99.7 percent of the theoretical copper content.

[4] Titration showed the pyridine to have an effective strength of 98.4 percent, including 2½ percent of picoline as an impurity.

[5] These data apply also throughout the visible spectrum to a similar solution made up with 10.3 g of cobalt sulfate ($CoSO_4 \cdot 7H_2O$).

[6] Chemical analysis showed a cobalt (plus nickel) content of 100.0 percent of the theoretical, the ratio of nickel to cobalt (metals) being 1 to 200.

Glass-Water Double Cell

Three glass plates, each approximately 2.4 mm thick (borosilicate crown, refractive index, D line, = approximately 1.52); two 1.000-cm thicknesses of distilled water; two air-glass surfaces; four glass-water surfaces.

The spectral transmittancies of the A′, B_1', and B_2' solutions (relative to distilled water) were measured in 1.000-cm cells with quartz end plates over the range from 300 to 400 mμ and at 404.7 and 435.8 mμ.[7] The transmittance of the glass-water double cell was measured at the same wavelengths.[8]

Solution	Wavelength	Transmittancy	
		Observed	Reference [2]
	mμ		
A′	587.6	0.208	0.207
B_1'	667.8	.483	.480
B_2'	501.6	.679	.682

The purpose of the determinations at 435.8 and 404.7 mμ was to give correlation with the standard values in [2]. As is shown in that publication, the most extensive and reliable spectrophotometric determinations were made at eight Hg and He wavelengths, including these two. Below 404.7 mμ the standard values were subject to increasing uncertainty.

[7] In addition, a measurement at a region of relatively high absorption in the visible was made with each solution as a check on the concentration. The following values were obtained and were considered to be satisfactory checks, the deviation in each being less than 1 percent of the value:

[8] As a matter of interest, the spectral transmittancies of the three standard solutions were also examined in 1-cm thicknesses between 210 and 300 mμ. No measureable transmittancy was detected for the A′ solution below 320 mμ. The transmittancy of the B_1' solution decreases rapidly below 300 mμ, approaching zero at 270 mμ and having no measureable value below this wavelength. The B_2' solution transmits freely between 210 and 300 mμ.

It was believed that the best correlation between the present measurements and the previous determinations would be obtained if the present values of transmittancy and transmittance were adjusted slightly, if necessary, to bring them into agreement with the previous standard values at these two wavelengths, 435.8 and 404.7 mμ; the resulting degree of agreement from 400 to 350 mμ could then be studied and new standard values for the four components from 300 to 400 mμ thereupon adopted. These adjustment factors, the averages of $T_{[2]}/T_{1950\text{-}51}$ for the two Hg wavelengths, were as follows:

Component	Ratio: $T_{[2]}/T_{1950\text{-}51}$		Adjustment factor
	404.7 mμ	435.8 mμ	
A′	1.0130	1.0095	1.011
B_1'	1.0030	1.0040	1.004
B_2'	1.0073	1.0067	1.007
W	0.9966	1.0011	0.999

In table 1 are given these adjusted values of transmittancy or transmittance for the various components, together with the values previously published in [2] and the newly adopted values. The following comments may be made regarding these values:

1. In deriving the adopted values, weights of 10, 8, 6, 4, 2, and 0 were given to the former values at 400, 390, 380, 370, 360, and 350 mμ, respectively. Corresponding weights of 0, 2, 4, 6, 8, and 10 were given to the 1950–51 adjusted values at these same wavelengths. From 340 to 300 mμ the 1950–51 adjusted values were used.

2. Solutions B_1' and B_2' show very close agreement between the former values and the 1950–51 adjusted values. Although there are no certain differences

TABLE I. *Revision and extension of standard data for Davis-Gibson filter components*

Solutions A′, B_1', and B_2', and double glass cell filled with distilled water, W

Wavelength	Transmittancy, 10.00 mm, at 25° C									Transmittance at 25° C of glass-water cell, W		
	Solution A′			Solution B_1'			Solution B_2'					
	Reference [2]	1950–51 average, adjusted (f=1.011)	Adopted values	Reference [2]	1950–51 average, adjusted (f=1.004)	Adopted values	Reference [2]	1950–51 average, adjusted (f=1.007)	Adopted values	Reference [2]	1950–51 average, adjusted (f=0.999)	Adopted values
mμ												
300	.....	0.000	0.000	.....	0.548	0.548	.....	0.986	0.986	.....	0.010	0.010
310	.....	.000	.000	.....	.788	.788	.....	.988	.988	.....	.102	.102
320	.....	.006	.006	.....	.899	.899	.....	.989	.989	.....	.314	.314
330	.....	.069	.069	.....	.945	.945	.....	.991	.991	.....	.536	.536
340	.....	.214	.214	.....	.968	.968	.....	.992	.992	.....	.702	.702
350	0.339	.334	.334	0.979	.980	.980	0.991	.992	.992	0.817	.798	.798
360	.437	.426	.428	.986	.986	.986	.991	.992	.992	.851	.848	.849
370	.541	.528	.533	.989	.991	.990	.989	.990	.990	.873	.870	.871
380	.646	.636	.642	.992	.994	.993	.985	.986	.985	.885	.869	.879
390	.746	.737	.744	.994	.994	.994	.980	.978	.980	.889	.886	.888
400	.825	.821	.825	.995	.995	.995	.972	.969	.972	.891	.893	.891
404.7	.855	.854	.855	.995	.996	.995	.967	.967	.967	.892	.894	.892
435.8	.959	.960	.959	.997	.996	.997	.904	.904	.904	.895	.893	.895
750	.446	.....	.446	.132	.....	.132	.904	.....	.904	.861	.....	.861
760	[a] .471	.....	.471	[a] .130	.....	.130	[a] .904	.....	.904	[b] .862	.....	.862
770	[a] .497	.....	.497	[a] .129	.....	.129	[a] .904	.....	.904	[b] .864	.....	.864
780	[a] .522	.....	.522	[a] .122	.....	.122	[a] .904	.....	.904	[b] .866	.....	.866

[a] Extrapolated, unpublished.
[b] Unpublished experimental data obtained at same time as data of [2].

tween the two sets of data, the same system of ghting was used in adopting the final values.

3. Below 400 mμ there were slight but consistent ferences between the 1950 and 1951 data for the solutions. However, neither set of data differed n the average (either before or after adjustment) more than 0.01 at any wavelength. Further work s considered unwarranted.

4. With the double glass cell filled with water a ght absorption band centering at 380 mμ was noted the present determinations. This is caused by the ass plates and was not detected in the previous easurements. This is considered further in the next section.

5. The values at 750 mμ are as published in [2]. The values from 760 to 780 mμ for the three solutions were obtained by extrapolating the final $-\log_{10}T$ versus λ curves, on which the data of [2] are based. The uncertainty of this extrapolation increases of course as the wavelength interval from 750 mμ increases. At 760 and 770 mμ this uncertainty is considered very small, and the reliability of the values at these two wavelengths is considered wholly adequate for the purpose. For the glass-water cell, the values are as measured in 1926 and show clearly the water absorption band near 750 mμ.

2.2. Glass-Water Double Cell

A precise duplication of the spectral energy distributions given herein for sources B and C depends, among other things, on the adequate duplication of the spectral transmittance of the two-compartment glass cell when filled with distilled water. Borosilicate crown glass varies slightly in its index of refraction and in its spectral transmittance, particularly in the ultraviolet.

The *D*-line index of the glass used in 1926 to obtain the published data [2] was about 1.51. A new supply of borosilicate crown glass was obtained in 1929 with an index of about 1.52. This was used in the present measurements, the original pieces no longer being available. The agreement in spectral transmittance from 350 to 435.8 mμ, table 1, indicates that no important difference in the visible spectrum is to be expected. This has also been confirmed many times during the years by spectrophotometric measurements throughout the visible on various of the Davis-Gibson filters.

The slight absorption band centering at 380 mμ (table 1) was not detected in the 1926 measurements, those data having been derived from measurements made only at the mercury wavelengths below 400 mμ. With the Beckman spectrophotometer this band can be readily measured. It is present in all of the few samples of borosilicate crown recently measured, but in varying degree. It is probably caused by iron impurities since a greenish slide rule glass showed the band very strikingly.

This slight absorption has been ignored because (1) it varies from one glass to another, so that an extensive study would be necessary to determine what would be the most probable or representative value. It is, of course, also possible that some borosilicate crown glass would not show this slight absorption band, (2) needless confusion would be caused by the resulting trivial and unimportant changes in the energy distributions of the B and C sources.

Below 360 mμ there is some scatter among the spectral transmittances of different borosilicate crown glasses. This is also of little importance, however, because of the much greater absorption of the copper-pyridine (A′) solution, as shown in table 1.

In accordance with the CIE request there are given in table 2 the complete spectral transmittance data for the double glass cell filled with water entering into the derivation of the energy distributions of the B and C sources over the range from 300 to 780 mμ.[9]

TABLE 2. *Spectral transmittance of glass-water double cell*

Three glass plates, each 2.4[a] mm thick (borosilicate crown, refractive index, *D* line = 1.52)[a], two 1.000-cm thicknesses of distilled water; two air-glass surfaces, four glass-water surfaces.

Wavelength	Transmittance	Wavelength	Transmittance
mμ		mμ	
290	0.000	550	0.904
300	.010	60	.904
10	.102	70	.904
20	.314	80	.904
30	.536	90	.903
40	.702	600	.902
350	.798	10	.902
60	.849	20	.902
70	.871	30	.901
80	.885	40	.900
90	.889	650	.900
400	.891	60	.900
10	.892	70	.900
20	.893	80	.900
30	.894	90	.898
40	.895	700	.897
450	.896	10	.893
60	.897	20	.883
70	.898	30	.871
80	.900	40	.863
90	.901	750	.861
500	.902	60	.862
10	.903	70	.864
20	.904	80	.866
30	.904		
40	.904		

[a] From 380 to 780 mμ the values were obtained with 2.5-mm plates with index 1.51 [2], but within the uncertainties of the data and the variability of borosilicate crown glass the data are valid for the conditions specified.

By measuring the spectral transmittance of his own glass-water cell, any user of these filters can tell if there are any important deviations of his cell from those of the authors.

2.3. B and C Filters

a. Computed Values

Based on the newly adopted standard components data of table 1, and by the same methods as previously used in the computation of such filters [2], the spectral transmittances of the B and C filters were computed and are shown in table 3.

b. Observed Values

In both 1950 and 1951, as already noted, spectrophotometric measurements were made directly on B

[9] At 380 and 390 mμ these values agree with the "Reference [2] values" rather than with the "adopted values" of table 1. The adopted values of table 1 were used in deriving the computed values of table 3, as indicated. However, since the energy distributions of the B and C sources and the spectral transmittances of the B and C filters were kept unchanged at 380 and 390 mμ for reasons given in section 2.3. c, the appropriate values for table 2 should be as given therein.

TABLE 3. *Revision and extension of standard data for filters and light sources B and C*

Wavelength	Spectral transmittance of filter B				Relative energy distribution of source B		Spectral transmittance of filter C				Relative energy distribution of source C	
	Former values	1950–51 data		New values	Former values	New values	Former values	1950–51 data		New values	Former values	New values
		Computed from adopted values of table 1	Observed values (no adjustment)					Computed from adopted values of table 1	Observed values (no adjustment)			
mμ												
300	.....	0.000	0.000	0.000	.....	.....	.....	0.000	0.000	0.000	.....	.....
310	.....	.000	.001	.000	.....	.....	.....	.000	.000	.000	.....	.....
320	.....	.003	.004	.003	.....	0.0[1]	.....	.001	.001	.001	.....	0.0[1]
330	.....	.049	.047	.048	.....	.5	.....	.027	.022	.025	.....	.4
340	.....	.176	.173	.175	.....	2.4	.....	.126	.114	.120	.....	2.7
350	0.309	.298	.304	.301	5.7	5.6	0.243	.234	.228	.231	7.4	7.0
360	.403	.396	.407	.402	9.7	9.6	.335	.328	.331	.330	13.2	12.9
370	.498	.492	.504	.498	15.2	15.2	.433	.427	.431	.429	21.6	21.4
380	.588	.585	.585	.588	22.4	22.4	.529	.525	.520	.529	33.0	33.0
390	.666	.664	.666	.666	31.3	31.3	.615	.613	.612	.615	47.4	47.4
400	.721	.722	.725	.721	41.3	41.3	.675	.676	.680	.675	63.3	63.3
720	.1134	.....	.....	.1134	92.9	92.9	.0509	.....	.....	.0509	68.3	68.3
730	*.1063	.....	.....	.1063		89.4	*.0457	.....	.....	.0457		64.4
740	*.1007	.....	.....	.1007		86.9	*.0435	.....	.....	.0435		61.5
750	*.0964	.....	.....	.0964		85.2	*.0409	.....	.....	.0409		59.2
760	*.0938	.....	.....	.0938		84.7	*.0392	.....	.....	.0392		58.1
770	*.0926	.....	.....	.0926		85.4	*.0385	.....	.....	.0385		58.2
780	*.0925	.....	.....	.0925		87.0	*.0384	.....	.....	.0384		59.1

* From 730 to 750 mμ these values are derived from the published data of [2].
From 760 to 780 mμ the values are derived from the data of table 1

and C filters prepared according to the specifications. These consisted of two-compartment glass cells (index 1.52) filled with the appropriate solutions prepared in the respective years. The filters were kept at 25° C during the measurements. The average values so obtained are given in table 3. These are as directly observed, without any adjustment. (No values are given at 404.7 and 435.8 mμ, because data at these wavelengths were not published in [2 and 7] for the filters themselves.)

c. New Values

In table 3, in addition to the computed and observed values of spectral transmittance, are given the new transmittance values for filters B and C, together with the values previously derived by the methods and data of [2]. With respect to the new values it may be noted that:

1. The former values are retained without change from 380 to 400 mμ. This is highly desirable, as already implied, because these values from 380 to 400 mμ were incorporated in the energy distributions of sources B and C in 1931, and have been used in thousands of colorimetric computations since that date.[10] If the 1950–51 values differed certainly and importantly from the former values from 380 to 400 mμ, serious consideration would have to be given to changing the standard values. However, inspection of the data of table 3 at these wavelengths shows that in only one case out of 12 (observed value at 380 mμ for the C filter) does a computed or observed 1950–51 value differ from the former value by as much as 1 percent of the value.

[10] Although the CIE adopted values of energy distribution also at 370 mμ, the standard observer was defined by data ending at 380 mμ. The energy values at 370 mμ, so far as known, have never been used in colorimetric computations. The authors, therefore, felt free to revise both the values of transmittance and the resulting energy at 370 mμ.

2. At 350 mμ the slight absorption found in the 1950–51 borosilicate crown glass plates is reflected in the relatively low values for both the computed and observed data for both the B and the C filters. However, even if it were not desirable to retain the values at 380 mμ, for the reason just stated, one would hesitate to make any change on the basis of the present data alone, without a thorough study of borosilicate crown glass plates.

3. From 320 to 370 mμ the new values are taken as the average of the observed and computed values. While one might believe that the observed values should be given more weight than the computed values, the experimental conditions render the measurements somewhat more difficult and uncertain in the former case. Furthermore, at the very low values of transmittance the computed values are considered more reliable than the directly observed values.

4. The values of transmittance at 720 mμ are as given in figures 2 and 3. The values of transmittance from 730 to 780 mμ are derived from the data of table 1 or the published data of [2] by the same computational procedures used to derive the corresponding values of figures 2 and 3 at the other wavelengths.

2.4. Light Sources B and C

The values of relative spectral energy distribution for sources B and C are derived by multiplying, wavelength by wavelength, the relative-energy values of source A by the respective spectral transmittances of filters B and C, and reducing in each case by a factor to the same scale as used in [2].

In table 3 are given the values of relative energy for sources B and C, first the former values, which are consistent with the data of [2], and then as revised on

TABLE 4. *Relative spectral-energy distributions E of CIE light sources A, B, and C, and spectral transmittances T of CIE filters B and C*

Wavelength	E_A	E_B	E_C	T_B	T_C
mμ					
320	1.92[a]	0.0$_2$	0.0$_2$	0.003	0.001
30	2.66	.5	.4	.048	.025
40	3.58	2.4	2.7	.175	.120
350	4.74	5.6	7.0	.301	.231
60	6.14	9.6	12.9	.402	.330
70	7.82	15.2	21.4	.498	.429
80	9.79	22.4	33.0	.588	.529
90	12.09	31.3	47.4	.666	.615
400	14.71	41.3	63.3	.721	.675
10	17.68	52.1	80.6	.757	.714
20	21.00	63.2	98.1	.774	.733
30	24.67	73.1	112.4	.761	.714
40	28.70	80.8	121.5	.723	.663
450	33.09	85.4	124.0	.663	.587
60	37.82	88.3	123.1	.601	.511
70	42.87	92.0	123.8	.551	.453
80	48.25	95.2	123.9	.507	.402
90	53.91	96.5	120.7	.460	.351
500	59.86	94.2	112.1	.404	.293
10	66.06	90.7	102.3	.353	.243
20	72.50	89.5	96.9	.317	.210
30	79.13	92.2	98.0	.300	.194
40	85.95	96.9	102.1	.290	.186
550	92.91	101.0	105.2	.279	.178
60	100.00	102.8	105.3	.264	.165
70	107.18	102.6	102.3	.246	.1497
80	114.44	101.0	97.8	.227	.1338
90	121.73	99.2	93.2	.209	.1199
600	129.04	98.0	89.7	.195	.1080
10	136.34	98.5	88.4	.186	.1016
20	143.62	99.7	88.1	.178	.0961
30	150.83	101.0	88.0	.172	.0914
40	157.98	102.2	87.8	.166	.0871
650	165.03	103.9	88.2	.162	.0838
60	171.96	105.0	87.9	.157	.0801
70	178.77	104.9	86.3	.151	.0756
80	185.43	103.9	84.0	.1440	.0710
90	191.93	101.6	80.2	.1360	.0654
700	198.26	99.1	76.3	.1284	.0604
10	204.41	96.2	72.4	.1210	.0555
20	210.36	92.9	68.3	.1134	.0509
30	216.12	89.4	64.4	.1063	.0467
40	221.66	86.9	61.5	.1007	.0435
750	227.00	85.2	59.2	.0964	.0409
60	232.11	84.7	58.1	.0938	.0392
70	237.01	85.4	58.2	.0926	.0385
80	241.67	87.0	59.1	.0925	.0384

[a] E_A=0.93 at 300 mμ and 1.36 at 310 mμ.

the basis of the new spectral transmittances. The following points may be noted: (1) The values from 380 to 400 mμ are kept unchanged. This follows from the fact that the new spectral transmittances are kept unchanged at these wavelengths, for the reason already stated. (2) From 350 to 370 mμ the new values do not differ importantly from the former values. For source B they are not considered certainly different except at 350 mμ. For source C the new values are considered certainly different from the old values at both 350 and 360 mμ. (3) Effective termination of the energy distribution at 320 mμ results primarily from the absorption of the copper-pyridine component, with the increasing absorption of the glasses and the decreasing energy of source A contributing secondarily.

3. Final Data

As a matter of convenient reference there are given in table 4 over the spectral range from 320 to 780 mμ the relative spectral-energy distributions of CIE sources A, B, and C and the spectral transmittances of filters B and C.

For source A, the values from 380 to 780 mμ are identical with those published by Smith and Guild [3] and by Judd [4]. From 320 to 370 mμ the values have been derived by the authors from previous publications [10, 11], with allowance for differences in c_2 of Planck's equation.

For sources B and C the values from 380 to 720 mμ are identical with the published CIE values [11] [1], and with values published by Smith and Guild [3] and by Judd [4]. From 320 to 370 mμ the values are taken from table 3 of the present paper. From 730 to 780 mμ, the values are as published by Smith and Guild and by Judd.

For filters B and C the values from 380 to 720 mμ are unchanged from previous data. From 320 to 370 and from 730 to 780 mμ, the values are taken from table 3 of the present paper.

4. References

[1] CIE Compt. rend. p. 19–29 (1931).

[2] Raymond Davis and K. S. Gibson, Filters for the reproduction of sunlight and daylight and the determination of color temperature, NBS Misc. Pub. No. 114 (1931).

[3] T. Smith and J. Guild, The C. I. E. colorimetric standards and their use, Trans. Opt. Soc. (London) **33,** 73 (1931–32).

[4] Deane B. Judd, The 1931 I. C. I. standard observer and coordinate system for colorimetry, J. Opt. Soc. Am. **23,** 359 (1933).

[5] CIE, Compt. rend. **1,** Tech. Rept. 7, p. 11 (1951).

[6] Deane B. Judd, Color in business, science, and industry p. 96 (John Wiley & Sons, Inc., New York, N. Y., 1952).

[7] Raymond Davis and K. S. Gibson, The relative spectral energy distribution and correlated color temperature of the N. P. L. white-light standard, BS J. Research **7,** 791 (1931) RP374.

[8] CIE, Compt. rend. p. 16, 238 (1948).

[9] CIE, Compt. rend **3,** 116 (1951).

[10] R. Stair and W. O. Smith, A tungsten-in-quartz lamp and its applications in photoelectric radiometry, J. Research NBS **30,** 449 (1943) RP1543.

[11] J. F. Skogland, Tables of spectral energy distribution and luminosity for use in computing light transmissions and relative brightnesses from spectrophotometric data, NBS Misc. Pub. 86 (1929).

[11] Except for the erroneous published value at 380mμ for source C.

WASHINGTON, August 28, 1952.

nal of Research of the National Bureau of Standards Vol. 50, No. 1, January 1953 Research Paper 2385

The Constants in the Equation for Atmospheric Refractive Index at Radio Frequencies

Ernest K. Smith, Jr., and Stanley Weintraub

Recent improvements in microwave techniques have resulted in precise measurements at the National Bureau of Standards, the National Physical Laboratory, and elsewhere, which indicate that the conventional constants $K_1=79°$ K/mb and $K_2'=4{,}800°$ K in the expression for the refractivity of air, $N=(n-1)10^6=(K_1/T)\,[p+K_2'(e/T)]$ should be revised. Various laboratories appear to have arrived at this conclusion independently, with the result that there are several different sets of constants in current use. In much of propagation work the absolute value of the refractive index of the atmosphere is of small moment. However, in some work it is important, and it seems highly desirable to decide upon a particular set of constants.

Through consideration of the various recent experiments a relation $N=(77.6/T)\,[p+4810\,(e/T)]$ is derived, where p is the total pressure, in millibars, e is the partial pressure of water vapor, in millibars, and T is absolute temperature (°C+273). This expression is considered to be good to 0.5 percent in N for frequencies up to 30,000 megacycles and normally encountered ranges of temperature, pressure, and humidity.

Recent improvements in microwave techniques have resulted in measurements at the National Bureau of Standards [1],[1] the National Physical Laboratory [2], and elsewhere [3, 4, 5], which have indicated that the conventional constants in the expression for the refractive index of air at radio frequencies should be revised. Various laboratories appear to have arrived at this conclusion independently, with the result that there are several different sets of constants in current use [6, 7, 8, 9]. The sources of these recent changes, such as have been run to earth, have been found to be based on individual rather than collective results. Almost all the proposed constants seem to represent a substantial improvement over the former values. The authors propose a set of constants derived from what is felt to be the most reliable of the recent microwave and optical measurements of the refractive index of dry air and from a recent survey of water vapor Debye constants. It is hoped that these new constants will provide a common meeting ground for the laboratories desiring change rather than inject just another set of values into the field.

For an accuracy of 0.5 percent in N, the scaled-up refractivity of moist air $[N=(n-1)10^6]$, where n is the refractive index, some simplifying assumptions may be made if the use of the relation is to be restricted to certain limits of the variables. The limits in this case restrict its use to temperatures of -50 to $+40°$ C, total pressures of 200 to 1,100 mb, water-vapor partial pressures of 0 to 30 mb, and a frequency range of 0 to 30,000 Mc. The constituents of dry air and even water vapor may be assumed to obey the ideal gas law [10]. The refractive index of water vapor, a polar molecule with an electric dipole, may be represented by a two-term Debye relation [11]. The permeability of air at radio frequencies due to oxygen may be taken as $1+0.4\times10^{-6}$ [1]. Dispersion may be neglected. The Lorentz polarization term may be ignored. Absolute zero for temperature may be taken as $-273°$ C rather than $-273.16°$ C [12].

There has been no proof of variation in the composition of the dry gases of the free atmosphere either with latitude or with height up to the ionosphere [13]. The water vapor content, of course, varies widely. As contributions to the total refractive index obey an additive rule, a three-term expression may be formulated [11], in which the first term expresses the sum of the distortions of electronic charges of the dry-gas molecules under the influence of an applied electromagnetic field; the second term, these distortions for water vapor; and the third term, the effect of the orientation of the electric dipoles of water vapor under the influence of a field. Thus, using N for the scaled-up refractivity $[N=(n-1)10^6]$,

$$N=K_1\left(\frac{P_d}{T}\right)+K_2\left(\frac{e}{T}\right)+K_3\left(\frac{e}{T^2}\right), \qquad (1)$$

where n is the refractive index at radio frequencies; P_d, the partial pressure of the dry gases; e, the partial pressure of water vapor; and T, the absolute temperature.

In radio work one is interested in propagation through the free atmosphere. Therefore, the composition of air should be taken to include an average amount of carbon dioxide. However, laboratory measurements usually are made on CO_2-free air because of variable concentrations of CO_2 in the laboratory. Hence, those values of $\epsilon-1$ originally published for CO_2-free air have been adjusted for 0.03 percent CO_2 content by raising them 0.02 percent. These values are also given on a real rather than an ideal gas basis. Three determinations shown in table 1 are considered. The first shown, that of Barrell [14], is an average of the constant term (n for $\lambda=\infty$) of the optical Cauchy dispersion equations for standard air used in three of the principal metrology laboratories of the world. Theoretical considerations indicate that the dielectric constant

[1] Figures in brackets indicate the literature references at the end of this paper.

for dry air will be the same for optical and radio frequencies. Barrell's value is converted to dielectric constant from the relation $n=\sqrt{\mu\epsilon}$ with μ, the permeability, taken as unity at optical frequencies. The second value, that of Birnbaum, Kryder, and Lyons [1], was originally published on an ideal basis but has here been converted to the value pertinent to real gases. The last determination, that of Essen and Froome [2], has been adjusted to include CO_2. The uncertainties listed are standard errors.

TABLE 1. *Dry-air refractive index and dielectric constant at 0° C and 1 atmosphere*

	Frequency of measurement	Measured N	$(\epsilon-1)10^6$	Year
Barrell [14]	Optical	$287.7_6\pm0.0_3$	$575.6\pm0.1_2$	1951
Birnbaum, Kryder and Lyons [1].	9,000 Mc		$575.8\pm0.3_6$	1951
Essen and Froome [2].	24,000 Mc	$288.2_1\pm0.1$	576.1 ± 0.2	1951
Mean value		$*288.0_{17}\pm0.0_5$	$575.7_3\pm0.1_0$	

* Derived from $n=\sqrt{\mu\epsilon}$, where $\mu-1=0.4\times10^{-6}$ is taken for radio frequencies to account for the permeability.

The statistical mean value of dielectric constant is then converted to refractive index. The constant K_1 is evaluated from

$$N=K_1\frac{p_d}{T}, \tag{2}$$

which stems from (1) when $e=0$. Setting $N=288.04$, $p=1013.25$ mb, $T=273°$ C and solving for K_1:

$$K_1=77.60_7\pm0.01_2\ \frac{°\text{K}}{\text{mb}} \tag{3}$$

A recent survey of determinations of the dielectric constant of water vapor in the microwave region by Birnbaum and Chatterjee [15] is used to evaluate the water-vapor constants K_2 and K_3 in (1). Assuming ideal gas behavior, which is permissible here as only low partial pressures are of interest, the constants may be evaluated from the Debye constants A and B (molar polarization $P=A+B/T$) determined by Birnbaum and Chatterjee. This results in

$$K_2=71._6\pm8._5\ \frac{°\text{K}}{\text{mb}} \tag{4}$$

$$K_3=(3.74_7\pm0.03_1)10^5\ \frac{°\text{K}^2}{\text{mb}}, \tag{5}$$

where the uncertainties are again standard errors. Substituting the values of (3), (4), and (5) in (1), and reducing the values to three figures where significant

$$N=77.6\frac{p_d}{T}+72\frac{e}{T}+3.75\times10^5\frac{e}{T^2}. \tag{6}$$

Utilizing the total pressure, $p=P_d+e$, one may write

$$N=77.6\frac{p}{T}-6\frac{e}{T}+3.75\times10^5\frac{e}{T^2}. \tag{7}$$

For use in the limited temperature range $-50°$ to $+40°$ C, negligible error is incurred through lumping the second and third terms in (7). This may be accomplished by dividing these terms by e/T and solving for the composite constant, K_4, in the relation

$$\frac{3.75\times10^5}{T}-6=\frac{K_4}{T}, \tag{8}$$

which, for $T=273°$ K, results in

$$K_4=3.73\times10^5. \tag{9}$$

The two-term formula for dry air is now

$$N=77.6\frac{p}{T}+3.73\times10^5\frac{e}{T^2}, \tag{10}$$

which may be written

$$N=\frac{77.6}{T}\left(p+4.81\times10^3\frac{e}{T}\right). \tag{11}$$

These last two relations are the ones proposed for general radio meteorological use.

Listed in table 2 are some of the values of K_1, K_2, and K_3, that have been used by authors through the years. In examples 1 through 7 the constant K_1 was drawn from the Smithsonian Physical Tables (1933). The water-vapor constants K_2 and K_3 in examples 2 to 7 represent an average of the determinations of several different workers in each case. Essen and Froome in example 8 relied on their own excellent experimental work to evaluate K_1 and K_3. Their value of K_1 is seen from table 1 to be in excellent agreement with the values of Barrell and of Birnbaum, Kryder, and Lyons. However, their value for K_3 is low because of the fact that their measured value of the dielectric constant of water vapor is about 1 percent lower than those determined

TABLE 2. *Constants used by different authors*

$$N=(n-1)10^6=K_1\frac{p}{T}+K_2\frac{e}{T}+K_3\frac{e}{T^2}$$

Author	Year	K_1	K_2	K_3
1. Schelleng, Burrows, and Ferrell [16]	1933	79	675	1.35×10^5
2. Englund, Crawford, and Mumford [17]	1935	79.1	68.3	3.81
3. Waynick [18]	1940	79	68.5	3.72
4. Smith-Rose and Stickland [19]	1943	79	68	3.77
5. NDRC, Burrows and Attwood [20]	1946	79	68	3.8
6. Meteorological Factors in Propagation [21]	1946	79	68	3.8
7. Radiation Laboratory, vol. 13 (Kerr) [11]	1951	79	(79)	3.8
8. Essen and Froome [2]	1951	77.64	64.68	3.718
9. Smith and Weintraub	1952	77.6	72	3.75

other recent workers in the field. It is true that ir measurements were performed in a region jacent to the 1.35-cm water-vapor absorption nd, but this effect has been shown to be too small account for the discrepancy. As Essen and oome did not have refractive-index determinations er the wide temperature range necessary to evalate K_2 and K_3 independently, they utilized an ptical value of refractive index ($K_3=0$) to deterine K_2. Consequently, their value for K_2 is about 0 percent low at radio frequencies. However, the ffect of this on the equation is negligible.

The authors thank George Birnbaum, Arthur Maryott, Jack W. Herbstreit, and Kenneth A. Norton for their advice and assistance in this work.

References

[1] G. Birnbaum, S. J. Kryder, and H. Lyons, J. Applied Phys. **22,** 95 (1951).
[2] L. Essen and K. D. Froome, Proc. Phys. Soc. (London) [B] **64,** 862 (1951).
[3] C. M. Crain, Phys. Rev. **74,** 691 (1948).
[4] W. F. Gabriel, Proc. Inst. Radio Engrs. **40,** 940 (Aug. 1952).
[5] W. E. Phillips, Proc. Inst. Radio Engrs. **38,** 786 (1950); C. M. Crain, Proc. Inst. Radio Engrs. **40,** 164 (Feb. 1952).
[6] C. I. Aslakson and O. O. Fickeissen, Trans. Am. Geophys. Union **31,** 819 (1950).
[7] Cornell E. E. Research Interim Engineering Report No. 13, p. 23 (October 27, 1951).
[8] L. Essen and K. D. Froome, Nature **167,** 512 (1951).
[9] L. J. Anderson, NEL Report No. 279 (1952).
[10] H. Barrell and J. E. Sears, Philos. Trans. [A] **238,** 2 (1940).
[11] Propagation of Short Radio Waves, Edited by D. E. Kerr, Radiation Laboratory Series 13, p. 189 (McGraw-Hill Book Co., Inc., New York, N. Y., 1951).
[12] ibid. p. 643.
[13] Ionospheric Radio Propagation, NBS Circ. 462, p. 35 (June 1948).
[14] H. Barrell, J. Optical Soc. Am. **41,** 295 (1951).
[15] G. Birnbaum and S. K. Chatterjee, J. Applied Phys. **23,** 220 (Feb. 1952).
[16] J. C. Schelleng, C. R. Burrows, and E. B. Ferrell, Proc. Inst. Radio Engrs. **21,** 427 (1933).
[17] C. R. Englund, A. B. Crawford, and W. W. Mumford, Bell System Tech. J. **14,** 369 (1935).
[18] A. H. Waynick, Proc. Inst. Radio Engrs. **28,** 468 (1940).
[19] R. L. Smith-Rose and A. C. Stickland, J. Inst. Elec. Engrs. (London) **90,** pt. III, 12 (1943).
[20] Radio Wave Propagation, Consolidated Summary Technical Report of the Committee on Propagation, NDRC, Edited by C. R. Burrows and S. S. Attwood (Academic Press, Inc., New York, N. Y., 1949), p. 219.
[21] Meteorological Factors in Radio Wave Propagation, Foreword (Phys. Soc., London, 1946).

Boulder, Colo., October 6, 1952.

233150—53——4

Tables of Complete Elliptic Integrals[1]

J. M. Hammersley [2]

The complete elliptic integrals

$$K=\int_0^{\pi/2}(1-k^2\sin^2\phi)^{-\frac{1}{2}}d\phi,$$

$$E=\int_0^{\pi/2}(1-k^2\sin^2\phi)^{\frac{1}{2}}d\phi$$

and the associated function

$$M=\frac{\pi}{2K}$$

have been tabulated extensively [3,4] with k^2 and k and arcsin k as arguments. This replication of tables with a variety of closely related arguments is partly due to the difficulty of interpolating in the neighborhood of $k=1$. Legendre considered that interpolation was unsatisfactory in the range $1\leq 1/k\leq\sqrt{2}$. Recently the author needed tables of K and E with $1/k$ as argument. This is quite a common need. For example, it arises in evaluating integrals of the form

$$\int_0^1 \frac{dx}{\sqrt{\{(1-x^2)(p^2-x^2)\}}}, \quad pk=1.$$

The tables, given below, were computed by Gauss's arithmetic-geometric mean. The last significant figure is doubtful, but is retained in accordance with Fisher and Wishart.[5]

[1] This paper was prepared under a National Bureau of Standards contract with American University.
[2] Oxford University and American University.
[3] A. Fletcher, J. C. P. Miller, and L. Rosenhead, An index of mathematical tables (Scientific Computing Service, London, 1946).
[4] A. Fletcher, Guide to tables of elliptic functions, MTAC 3, 229-281 (1948).
[5] R. A. Fisher and J. Wishart, On the distribution of the error of an interpolated value, and on the construction of tables, Proc. Cambridge Phil. Soc. **23**, 912-921 (1927).

$1/k$	K	E	M
1.00	∞	1.	0.
1.01	3.36145 8120	1.02824 2731	0.46729 61170
1.02	3.03047 9311	1.04930 1697	0.51833 26351
1.03	2.84195 7373	1.06755 5825	0.55271 63573
1.04	2.71141 0062	1.08395 7261	0.57932 82058
1.05	2.61243 9112	1.09896 6268	0.60127 57656
1.06	2.53331 9380	1.11285 8448	0.62005 45970
1.07	2.46781 4067	1.12581 8774	0.63651 32398
1.08	2.41221 1023	1.13798 0652	0.65118 52868
1.09	2.36412 2792	1.14944 5208	0.66443 09393
1.10	2.32192 4037	1.16029 1946	0.67650 63378
1.11	2.28445 8951	1.17058 5138	0.68760 10297
1.12	2.25087 6725	1.18037 7893	0.69785 97760
1.13	2.22053 3243	1.18971 4883	0.70739 59970
1.14	2.19292 9400	1.19863 4233	0.71630 04550
1.15	2.16767 0799	1.20716 8882	0.72464 70855
1.16	2.14444 0528	1.21534 7583	0.73249 70342
1.17	2.12298 0225	1.22319 5658	0.73990 15350
1.18	2.10307 6584	1.23073 5581	0.74690 40066
1.19	2.08455 1532	1.23798 7432	0.75354 16145
1.20	2.06725 4932	1.24496 9258	0.75984 64529
1.21	2.05105 9081	1.25169 7363	0.76584 64553
1.22	2.03585 4498	1.25818 6552	0.77156 61060
1.23	2.02154 6642	1.26445 0315	0.77702 70023
1.24	2.00805 3348	1.27050 1000	0.78224 83048
1.25	1.99530 2778	1.27634 9943	0.78724 71008
1.26	1.98323 1784	1.28200 7587	0.79203 87014
1.27	1.97178 4578	1.28748 3577	0.79663 68863
1.28	1.96091 1645	1.29278 6848	0.80105 41070
1.29	1.95056 8854	1.29792 5693	0.80530 16554
1.30	1.94071 6711	1.30290 7829	0.80938 98084
1.32	1.92234 6001	1.31243 0289	0.81712 46622
1.34	1.90555 5240	1.32140 6374	0.82432 47395
1.36	1.89014 3668	1.32988 1897	0.83104 59960
1.38	1.87594 4456	1.33789 7365	0.83733 62664
1.40	1.86281 7607	1.34548 8787	0.84323 67835
1.42	1.85064 4602	1.35268 8327	0.84878 33512
1.44	1.83932 4316	1.35952 4838	0.85400 72640
1.46	1.82876 9850	1.36602 4314	0.85893 60368
1.48	1.81890 6041	1.37221 0246	0.86359 39910
1.50	1.80966 7496	1.37810 3938	0.86800 27302
1.52	1.80099 7013	1.38372 4769	0.87218 15280
1.54	1.79284 4308	1.38909 0414	0.87614 76498
1.56	1.78516 4971	1.39421 7036	0.87991 66198
1.58	1.77791 9616	1.39911 9448	0.88350 24444
1.60	1.77107 3176	1.40381 1262	0.88691 78010
1.62	1.76459 4312	1.40830 5004	0.89017 41982
1.64	1.75845 4921	1.41261 2228	0.89328 21127
1.66	1.75262 9723	1.41674 3613	0.89625 11056
1.68	1.74709 5907	1.42070 9039	0.89908 99244
1.70	1.74183 2833	1.42451 7669	0.90180 65896
1.72	1.73682 1775	1.42817 8011	0.90440 84715
1.74	1.73204 5702	1.43169 7974	0.90690 23555
1.76	1.72748 9086	1.43508 4926	0.90929 45015
1.78	1.72313 7737	1.43834 5734	0.91159 06946
1.80	1.71897 8667	1.44148 6811	0.91379 62892
1.82	1.71499 9953	1.44451 4152	0.91591 62509
1.84	1.71119 0637	1.44743 3363	0.91795 51902
1.86	1.70754 0629	1.45024 9701	0.91991 73949
1.88	1.70404 0617	1.45296 8092	0.92180 68582
1.90	1.70068 1997	1.45559 3163	0.92362 73036
1.92	1.69745 6806	1.45812 9262	0.92538 22079
1.94	1.69435 7662	1.46058 0475	0.92707 48213
1.96	1.69137 7713	1.46295 0655	0.92870 81858
1.98	1.68851 0587	1.46524 3426	0.93028 51514
2.00	1.68575 0355	1.46746 2209	0.93180 83916

Washington, October 27, 1952.

Assembled Polygon for the Calibration of Angle Blocks

Clyde E. Haven and Arthur G. Strang

A method is described for constructing and calibrating an assembled, multiple-sided, angular standard of exceptional accuracy. Although designed as a master for the 30- and 45-degree angle blocks of a series made in this country, the polygon is equally suitable for the test or calibration of circular dividing equipment. Simpler forms may be easily and economically constructed as masters for a variety of applications in the mechanical and optical industries.

1. Introduction

The advent of World War II produced an acute shortage of precise angular dividing equipment in England and led to the development by the National Physical Laboratory of a series of solid angular standards.[1] These are hardened, ground, and lapped steel blocks about ⅝ in. wide, 3 in. long, and having specified angles between the two contact surfaces. Like gage blocks, they can be combined with little error by wringing, but since they may be combined to form the sum or difference of a pair, a series of as few as 12 blocks will form any angle up to a little over 80 deg. in increments of 3 sec. By mounting these blocks and a solid square (a rectangular prism having four finished faces), in various positions, any subdivision of a circle to the nearest 3 sec. may be obtained.

The angles of the individual blocks in the NPL set are, in general, based on the mathmatical relationship whereby each successively larger block is twice the sum of the preceding blocks plus 1, respectively, in seconds, minutes, and degrees. Exceptions to the general relationship are the omission of a 1-sec. block, and the use of a 41-deg. block instead of an 81-deg. block. A 1-sec. block is unwarranted in a set having permissible errors of 1 sec., and the 41-deg. block provides a more convenient size than the 81-deg. block. The series is thus comprised of blocks having angles of 3, 9, and 27 sec., 1, 3, 9, and 27 min., and 1, 3, 9, 27, and 41 deg.

At about the same time that the English series of blocks was developed, a similar series was patented in this country.[2] The American series differs from the English in that it is made up of more commonly used sizes and thus requires a few more blocks for the same angular coverage. The series is 1, 3, 5, 20, and 30 sec.; 1, 3, 5, 20, and 30 min.; 1, 3, 5, 15, 30, and 45 deg.

Because the generation of nearly optically plane surfaces and the control of pyramidal error within the required limits are not excessively difficult, it is possible to produce blocks that are susceptible to very precise calibration.

One of the most satisfactory methods of calibrating angle blocks is by comparison with a master set, provided that the angular values of the masters can be determined with adequate accuracy. Knoyle[3] has described a primary determination of the angles of all the blocks in a set without reference to an external standard. Using an interferometric method for the required comparisons, we have found his procedure entirely satisfactory except for measurements on master blocks or combinations of master blocks having angles of 45 deg or larger and particularly on the 90-deg combination, which is used in the primary determination for the entire series. Alinement of the sides of the blocks in a combination becomes increasingly critical as the angle increases, and some difficulty has been experienced in obtaining satisfactory agreement on 90-deg combinations.

Similar types of alinement difficulties arise in the comparison of 45-deg blocks by interferometric methods wherein two blocks are wrung side by side on an optical flat and the difference in angle established by the difference in fringe count over a specific length on the unwrung surfaces of the blocks. If, for example, the adjacent sides of the two 45-deg blocks are more than 0.00005 in./in. out of parallel along the length of the blocks, interference bands on the two blocks form too large an angle with each other to permit an accurate fringe count. Considering the errors that may accrue in the determination of the angle of 45-deg blocks, and possibly 30-deg blocks, an alternative method of determining their angles is clearly desirable.

The success of the National Physical Laboratory in the calibration of angular-dividing equipment by means of multiple-sided solid angular standards[4] suggested the possibility of using a 24-sided solid polygon having 15-deg exterior angles between adjacent faces. Such a polygon would permit direct calibration of both 30- and 45-deg blocks. The mechanical requirements for a polygon of the requisite accuracy are quite severe; the defining surfaces must be flat over practically their entire area to one or two millionths of an inch, the surface roughness of the faces must be less than 0.5 μin. rms with practically no visible scratches perpendicular to the side of the polygon, and the variations in the angle between the defining faces and the axis of the polygon not in excess of 15 sec. Convenience dictates a maximum departure of the angular intervals from nominal value of not more than 10 sec. The con-

[1] British patent 569,002.
[2] U. S. Patent 2,134,062.

[3] C. H. Knoyle, NPL combination angle gauges, Machinery (London) **77**, 1975 (1950).
[4] C. O. Taylerson, Testing circular division by means of precision polygons, Machinery (London) **71**, 1821 (1947).

struction of a conventional, solid 24-sided polygon to these limits constitutes a challenge to the best mechanical skill and equipment.

2. Construction of the Polygon

As a substitute for such a formidable undertaking, the possibility of assembling a polygon from more easily fabricated units was considered. The availability of satisfactory defining faces in the form of gage blocks suggested the assembly of modified blocks on a suitable base, using one finished surface of each block to define the polygon. Conventional gage blocks could readily be modified by lapping the side faces plane and parallel, with, of course, due control of the angle between adjacent lapped faces and by providing holes for fastening the blocks to the base. With this type of construction, control of any of the required features of the polygon could be readily accomplished, usually with little effect on the other dimensions.

In order to determine the merits of this method of construction, an experimental polygon was made. The base of the polygon was ¾ in. thick and 8 in. in diameter. It was made of oil hardened steel and heat treated for maximum dimensional stability. A 1¾-in.-diameter center hole and appropriate tapped holes in the base provided means for attaching a bushing so that the polygon could be used on centers if desired. In order to keep the diameter of the plate within reasonable limits, the gage blocks were placed in two layers of twelve each.

Twenty-four tapped holes were equally spaced on a circle of a radius such that the chord of a 30-deg sector corresponded to the spacing of the holes in the gage blocks. This permitted the use of the same screws for fastening both the upper and lower layers of blocks. The tapped holes in the base were countersunk and then counterbored to a depth of ¼ in. to minimize distortion of the base due to tension of the clamping screws.

After hardening, the base was ground on both sides and then hand-lapped until the error in parallelism of the two surfaces was less than 0.0001 in. and the maximum error in flatness of each surface less than 0.00006 in. A relatively high finish was imparted to one surface in the final lapping to permit wringing the special gage blocks in position.

Modified 0.750-in. rectangular gage blocks were obtained from a gage-block manufacturer for use as the defining faces. All four lapped sides were plane to 0.000005 in. or better, and adjacent sides were square to 2 sec of arc. The surface roughness of each of the sides was less than 1 μin. rms. The thickness (¾-in. dimension) of the 24 blocks in the group varied less than 0.00003 in. Each block was measured and the bottom layer of blocks so selected that adjacent blocks did not differ in thickness by more than 0.00001 in. This permitted at least partial wringing of the blocks in the upper layer to their supporting blocks and reduced distortion arising from the pressure of the clamping screws.

Commercial gage blocks are frequently used as mirrors for an autocollimator, and as such form reasonably sharp images of the reticle. It was found, however, that the crispness of the image could be further enhanced by a limited amount of polishing on a cloth lap, and each of the defining faces was so finished. Figure 1, illustrating the finish before and after polishing, was made with the Ziess microinterferometer.

The assembly of the components of the polygon

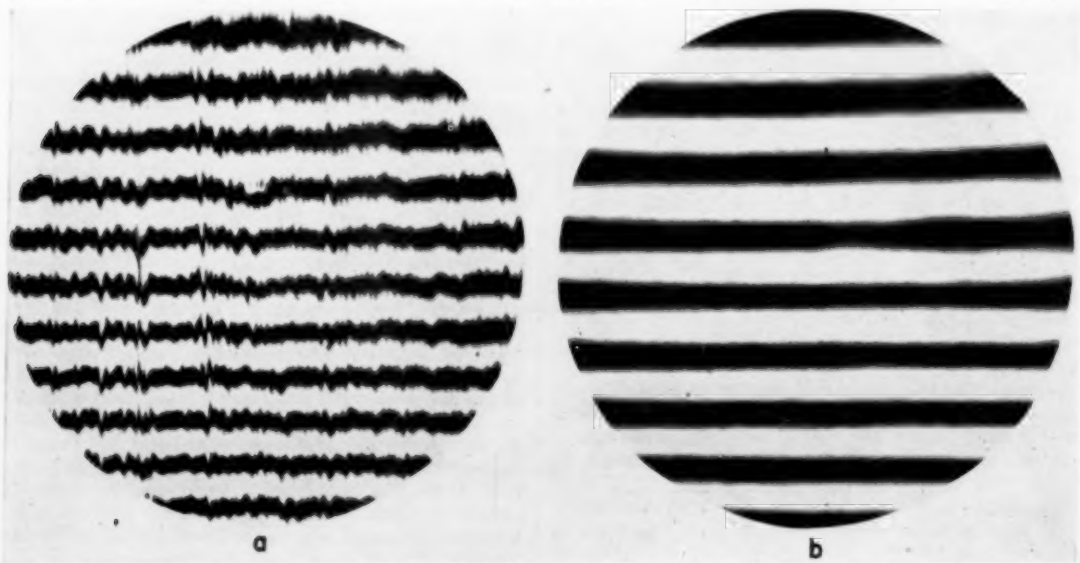

FIGURE 1. *Interference micrographs of a reflecting face (a) before and (b) after cloth polishing,* $\times$ *400.*

The interference fringes may be considered as contour lines with the distance between adjacent fringes equal to 0.000011 inch. Thus the excursion of a fringe one-half way toward an adjacent fringe indicates a hill or valley 0.0000055 inch high or low with the nature of the irregularity determined by the direction of the fringe displacement.

as made on a rotary table by the use of 15-, 30-, and 45-deg angle blocks, a solid square, and an autocollimator. The rotary table had previously been adjusted so that its surface was closely perpendicular to its axis of rotation and, for convenience in alining the autocollimator, parallel to the surface plate on which it rested. The autocollimator was mounted on a rigid base with its axis parallel to the surface plate at an appropriate height to cover both the polygon faces and the square or angle block.

The 0-, 90-, 180-, and 270-deg faces were positioned by means of the square and the intermediate faces by adding or subtracting 15, 30, and 45 deg from these positions. For example, the 0-deg block was wrung to the base with its two holes approximately concentric with two of the tapped holes; one face of a 30-deg angle block was adjusted parallel to the 0-deg block by means of the autocollimator; the base and the angle block were rotated through 30 deg by means of the rotary table, and the 30-deg polygon block was positioned parallel to the second face of the angle block. Because the 0- and 30-deg blocks could not be fastened to the base until the 15-deg block was in place, this block was positioned next, using the same method as for the 30-deg block. All the other blocks of the polygon were similarly located, working alternately in clockwise and counterclockwise directions from the 0-deg block.

The use of the same screws for holding both layers of blocks to the base made the assembling somewhat tedious, as the top block frequently moved when the screws were tightened, even though well lubricated, cupped, brass washers were used between the screw heads and the blocks. At least a part of this difficulty arose from the fact that some of the tapped holes were not accurately square with the base. The angular position of the top block was observed as the screws were tightened and, when necessary, the positioning repeated until the block was located within the required limits. The blocks in the lower layer had little tendency to move as they wrung quite firmly to the base, but their position was checked, as a precautionary measure, after the fastening screws were tightened.

It was found that quite accurate settings could be made by gently tapping a block to its final position, and, if only a single layer of blocks had been involved, it is believed that the angular intervals could easily have been set to an accuracy of 2 sec.

On this particular polygon no further adjustment was attempted when a block was once located to an accuracy of ± 10 sec, as moderate random departures from nominal angle may, in some applications, be used to good advantage to confirm the direction of corrections.

3. Calibration of Equipment

The autocollimators used in the calibration have a total range of 10 min and a least reading of 0.5 sec.

In order to reduce autocollimator errors to a minimum, a number of precautions were observed. Rotation of the reticle from its true position in a plane perpendicular to the optical axis introduces an error. The true position of the reticle is parallel to the setting hairlines of the micrometer eyepiece and perpendicular to their direction of travel. When the autocollimator is properly alined, the setting hairlines are parallel to the axis of rotation of the work. The relationship can be expressed by the formula $\theta = \beta \tan \alpha$, where θ is the error in seconds of the reading, β the departure in seconds of the reflecting surface from the plane of measurement of the micrometer eyepiece, and α the deviation of the reticle line from its true position. For a 30-sec change in vertical angle of the polygon reflecting surface and for a 2-deg rotation of the reticle line, the error is 1.05 sec. Because visual alinement of a reticle line is usually limited to an accuracy of about 2 deg, a more accurate method of alinement was required. Accordingly, we removed all the lenses of the autocollimator, projected an image of the reticle on a screen, and, by adjustment of the autocollimator rotational stops, brought the image into coincidence with the image of a suitably disposed machinist square. By this method the reticle line could be set perpendicular to the base of the instrument to within less than 15 min.

After adjustment of the reticle line, the autocollimator microscope was carefully focused on the reticle and the autocollimator objective adjusted to form a crisp image with a representative polygon face.

The two lines of the micrometer eyepiece so closely bracketed the reticle image that traces of color along each edge of the image affected the precision of setting. After some experimentation, a blue-green Wratten filter (B2–58) was found that transmitted an adequate amount of light but largely suppressed the objectionable colors. The remaining secondary chromatic aberration appeared to the operator to be equal on both sides of the reflected line.

Both autocollimators were calibrated over the central 9 min of range in 3-min intervals and over the central 5 min in 1-min intervals by means of master angle blocks. No error in excess of 0.3 sec/min was found in the central part of the range on either autocollimator. Because the differences in the angles to be measured were not expected to exceed 10 sec, it was considered that the progressive errors of the autocollimators could be neglected. As a check on the possibility of periodic errors in the micrometer eyepiece screws, comparisons were made of the angular value of the micrometer eyepiece screws of the two autocollimators in 5-sec intervals over a 1-min range by directing the autocollimators at separate faces of an angle block and rotating it in 5-sec increments between readings. The angular values of the screws on both instruments were found to be uniform within 0.3 sec, which is about the limit to which two settings can be repeated.

4. Calibration of Polygon

All the equipment for the calibration of the polygon was then assembled on a large surface plate. The

polygon was mounted on a rotary table and each autocollimator on a substantial iron base with its optical axis in line with the junction of the upper and lower layers of blocks. Each autocollimator was centered on the appropriate polygon face by viewing with a low-power microscope the real image of the face that is formed in the exit pupil of the autocollimator eyepiece. At the same time, the position of the autocollimator light source was adjusted to provide uniform illumination over the entire polygon face.

Preliminary observations soon indicated that, after handling of the equipment, the entire setup required a fairly long stabilizing period in a constant-temperature room and that temperature gradients in the surface plate due to the presence of observers changed the angle between the autocollimators enough to introduce intolerable errors when the observations extended over a period of 1 or 2 hr. These effects were largely overcome by erecting an insulating barrier completely around and over the top of the setup and scheduling the observations so that at least 4 hr intervened between the readjustment of units and a series of measurements. Small openings in the insulating wall at each autocollimator position permitted reading of the autocollimator. As a check on angular change in autocollimator positions, the initial interval was remeasured after six (or fewer) consecutive intervals were observed.

Measurements were made by directing each autocollimator toward the center of the appropriate polygon face at such an angle that the reflected image of the reticle came within the selected range of the autocollimator. Figure 2 shows the disposition of polygon and autocollimators for the measurement of the 30-deg intervals. After recording the reading of the two autocollimators, the rotary table on which the polygon was mounted was then turned to present the faces of the adjacent angular interval. This process was repeated until every interval of the same nominal size had been measured and the circuit closed. Because some of the intervals are aliquot parts of 360 deg and others are aliquots of a multiple of 360 deg, a closure consisted of from 2 to 24 readings. Where a closure consisted of less than 24 readings, additional closures were required to cover all the intervals. For example, 12 closures of two readings each were required to cover the 180-deg intervals, whereas one closure consisting of 24 readings over 3,960-deg (11 revolutions) was required for the 165-deg intervals.

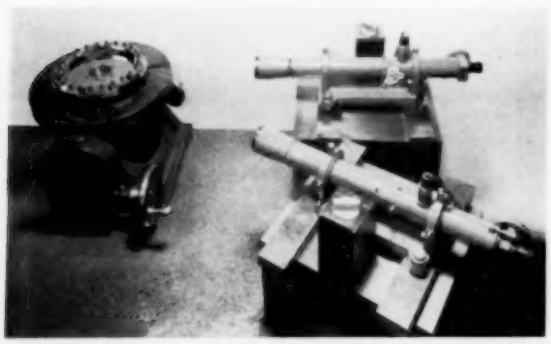

FIGURE 2. *Arrangement of polygon and autocollimators for the measurement of 30-degree intervals.*

One autocollimator is directed at a selected face and the other at a face 30 degrees away.

The difference between the readings of the two autocollimators is an estimate of the difference in angle defined by the two autocollimators and the angle between the two polygon faces. Because the angle between the collimators was only approximately equal to the nominal polygon interval, each difference, d_i, in any particular closure is an estimate of the error of the polygon interval, γ_i, plus a constant error, Δ, due to the deviation from nominal of the angle between the autocollimators. Thus $d_i = \gamma_i + \Delta$.

For a complete closure

$$\sum_{i=1}^{n} d_i = \sum_{i=1}^{n} \gamma_i + n\Delta,$$

where n is the number of readings required for a closure. But since $\sum_{i=1}^{n} \gamma_i$ for a circle or any multiple thereof equals 0,

$$\Delta = \frac{1}{n} \sum_{i=1}^{n} d_i.$$

Therefore,

$$\gamma_i = d_i - \frac{1}{n} \sum_{i=1}^{n} d_i,$$

from which values for each polygon interval of a closure can be obtained. However, each difference is subject to a random error ϵ, so that we have an ϵ_i associated with each d_i. It is reasonable to assume that all errors, ϵ_i, arise independently and randomly from the same error distribution, and that the distribution is characterized by an average value of zero and a dispersion of the magnitude indicated by a standard deviation, σ. This standard deviation is a measure of the precision of an individual difference by this processs of measurement; an average of n individual values will have the precision indicated by a standard deviation of $\sigma/\sqrt{n}$ and the sum of k individual values will have a standard deviation of $\sigma\sqrt{k}$.

If only the closure for the 15-deg interval is made, the precision with which the corrections to each of the 24 basic angles is known would be the same for all angles, but that of any angle comprised of the sum of two or more 15-deg angles would vary with the number of 15-deg angles involved.

In order to provide corrections of equal precision for all intervals, 552 measurements involving 76 closures were made to obtain all possible sums of consecutive angles. From these measurements corrections were derived for each interval. For example, in the determination of the correction for the 0- to 15-deg interval, 48 values were obtained from the following two series of differences:

[(0- to 15-deg correction)−(15- to 15-deg correction)],
[(0- to 30-deg correction)−(15- to 30-deg correction)], . . .,
(0- to 360-deg correction)−(15- to 360-deg correction)], and

(360- to 15-deg correction)−(360- to 0-deg correction)],
(345- to 15-deg correction)−(345- to 0-deg correction)], . . .,
[(15- to 15-deg correction)−(15- to 0-deg correction)].

The least-squares estimate for each angular interval involves the same number of measurements, and the precision with which the correction to any angle is known is $\sigma/\sqrt{24}$. An estimate of the standard deviation, σ, was determined from the least-squares solution. For any single measurement, the standard deviation, σ, was found to be 0.22 sec. Hence, the final value for each of the intervals had a standard deviation of $0.22/\sqrt{24}$, or 0.045 sec.

In addition to random errors, any calibration process commonly has systematic errors associated with it. In this case, however, no error existed in the primary standard, a circle, and any possible small errors in the autocollimator screws were so distributed over the entire series of measurements that their effect largely assumed a random characteristic. Accordingly, it is believed that the systematic errors may be considered negligible and, therefore, disregarded. Knowledge of the true corrections is, therefore, obscured solely by the random errors of measurement, and the accuracy of the process involves only some upper limit to the magnitude of the random errors.

A reasonable upper limit for the magnitude of the random errors can be set by selecting the value from the error distribution for which there is a chance of only one in one hundred of a greater discrepancy occurring. For this definition (assuming a normal distribution of errors), the accuracy of the corrections is $\pm 2.58(.045) = \pm .12$ sec.

The actual values of the intervals are of no particular interest to a reader of this paper, but it may be noted that the maximum deviation from nominal size of any 15-deg interval was 8.2 sec and for any iterval, 9.0 sec.

5. Application of the Polygon

The polygon was used to calibrate a master 45-deg. angle block belonging to the Bureau. The calibration could be made either by comparing the angle block with one or more intervals of the polygon or by comparing the angle block with a sufficient number of consecutive intervals to encompass an integral number of polygon rotations or circuits. In the case of a 45-deg block, whose external angle is 135 deg, eight consecutive readings covering 1,080 deg are required for a closure. Two additional series of eight readings each are required to provide comparisons with every 135-deg interval of the polygon.

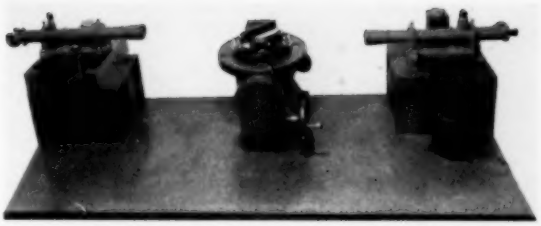

FIGURE 3. *Arrangement of polygon, angle block, and autocollimators for calibration of 45-degree angle block.*

One autocollimator is directed at the polygon and the other at the angle block.

The disposition of the equipment for the calibration of a 45-deg angle block is shown in figure 3. The polygon and angle block were mounted on a rotary table with the angle block elevated just above the polygon faces by means of a plane parallel block interposed between the polygon base and the block. Two autocollimators were positioned 180 deg apart, with one directed at a polygon face and the other at an angle-block face. The same care was observed in alining the equipment as for the calibration of the polygon, but temperature effects were largely eliminated by the 180-deg disposition of the autocollimators.

With the autocollimators appropriately alined, the readings of the two instruments were recorded. The assembly of polygon and angle block was then rotated 135 deg by means of the rotary table, and the autocollimator readings were again noted. The angle block was next rotated 135 deg with respect to the polygon, and comparison of the angle block with the adjacent 135-deg polygon interval was obtained by observing readings of both autocollimators at that position and after another 135-deg rotation of both polygon and angle block. Similar comparisons with the next six consecutive intervals of the polygon completed a closure and permitted computation of the angle of the angle block. In order to obtain a more accurate value, additional closures were made, relating the angle block to other 135-deg-polygon intervals.

Table 1 is a tabulation of two closures on a 45-deg angle block. Column 1 is the polygon interval; column 2, the difference in autocollimator readings on the polygon; column 3, the difference in autocollimator readings on the angle block; column 4, the difference between columns 2 and 3; column 5, the error in the polygon interval by the previous calibration; column 6, the error of the angle block by direct comparison with the polygon interval; and column 7, the error of the angle block by comparison with all the polygon intervals in each of the separate closures. The latter is wholly independent of any errors in the values for the polygon intervals and therefore somewhat more accurate than the average of eight values not constituting a closure.

The angular rotation of the block and polygon between readings was 135 deg$+\epsilon_p+d_1$ in terms of polygon values and 135 deg$+\epsilon_b+d_2$ in terms of angle block values, where ϵ_p is the error in the polygon interval, d_1 is the difference in autocollimator

readings on the polygon, e_b is the error in the angle of the block, and d_2 is the difference in autocollimator readings on the angle block.

Equating the two expressions, we have $e_b = d_1 - d_2 + e_p$. The values of e_b are given in column 6 of table 1. Since the sum of the e_p's for a closure is zero, e_b is estimated by $\frac{1}{8}\Sigma(d_1 - d_2)$, where 8 is the number of readings in a closure. This estimate is given in column 7 of table 1, and it is independent of the errors in the polygon.

TABLE 1. *Measurements of a 45-deg angle block by comparison with 135-deg intervals of polygon*

1	2	3	4	5	6	7
Polygon interval	Difference in polygon readings, d_1	Difference in block readings, d_2	$d_1 - d_2$	Error of polygon intervals	Error of angle block	$\frac{\Sigma(d_1 - d_2)}{8}$
deg	*sec*	*sec*	*sec*	*sec*	*sec*	*sec*
0 to 135	12.13	10.10	2.03	−1.76	0.27	.....
135 to 270	1.77	0.63	1.14	−1.19	−.05	.....
270 to 45	−5.57	−3.20	−2.37	2.34	.03	.....
45 to 180	12.86	12.03	0.83	−0.45	.38	.....
180 to 315	13.60	14.70	−1.10	0.87	−.23	.....
315 to 90	4.13	1.47	2.66	−2.41	.25	.....
90 to 225	6.53	7.43	−0.90	0.48	−.42	.....
225 to 0	−5.14	−2.76	−2.38	2.12	−.26	−0.01
15 to 150	−7.34	−8.60	1.26	−1.17	.09	.....
150 to 285	6.97	2.06	4.97	−4.96	.01	.....
285 to 60	−3.17	−1.20	−1.97	1.82	−.15	.....
60 to 195	−11.13	−5.93	−5.20	4.81	−.39	.....
195 to 330	5.44	4.07	1.37	−0.76	.61	.....
330 to 105	1.47	−1.57	3.04	−3.02	.02	.....
105 to 240	12.70	10.94	1.76	−1.43	.33	.....
240 to 15	1.46	6.67	−5.21	4.71	−.50	0.00

Four additional measurements gave values of +0.01, −0.01, −0.12, and +0.03 sec for $\Sigma(d_1 - d_2)/8$. The standard deviation, σ, for the six values of $\Sigma(d_1 - d_2)/8$ is 0.02 sec. If we use a 99 percent confidence limit, as in the case of the polygon, the average value of −0.01 sec may be considered accurate to ±0.09 sec.

6. Other Possible Uses

Although designed primarily as a master for angle blocks, the polygon is equally suitable for the test or calibration of angular dividing equipment. Used alone, it permits the calibration of 15-deg. intervals and, in conjunction with other polygons, of intervals as small as 1 deg by the method described by Taylerson (see footnote [3]).

Simple arrangements of a few blocks can be easily assembled to serve as masters or gages in the optical or mechanical industry.

A further extension of the application of assembled polygons to the calibration of circular dividing equipment is being considered.

Taylerson's method for calibrating 1-deg intervals requires the use of a number of polygons, each having a different number of sides. The complete calibration, using one suggested group of polygons, requires 49 circuits of three polygons, with a total of 408 readings.

The ease and precision with which defining faces can be positioned on an assembled polygon suggests the possibility of using a single polygon having in addition to the usual large intervals, one or more blocks offset at such angles as to subdivide the principal intervals. If, for example, a 12-sided polygon having 30-deg intervals is used, the addition of a single block offset from any one of the faces by 1 deg permits the calibration of test equipment in 1-deg increments. The 1-deg interval would fix the relationship between successive series of comparisons with the equal intervals of the polygon and necessarily enter the complete calibration as many as 15 times. If, however, two additional blocks are offset 10 and 20 deg, respectively, no more than five 1-deg intervals need be added or subtracted to establish the relationship between circuits. The addition of three more blocks offset 5, 15, and 25 deg, respectively, further reduce the number of 1-deg intervals entering a calibration and also provides very convenient method of calibrating equipment in 5, 10, or 15-deg increments.

The procedure for calibrating a rotary table in increments of 1 deg with a 12-sided polygon having three additional blocks offset 1, 10, and 20 deg, respectively, is as follows: Every 30-deg interval of the polygon is compared with rotary-table intervals starting at zero, then at 1, 2, 3, etc. up to 29 deg, inclusive. Additional comparisons are made with the 1-, 10-, and 20-deg intervals starting at zero and with the 1-deg interval on succeeding circuits. From the values of the polygon intervals, the errors of the rotary table can be derived in 1-deg increments.

For simplicity of explanation, the additional 1-, 10-, and 20-deg blocks have been indicated as offset from the zero polygon face, whereas space limitations would require that they be distributed around the polygon and offset from other polygon faces. The only effect of such a distribution is to change the computational procedure.

The use of a single polygon having faces offset in fractions of the main intervals has two advantages over Taylerson's method:

1. Thirty circuits with 392 readings are required, as compared with 49 circuits with 408 readings. The minor reduction in the number of readings is of little importance, but the large reduction in the number of circuits and the concomitant manipulation of the polygon should effect an appreciable saving in time.

2. A major reduction in the cost of equipment is achieved by the substitution of a single polygon for a group of three.

The authors express their appreciation to J. M. Cameron and his associates of the Bureau's Statistical Engineering Laboratory for guidance in selecting the most suitable series of observations, development of formulas for the best utilization of the data, and computation of results.

WASHINGTON, September 16, 1952.

Journal of Research of the National Bureau of Standards Vol. 50, No. 1, January 1953 Research Paper 2388

On the Spectrum of Energy in Turbulent Shear Flow

C. M. Tchen

A turbulent flow with a given spatial pattern of mean motion invariant with time is treated. No solid boundary is considered. By means of the Fourier analysis of the Navier-Stokes equation, it is possible to obtain an equation of energy balance in spectral terms. This involves the following functions: Viscous dissipation, transfer, production, convection, and diffusion. The first two functions are common to the isotropic and homogeneous turbulence without mean motion. Assuming that eddies controlled by inhomogeneity are much larger than those controlled by anisotropy, stationary spectral laws are obtained for small eddies in the viscous and nonviscous ranges. The agreement between theory and experiment is shown.

1. Introductory Remarks and Hypotheses on the Energy Distribution

In the statistical theories of isotropic turbulence, the irregular motion of the fluid is described by some characteristic functions: the correlation function, and the spectral function. The statistical theories devoted to the analysis of the correlation function were developed by von Kármán, Burgers, and others [1].[1] The study of the spectral function is based on the analysis of an irregular motion into harmonic components, as was developed by Burgers, for a model of turbulence [2]. The nonlinear process of the balance of turbulent energy is controlled by a transfer function, describing the transfer of energy from large eddies into small ones. Certain shapes of the transfer function were studied by Onsager [3], Obukhoff [4], von Weizäcker [5], and Heisenberg [6], all leading to a spectral law in agreement with the Kolmogoroff [7] law of locally isotropic turbulence for the nonviscous range. It seems that the spectral law in isotropic turbulence is well determined, at least for the above range of small eddies. In the following pages an attempt is made to study the spectral law of small eddies in turbulent shear flow with a given pattern of mean motion without solid boundaries. In addition to the viscous dissipation function and the transfer function, as occurring in isotropic turbulence without mean motion, we have to consider the production function, the convection function, and the diffusion function, which arise from the presence of a pattern of mean motion.

The Navier-Stokes equation applied to a turbulent flow can be divided into two equations: an equation governing the mean, or primary motion U_i, and an equation governing the life history of the turbulent velocity, or velocity fluctuation u_i. The equation for the turbulent velocity that interests us the most is, for an incompressible flow:

$$\frac{\partial u_i}{\partial t}+\frac{\partial}{\partial x_j}(u_iU_j)=\nu\frac{\partial^2 u_i}{\partial x_j^2}-\frac{\partial}{\partial x_j}(U_iu_j)-\frac{\partial}{\partial x_j}\left(u_iu_j-\overline{u_iu_j}+\frac{p}{\rho}\delta_{ij}\right). \tag{1}$$

The mean velocity U_i and the velocity fluctuation u_i must fulfill the equations of continuity

$$\partial U_i/\partial x_i=0, \quad \partial u_i/\partial x_i=0. \tag{2}$$

The independent variables in the equations are the time t and the coordinates x_i, x_j. Like the velocity, the pressure is decomposed into a mean pressure P, and a superposed pressure fluctuation p. ρ represents the density of the fluid and μ its viscosity, while $\nu=\mu/\rho$. ρ, μ, ν are treated as constant. The indices i, j, denote projection components. They are $i=1, 2, 3$, $j=1, 2, 3$. A summation is understood where the indices repeat. The bar over a quantity represents a spatial mean value.

We shall study the spectral distribution of the energy of the turbulent motion in a given field of primary motion. The interaction between the primary and the turbulent motion is controlled by terms such as $\partial(u_iU_j)/\partial x_j$, and $\partial(U_iu_j)\partial x_j$ in the hydrodynamical equation (1). According to this equation, the structure of the field at a given instant is characterized by three kinds of motions—a mean or primary motion, which gives rise to production, convection, and diffusion of turbulence; a turbulent motion, which possesses a transfer of energy; and a molecular motion playing the role of viscous dissipation. The three motions have their own geometrical patterns generally different in average scales. In order to fix our ideas, we can choose a large

[1] Figures in brackets indicate the literature references at the end of this paper.

region of size R, in which the primary motion shows certain geometrical patterns. At a given point we draw an element of volume of dimensions $2X_1$, $2X_2$, $2X_3$, having several times the dimensions of the largest eddy to be included in the study. If we study the spectrum, or the energy carried by the eddies of different sizes contained in the element of volume, we can expect, according to the differential orders of the terms in the hydrodynamical equation, that the molecular action enters from the end of the small eddies, and the action of the primary motion from the end of the large eddies.

If we do not go down to the range of the molecular sizes, the action of the viscosity on the turbulent motion has a simple form, where the two motions are separated. On the other hand, if we do not go up to the very big eddies, and if the primary motion has a slowly varying pattern, or simple pattern, so that within the element of volume the velocity change can be considered constant and small, the action of the primary motion on the turbulent motion has also a simple form, where the two motions are separated without resonance. On the contrary, if the primary motion has a complexly varying pattern, or rich pattern, so that in the volume element are presented various scales of the patterns of the primary motion, and that certain small scales are comparable to the eddies of the turbulent motion, the two motions will interact with resonance and are not separable. Such circumstances will occur when the average scale of the primary motion, as depending on U'/U'', U''/U''', etc., according to the similarity theory, is small and becomes comparable to the scales of the eddies to be studied.

Let us isolate the finite element of volume from its surroundings and study first, by means of an elementary method, the balance of energy per unit volume among the different eddies. For this purpose, let k be the wave-number magnitude, v_k the velocity, and $l \sim 1/k$ the mixing length. The vorticity of the turbulent motion can be represented by v_k/l. The vorticity presented in the pattern of the primary motion, averaged over the element, is supposed to be given, and is denoted by U'.

Let S_k be the flow of energy from larger eddies (larger than the eddy k) to smaller eddies (smaller than the eddy k). Such a flow of energy corresponds to a dissipation due to the following exchanges of momentum: between the molecular motion and the turbulent motion, between the small and large eddies, and between the turbulent motion and the primary motion. According to Prandtl and Boussinesq, it is known that the dissipation is the product of the viscosity with the square of the vorticity.

For the dissipation of molecular origin, we can write $\mu v_k^2/l^2$, where μ is the coefficient of viscosity due to molecular agitations. For the dissipation of turbulent origin, that is, the dissipation due to the exchange of momentum between the eddies of the turbulent motion itself, and between the turbulent motion and the primary motion, we can write

$$\text{turbulent dissipation} = \rho\nu_k \cdot \text{compound square velocity}.$$

Here ν_k is the turbulent viscosity of Heisenberg $\nu_k = v_k l$. If there is no resonance between the primary motion and the turbulent motion, the compound square vorticity is formed by the following independent terms:

$$\frac{v_k^2}{l^2} + U'^2,$$

the interaction term $(v_k/l)U'$ being dropped out. If there is strong resonance between the two motions, the independent term U'^2 must be dropped out, because any primary vorticity field that is able to create momentum exchange with eddies must be coupled to the turbulent vorticity. Thus the compound square vorticity becomes in this case

$$\frac{v_k^2}{l^2} + \frac{v_k}{l} U'.$$

Hence the equation of total dissipation is

$$S_k = \mu \frac{v_k^2}{l^2} + \rho v_k l \begin{cases} \dfrac{v_k^2}{l^2} + U'^2 & \text{no resonance.} \\ \dfrac{v_k}{l} U' & \text{strong resonance.} \end{cases}$$

The case of intermediate resonance is not investigated here.

A spectral function $F(k)$ can be introduced such that $\rho F(k)dk$ is the turbulent energy between k and $k+dk$. Then by means of dimensional reasoning, the dissipation equation can be put

in spectral terms as follows:

$$\frac{S_k}{\rho}=2\nu\int_0^k dk'\,k'^2F(k')+2\kappa\int_k^\infty dk''\sqrt{\frac{F(k'')}{k''^3}}\int_0^k dk'\,k'^2F(k')+$$

$$\kappa'\int_k^\infty dk''\sqrt{\frac{F(k'')}{k''^3}}\,U'\cdot\begin{cases}U' & \text{no resonance}\\ \dfrac{\kappa''}{\kappa'}\left[2\displaystyle\int_0^k dk'\,k'^2F(k')\right]^{\frac{1}{2}} & \text{strong resonance,}\end{cases}$$

where κ, κ', κ'' are numerical constants to be determined by experiments.

We shall study the spectral laws in the equilibrium range of spectrum, which, as defined by Heisenberg, is the range controlled by a constant flow of energy S_k, independent of k. In the equilibrium range, two subranges are defined: the nonviscous, or inertial, subrange, as characterized by $v_k/k\nu \gg 1$, and the viscous subrange, as characterized by $v_k/k\nu \ll 1$. For the nonviscous subrange we obtain

$$v \sim k^{-1/3}, \qquad \text{or} \qquad F\sim k^{-5/3} \qquad \text{for small } U' \text{ and no resonance;}$$

and

$$v_k\sim\text{constant}, \qquad \text{or} \qquad F\sim k^{-1} \qquad \text{for large } U' \text{ and strong resonance.}$$

For the viscous subrange we obtain

$$v_k\sim k^{-3}, \qquad \text{or} \qquad F\sim k^{-7} \qquad \text{for arbitrary } U' \text{ and resonance.}$$

The spectral law k^{-7} is not expected to go down to molecular scales, as then the strong interference between the molecular motion and the turbulent motion will alter the above simple forms of the molecular and turbulent dissipations.

The above elementary study of the spectrum of turbulence is based on the considerations of the different forms of the exchange of momentum within an isolated volume element. Actually, the volume element is not isolated, and the general character of the field from one element to another may vary. Under those circumstances we may expect that the general spectrum depends on the position of the element analyzed, and that there exists an exchange of momentum between the element chosen and its neighbors, in the forms of convection and diffusion. However, the latter forms of exchange, called inhomogeneous exchange, have scales comparable to the dimensions of the volume elements and thus affect predominantly the large eddies rather than the eddies in the equilibrium range in which we are interested for the present. We shall return to the discussions of convection and diffusion in sections 3 and 4. We conclude that in the study of the equilibrium range of spectrum, we can analyze the inhomogeneous field as follows:

1. We choose a finite element of volume $2X_1\cdot 2X_2\cdot 2X_3$, which is of the order of several times the scales of the largest eddy of the equilibrium range. In the element of volume a turbulent motion is superposed to a primary motion exhibiting certain geometrical patterns. Both motions can be analyzed into Fourier components by the same method as applied to a homogeneous field.

2. The inhomogeneity of the general field creates an inhomogeneous exchange of momentum between the chosen element of volume and its neighbors, resulting in convection and diffusion. Such an exchange of large scales is not important to the study of eddies in the equilibrium range (small eddies). Thus it can be estimated approximately and added to the homogeneous exchange as small corrections.

2. Harmonic Analysis of a Turbulent Motion

The results predicted in section 1 by means of elementary considerations of energy distribution can be obtained by a harmonic analysis of the hydrodynamical equations. Such an analysis will reveal some important details of the exchange mechanism and of the energy balance, which are rather obscure in the elementary considerations.

The applications of Fourier analysis to a turbulent field has the difficulty that Fourier integrals can be defined only for functions that vanish at infinity in such a way that their squares take a finite integrable value. To overcome this difficulty, one usually assumes in the harmonic analysis of turbulence that we can restrict to the values of the function within a finite domain, say a finite element of volume $2X_1\cdot 2X_2\cdot 2X_3$ taken at a point x_1, x_2, x_3 as center, while outside

this domain the function is replaced by zero.[2] For the purpose of the analysis of turbulence, the Fourier integral of the turbulent velocity in such a finite domain will be sufficiently representative of the energy distribution of eddies smaller than the element. The amplitude functions of the Fourier coefficients are then obtained from

$$a_i(\boldsymbol{k})=\frac{1}{(2\pi)^3}\int_{x-X}^{x+X} d\boldsymbol{x}' u_i(\boldsymbol{x}')e^{-\iota\boldsymbol{k}\cdot\boldsymbol{x}'} \tag{3}$$

$$A_i(\boldsymbol{k})=\frac{1}{(2\pi)^3}\int_{x-X}^{x+X} d\boldsymbol{x}' U_i(\boldsymbol{x}')e^{-\iota\boldsymbol{k}\cdot\boldsymbol{x}'} \tag{3a}$$

$$c(\boldsymbol{k})=\frac{1}{(2\pi)^3}\int_{x-X}^{x+X} d\boldsymbol{x}' p(\boldsymbol{x}')e^{-\iota\boldsymbol{k}\cdot\boldsymbol{x}'} \tag{3b}$$

with the equations of continuity

$$k_i a_i(\boldsymbol{k})=0, \qquad k_i A_i(\boldsymbol{k})=0. \tag{4}$$

Here u_i, U_i, p are real quantities representing the turbulent velocity components, the mean velocity components, and the turbulent pressure, respectively, $a_i(\boldsymbol{k})$, $A_i(\boldsymbol{k})$, $c(\boldsymbol{k})$ are the corresponding Fourier coefficients at the wave-number vector $\boldsymbol{k}$ ($\boldsymbol{k}=2\pi/$wavelength), and are complex quantities, with $a_i^*(\boldsymbol{k})=a_i(-\boldsymbol{k})$, etc. An asterisk over a quantity denotes its conjugate, and $\iota=\sqrt{-1}$. The following symbol for the volume integral is used:

$$\int_a^b d\boldsymbol{x}'=\int_{a_1}^{b_1}\int_{a_2}^{b_2}\int_{a_3}^{b_3} dx_1' dx_2' dx_3'.$$

The actual change of u_i and p in the course of time is resolved into the change of the Fourier coefficients a_i and c with the time. Provisionally, we restrict to the single instant. The analysis in a finite volume renders the Fourier coefficients bounded. Outside and on the boundary of the finite volume ($\boldsymbol{x}'\leq\boldsymbol{x}-\boldsymbol{X}$, $\boldsymbol{x}'\geq\boldsymbol{x}+\boldsymbol{X}$), the function $u_i(\boldsymbol{x}')$ and its derivative $\partial u_i(\boldsymbol{x}')/\partial x_j'$ are supposed to vanish; so also do $p(\boldsymbol{x}')$ and $U_i(\boldsymbol{x}')$. Such functions are called *truncated functions*.

To show the significance of the limit $\boldsymbol{X}$, we form:

$$u_i(\boldsymbol{x})u_j(\boldsymbol{x}+\boldsymbol{r})=\int_{-\infty}^{+\infty} d\boldsymbol{k}'\int_{-\infty}^{+\infty} d\boldsymbol{k}'' a_i(\boldsymbol{k}')a_j(-\boldsymbol{k}'')e^{\iota(\boldsymbol{k}'-\boldsymbol{k}'')\cdot\boldsymbol{x}-\iota\boldsymbol{k}''\cdot\boldsymbol{r}}$$

The mean value $\overline{u_i(\boldsymbol{x})u_j(\boldsymbol{x}+\boldsymbol{r})}$ is obtained by integrating with respect to $\boldsymbol{x}$ from $-\boldsymbol{X}'$ to $+\boldsymbol{X}'$, where $\boldsymbol{X}'>\boldsymbol{X}$. We have

$$\overline{u_i(\boldsymbol{x})u_j(\boldsymbol{x}+\boldsymbol{r})}=\frac{1}{X_1X_2X_3}\int_{-\infty}^{+\infty} d\boldsymbol{k}'\int_{-\infty}^{+\infty} d\boldsymbol{k}'' e^{-\iota\boldsymbol{k}''\cdot\boldsymbol{r}}a_i(\boldsymbol{k}')a_j(-\boldsymbol{k}'')\cdot \frac{(\sin k_1'-k_1'')X_1'}{k_1'-k_1''}\ \frac{\sin(k_2'-k_2'')X_2'}{k_2'-k_2''}\ \frac{\sin(k_3'-k_3'')X_3'}{k_3'-k_3''},$$

which for $\boldsymbol{X}'\to\infty$ leads to

$$\overline{u_i(\boldsymbol{x})u_j(\boldsymbol{x}+\boldsymbol{r})}=\frac{\pi^3}{X_1X_2X_3}\int_{-\infty}^{+\infty} d\boldsymbol{k}\, a_i(\boldsymbol{k})a_j(-\boldsymbol{k})e^{-\iota\boldsymbol{k}\cdot\boldsymbol{r}}.$$

Since $\overline{u_i(\boldsymbol{x})u_j(\boldsymbol{x}+\boldsymbol{r})}$ must be independent of $\boldsymbol{X}$, it follows that the absolute value of the amplitude function must be proportional to $(X_1X_2X_3)^{1/2}$. As a_i is obtained by the summation of a large number of variables like $u_i(\boldsymbol{x}')e^{\iota\boldsymbol{k}\cdot\boldsymbol{x}'}$ according to (3), the fact that its absolute value is proportional to the square root of the volume must be related to the same results found in problems of radom walk, even though the paths may be correlated [10].

[2] To avoid discontinuities that may arise by such a method at the edges of the elementary volume, we may instead multiply the function by a certain function that is unity within the volume, and decays rapidly to zero beyond the volume.

If we take $r=0$ and $j=i$, we find

$$\overline{u_i^2}=\frac{\pi^3}{X_1X_2X_3}\int_{-\infty}^{+\infty}d\boldsymbol{k}\,a_i(\boldsymbol{k})a_i(-\boldsymbol{k}).$$

Instead of extending the integral over the whole $\boldsymbol{k}$-space, we can integrate over a spherical shell of radii between k and $k+dk$, and we find

$$2F(k)=\frac{\pi^3}{X_1X_2X_3}\int_0^{2\pi}d\varphi\int_0^{\pi}d\theta\sin\theta\,k^2a_i(\boldsymbol{k})a_i(-\boldsymbol{k})\quad\text{with}\quad 2\int_0^{\infty}dk'F(k')=\overline{u_i^2}\tag{5}$$

Here $k^2\sin\theta\,d\theta\,d\varphi$ is the volume element with polar angles θ, φ, and $F(k)dk$ is the energy associated with the wave numbers ranged between k and $k+dk$. $F(k)$ will be referred to customarily as spectral function of turbulent energy. Also we can define a spectral function of the turbulent shear stress $F_{ij}(k)$ such that

$$2F_{ij}(k)=\frac{\pi^3}{X_1X_2X_3}\int_0^{2\pi}d\varphi\int_0^{\pi}d\theta\sin\theta\,k^2\,\tfrac{1}{2}\,[a_i(\boldsymbol{k})a_j(-\boldsymbol{k})+a_i(-\boldsymbol{k})a_j(\boldsymbol{k})]\quad\text{with}\quad 2\int_0^{\infty}dk'F_{ij}(k')=\overline{u_iu_j}.\tag{6}$$

By a Fourier transform of (1) term by term, we have

$$\frac{\partial a_i(\boldsymbol{k})}{\partial t}+\int_{-\infty}^{+\infty}d\boldsymbol{n}\,\iota n_jA_i(\boldsymbol{n})A_j(\boldsymbol{k}-\boldsymbol{n})=-\nu k^2a_i(\boldsymbol{k})-\int_{-\infty}^{+\infty}d\boldsymbol{n}\,\iota n_jA_i(\boldsymbol{n})a_j(\boldsymbol{k}-\boldsymbol{n})-$$
$$\int_{-\infty}^{+\infty}d\boldsymbol{n}\,\iota n_ja_i(\boldsymbol{n})a_j(\boldsymbol{k}-\boldsymbol{n})-\frac{1}{\rho}\iota k_ic(\boldsymbol{k})-\text{inhomogeneous terms},$$

where the inhomogeneous terms arise from the inhomogeneous exchange as explained in section 1 and to be determined in sections 3 and 4. In the above equation c can be eliminated by its value obtained from the above equation multiplied by k_i, subjected to the conditions of continuity (4). The transformed equation is then

$$\frac{\partial a_i(\boldsymbol{k})}{\partial t}=-\nu k^2a_i(\boldsymbol{k})-\int_{-\infty}^{+\infty}d\boldsymbol{n}\,\iota n_ja_j(\boldsymbol{k}-\boldsymbol{n})\left[a_i(\boldsymbol{n})-\frac{k_ik_s}{k^2}a_s(\boldsymbol{n})\right]-$$
$$\int_{-\infty}^{+\infty}d\boldsymbol{n}\,\iota n_ja_j(\boldsymbol{k}-\boldsymbol{n})\left[A_i(\boldsymbol{n})-\frac{k_ik_s}{k^2}A_s(\boldsymbol{n})\right]-$$
$$\int_{-\infty}^{+\infty}d\boldsymbol{n}\,\iota n_jA_j(\boldsymbol{k}-\boldsymbol{n})\left[a_i(\boldsymbol{n})-\frac{k_ik_s}{k^2}a_s(\boldsymbol{n})\right]-\text{inhomogeneous terms}.$$

An equation describing the rate of change of the energy distribution can be obtained by forming the differential quotient $(\partial/\partial t)a_i(\boldsymbol{k})a_i(-\boldsymbol{k})$ as follows:

$$\frac{\partial}{\partial t}a_i(\boldsymbol{k})a_i(-\boldsymbol{k})=-2\nu k^2a_i(\boldsymbol{k})a_i(-\boldsymbol{k})-$$
$$\int_{-\infty}^{+\infty}d\boldsymbol{n}\,\iota n_ja_i(\boldsymbol{n})\,[a_j(\boldsymbol{k}-\boldsymbol{n})a_i(-\boldsymbol{k})+a_j(-\boldsymbol{k}-\boldsymbol{n})a_i(\boldsymbol{k})]-$$
$$\int_{-\infty}^{+\infty}d\boldsymbol{n}\,\iota n_jA_i(\boldsymbol{n})\,[a_j(\boldsymbol{k}-\boldsymbol{n})a_i(-\boldsymbol{k})+a_j(-\boldsymbol{k}-\boldsymbol{n})a_i(\boldsymbol{k})]-\tag{7}$$
$$\int_{-\infty}^{+\infty}d\boldsymbol{n}\,\iota n_ja_i(\boldsymbol{n})\,[A_j(\boldsymbol{k}-\boldsymbol{n})a_i(-\boldsymbol{k})+A_j(-\boldsymbol{k}-\boldsymbol{n})a_i(\boldsymbol{k})]-\text{inhomogeneous terms}.$$

The physical meaning of the equation for energy distribution (7) can be compared with the following equation for over-all balance obtained by multiplying (1) by u_i and taking the spatial mean values as follows:

$$\frac{\partial}{\partial t}\frac{\overline{u_i^2}}{2}=-\nu\overline{\left(\frac{\partial u_i}{\partial x_j}\right)^2}-\overline{u_iu_j}\frac{\partial U_i}{\partial x_j}-\frac{\partial}{\partial x_j}\left(\frac{\overline{u_i^2}}{2}U_j\right)+\nu\frac{\partial^2}{\partial x_j^2}\frac{\overline{u_i^2}}{2}-\frac{\partial}{\partial x_j}\left[\overline{u_j\left(\frac{u_i^2}{2}+\frac{p}{\rho}\right)}\right]\tag{7a}$$

Equation (7) represents the balance of energy associated with the wave number k, while eq (7a) represents the balance of energy covering the whole spectrum. The correspondence between terms of the two equations is as follows:

(a) Rate of change of energy:

$$\frac{1}{2}\frac{\pi^3}{X_1X_2X_3}\int_{-\infty}^{+\infty} d\boldsymbol{k}\frac{\partial}{\partial t}a_i(\boldsymbol{k})a_i(-\boldsymbol{k})=\frac{\partial}{\partial t}\frac{\overline{u_i^2}}{2}.$$

For a stationary flow these two terms vanish.

(b) Dissipation by viscosity:

$$\frac{1}{2}\frac{\pi^3}{X_1X_2X_3}\int_{-\infty}^{+\infty} d\boldsymbol{k}\,2\nu k^2a_i(\boldsymbol{k})a_i(-\boldsymbol{k})=\nu\overline{(\partial u_i/\partial x_j)^2}.$$

(c) Transfer of energy from eddies to eddies:

$$-\int_{-\infty}^{+\infty} d\boldsymbol{n}\,\iota n_j a_i(\boldsymbol{n})\,[a_j(\boldsymbol{k}-\boldsymbol{n})a_i(-\boldsymbol{k})+a_j(-\boldsymbol{k}-\boldsymbol{n})a_i(\boldsymbol{k})].$$

This term which figures in (7) has no corresponding term in (7a), because the total transfer must vanish for the whole spectrum.

(d) Production of turbulent energy by shearing stresses:

$$\frac{1}{2}\frac{\pi^3}{X_1X_2X_3}\int_{-\infty}^{+\infty} d\boldsymbol{k}\int_{-\infty}^{+\infty} d\boldsymbol{n}\,\iota n_j A_i(\boldsymbol{n})\,[a_j(\boldsymbol{k}-\boldsymbol{n})a_i(-\boldsymbol{k})+a_j(-\boldsymbol{k}-\boldsymbol{n})a_i(\boldsymbol{k})]=\overline{u_iu_j}\frac{\partial U_i}{\partial x_j}.$$

(e) Convection of turbulent energy by interaction with mean motion:

$$\frac{1}{2}\frac{\pi^3}{X_1X_2X_3}\int_{-\infty}^{+\infty} d\boldsymbol{k}\int_{-\infty}^{+\infty} d\boldsymbol{n}\,\iota n_j a_i(n)\,[A_j(\boldsymbol{k}-\boldsymbol{n})a_i(-\boldsymbol{k})+A_j(-\boldsymbol{k}-\boldsymbol{n})a_i(\boldsymbol{k})]=\frac{\partial}{\partial x_j}\left(\frac{\overline{u_i^2}}{2}U_j\right).$$

(f) Inhomogeneous transport: This is the part of convection from the inhomogeneity of the field. Thus in (7a) the terms

$$\frac{\partial}{\partial x_j}\frac{\overline{u_i^2}}{2},\qquad \frac{\partial^2}{\partial x_i^2}\frac{\overline{u_i^2}}{2},\qquad \frac{\partial}{\partial x_j}\left[\overline{u_j\left(\frac{u_i^2}{2}+\frac{p}{\rho}\right)}\right]$$

correspond to the inhomogeneous terms of (7), to be determined in sections 3 and 4. For a stationary condition the left-hand side of (7) must vanish. Integration between k and ∞ gives

$$2\nu\int_0^{\infty} dk'k'^2F(k')=2\nu\int_0^{k} dk'k'^2F(k')+W(k,\infty)+\psi(k,\infty)+C(k,\infty)+K(k,\infty). \tag{8}$$

This equation expresses the equilibrium in the exchange of energy. The left-hand side is the total viscous dissipation covering the whole spectrum. It is the total flow of energy. It is independent of k and will be represented by ϵ. The first term on the right-hand side gives the loss of energy through viscous dissipation associated with wave numbers not exceeding k. The other four terms give the flow of energy from this part of the spectrum through interaction with the remainder of the spectrum, respectfully, in the forms of transfer, production, convection, and diffusion, as to be obtained by integrating the corresponding terms of (7) for wave numbers not exceeding k.

3. Transfer, Production, and Convection of Turbulence

For the transfer function $W(k,\infty)$, we assume the Heisenberg formula [6].

$$W(k,\infty)=\kappa\int_k^{\infty} dk''\sqrt{\frac{F(k'')}{k''^3}}\,2\int_0^{k} dk'k'^2F(k'), \tag{9}$$

where κ is a numerical constant. The justification of the dissipative character of the transfer and hence of the Heisenberg theory, can be sought from the transport processes by turbulence on the basis of the hydrodynamical equations. We shall return to this problem in a subsequent communication.

For the production function $\Psi(k, \infty)$, we assume a gradient of U_1 in the x_2 direction, as expressed by $\partial U_1/\partial x_2$, all other gradients being negligible, and distinguish the case of no resonance and strong resonance, depending on the scale of the primary motion, as mentioned in section 1.

(a) When there is negligible resonance between the mean and the turbulent motions, we can neglect n compared to k in the following production term:

$$\int_{-\infty}^{+\infty} d\boldsymbol{n}\, \imath\, n_2 A_1(\boldsymbol{n})[a_2(\boldsymbol{k}-\boldsymbol{n})a_1(-\boldsymbol{k}) + a_2(-\boldsymbol{k}-\boldsymbol{n})a_1(\boldsymbol{k})] \simeq [a_1(-\boldsymbol{k})a_2(\boldsymbol{k}) + a_1(\boldsymbol{k})a_2(-\boldsymbol{k})] \cdot U'$$

where [2]

$$\int_{-\infty}^{+\infty} d\boldsymbol{n}\, \imath\, n_2 A_1(\boldsymbol{n}) = U'$$

is the magnitude of the average vorticity of the mean motion for a quickly dropping spectrum $A_1(\boldsymbol{n})$. Integration of the production term over the wave numbers of magnitudes between k and ∞ gives

$$\Psi(k, \infty) = 2\int_k^\infty dk' F_{12}(k') \cdot U'. \tag{10}$$

If, according to Prandtl and Broussinesq [8, 9,], we write

$$2\int_k^\infty dk' F_{12}(k') = \kappa' \int_k^\infty dk'' \sqrt{\frac{F(k'')}{k''^3}} \cdot U', \tag{11}$$

where $k' \int_k^\infty dk'' \sqrt{F(k'')/k''^3}$ is a turbulent viscosity, and κ' is a numerical constant, eq (10) is reduced to

$$\Psi(k, \infty) = \kappa' \int_k^\infty dk'' \sqrt{\frac{F(k'')}{k''^3}} \cdot U'^2, \text{ for negligible resonance.} \tag{12}$$

(b) When there is strong resonance between the mean and turbulent motions as described in section 1, in such a way that we cannot separate them *a priori* by the method used in (a), a new method has to be devised in order to formulate the production function Ψ. Integration of (7) outside the sphere of radius k gives the transfer and production functions as follows:

$$-W(k, \infty) = \frac{\pi^3}{X_1 X_2 X_3} \int_k^\infty d\boldsymbol{k}'' \int_0^\infty d\boldsymbol{n}\, \imath\, \boldsymbol{n}_j a_i(\boldsymbol{n}) a_j(\boldsymbol{k}''-\boldsymbol{n}) a_i(-\boldsymbol{k}'') + \text{conjugate}$$

$$-\Psi(k, \infty) = \frac{\pi^3}{X_1 X_2 X_3} \int_k^\infty d\boldsymbol{k}'' \int_0^\infty d\boldsymbol{n}\, \imath\, \boldsymbol{n}_j A_i(\boldsymbol{n}) a_j(\boldsymbol{k}''-\boldsymbol{n}) a_i(-\boldsymbol{k}'') + \text{conjugate}.$$

---

[2] By applying the Fourier formula (3a), the amplitude function of the vorticity is

$$\imath\, n_2 A_1(n_2) = \frac{1}{2\pi} \int_{-X_2}^{+X_2} dx_2 \frac{\partial U_1}{\partial x_2} e^{-\imath n_2 x_2}$$

and

$$\int_{-\infty}^{+\infty} dn_2\, \imath\, n_2 A_1(n_2) = \frac{1}{2\pi} \int_{-\infty}^{+\infty} dn_2 \int_{-X_2}^{+X_2} dx_2 \frac{\partial U_1}{\partial x_2} e^{-\imath n_2 x_2}$$

If the vorticity does not change too much within $(-X_2, +X_2)$, and has an average value U', as is the case here, we can write, as a first approximation:

$$\int_{-\infty}^{+\infty} dn_2\, \imath\, n_2 A_1(n_2) = \frac{1}{\pi} \int_{-\infty}^{+\infty} dn_2 \frac{\sin n_2 X_2}{n_2} \cdot U' = U',$$

the factor before U' being unity.

We notice that they are analogous in structural form, except that the transfer function contains a triple correlation

$$q(\boldsymbol{n}, \boldsymbol{k''}) \equiv \iota n_j \, a_i(\boldsymbol{n}) a_j(\boldsymbol{k''}-\boldsymbol{n}) a_i(-\boldsymbol{k''}) + \text{conjugate},$$

which is antisymmetrical: $q(\boldsymbol{n}, \boldsymbol{k''}) = -q(\boldsymbol{k''}, \boldsymbol{n})$, while the production function contains a triple correlation involving the gradient of the mean motion and is not antisymmetrical. For the antisymmetrical function, we can replace

$$\int_k^\infty dk'' \int_0^\infty dn \qquad \text{by} \qquad \int_k^\infty dk'' \int_0^k dn, \tag{13}$$

in agreement with the form of integrals given to $W(k, \infty)$ in (9). For the production function, we can take the following form, because of its structual analogy with the transfer function:

$$\Psi(k, \infty) = \kappa'' \int_k^\infty dk'' \sqrt{\frac{F(k'')}{k''^3}} \cdot (\text{vorticity of turbulent motion} \cdot \text{vorticity of mean motion}) \tag{14}$$

Now the vorticity of the turbulent motion can be written in the usual form

$$\left[2 \int_0^k dk' \, k'^2 F(k')\right]^{\frac{1}{2}},$$

while the vorticity of the mean motion is U'. We can remark that transformation (13) does not apply to correlations involving the mean motion, and therefore the vorticity of the mean motion is written for its whole spectrum. After substitution for the vorticities, (14) becomes:

$$\Psi(k, \infty) = \kappa'' \int_k^\infty dk'' \sqrt{\frac{F(k'')}{k''^3}} \left[2 \int_k^\infty dk' k'^2 F(k') \cdot U'^2\right]^{\frac{1}{2}}. \tag{15}$$

Finally we shall integrate the convection term of (7) for the region outside the sphere of radius k. We can remark that the transfer, production, and convection contain, respectively, the triple correlations

$$\iota n_j a_i(\boldsymbol{n}) a_j(\boldsymbol{k}-\boldsymbol{n}) a_i(-\boldsymbol{k}) + \text{conjugate}$$

$$\iota n_j A_i(\boldsymbol{n}) a_j(\boldsymbol{k}-\boldsymbol{n}) a_i(-\boldsymbol{k}) + \text{conjugate}$$

$$\iota n_j a_i(\boldsymbol{n}) A_j(\boldsymbol{k}-\boldsymbol{n}) a_i(-\boldsymbol{k}) + \text{conjugate}.$$

By analogy with the expression (9) and (15) for the transfer and the production, we can formulate an expression for the convection function. However, we assume that the apparent viscosity is much smaller for the mean motion than for the turbulent motion, for the sufficiently large value of k herewith considered; hence the convection function is negligible compared to $W(k, \infty)$ for sufficiently large k.

4. Diffusion by Inhomogeneity of the Field

Let us consider a case with the following simple conditions:

(a) The diffusion due to the inhomogeneity is primarily a large scale phenomenon, and hence the molecular diffusion can be neglected compared to the turbulent diffusion.

(b) The mean pressure is constant in time and space.

The difference of energy distribution in the space causes a flux of energy as a consequence of the exchange of matter. This flux of energy can be written as

$$\text{flux of energy} = \kappa''' \int_k^\infty dk'' \sqrt{\frac{F(k'')}{k''^3}} \cdot \frac{\partial}{\partial x_2} \left[\rho \int_0^k dk' F(k')\right].$$

The first integral is the turbulent viscosity, the gradient is the gradient of the energy distribution, and κ''' is a numerical constant to be determined by experiment. By taking the difference of the fluxes across opposite faces of the elementary space and dividing by ρ, we obtain the

rate of decrease of energy by diffusion per unit mass and unit time equal to

$$K(k,\infty)=\frac{\partial}{\partial x_2}\left[\kappa'''\int_k^\infty dk''\sqrt{\frac{F(k'')}{k''^3}}\cdot\frac{\partial}{\partial x_2}\int_0^k dk'F(k')\right].$$

Finally, if k is chosen sufficiently large so that the range from 0 to k includes practically all the energy gradient, we can write

$$\frac{\partial}{\partial x_2}\int_0^k dk'F(k')\cong\frac{\partial}{\partial x_2}\left(\frac{1}{2}\overline{u_i^2}\right).$$

Hence

$$K(k,\infty)\cong\frac{\partial}{\partial x_2}\left[k'''\int_k^\infty dk''\sqrt{\frac{F(k'')}{k''^3}}\,\frac{\partial}{\partial x_2}\left(\frac{1}{2}\overline{u_i^2}\right)\right] \tag{16}$$

5. Energy Spectrum of Turbulence

In the equilibrium range the energy spectrum is determined by eq 8, which becomes, after substitution of (9), (12), (15), and (16),

$$\epsilon=2\nu\int_0^k dk'k'^2F(k')+2\kappa\int_k^\infty dk''\sqrt{\frac{F(k'')}{k''^3}}\int_0^k dk'k'^2F(k')+$$

$$\kappa'\int_k^\infty dk''\sqrt{\frac{F(k'')}{k''^3}}\cdot U'^2\zeta+\frac{\partial}{\partial x_2}\left[\kappa'''\int_k^\infty dk''\sqrt{\frac{F(k'')}{k''^3}}\,\frac{\partial}{\partial x_2}\left(\frac{1}{2}\overline{u_i^2}\right)\right] \tag{17}$$

with

$$\zeta=\begin{cases}1, \text{ no resonance}\\ \dfrac{\kappa''}{\kappa'}\left[\dfrac{2\displaystyle\int_0^k dk'k'^2F(k')}{U'^2}\right]^{\frac{1}{2}}, \text{ strong resonance}\end{cases} \tag{17a}$$

We shall study the energy spectrum for the following subranges: (a) nonviscous subrange with large U' and strong resonance, (b) nonviscous subrange with small U' and no resonance, and (c) viscous subrange with arbitrary U' and arbitrary resonance.

(a) In the nonviscous subrange of the spectrum, if there is a strong resonance and if U' is large, along with sufficiently small k, we have

$$2\int_0^k dk'k'^2F(k')\ll U'^2,$$

thus the production function is predominant, and all other functions are negligible. In this way eq (17) reduces to

$$\frac{\epsilon}{\kappa''U'}=\int_k^\infty dk''\sqrt{\frac{F(k'')}{k''^3}}\left[2\int_0^k dk'k'^2F(k')\right]^{\frac{1}{2}}$$

and has the solution $F=(\epsilon/\kappa''U')k^{-1}$ to be obtained simply by introducing the new variable $g^2=2\int_0^k dk'k'^2F(k')$. If the diffusion term is small, but not negligible, then as a first approximation, the solution is

$$F=\frac{\epsilon}{\kappa''U'}k^{-1}(1-k_r/k),$$

where

$$k_r=\frac{\kappa''}{\epsilon}\,\frac{\partial}{\partial x_2}\left[\left(\frac{\epsilon}{\kappa''U'^2}\right)^{\frac{1}{2}}\frac{\partial}{\partial x_2}\left(\frac{1}{2}\overline{u_i^2}\right)\right]$$

and k_r/k is assumed to be small compared to unity.

(b) In the nonviscous subrange, if there is no resonance and U' is small, along with sufficiently large k, we have

$$2\int_0^k dk' k'^2 F(k') \gg U'^2.$$

Thus the production function and the diffusion function are small, although not negligible compared to the transfer function, and eq (17) gives the following solution as a first approximation:

$$F = \left(\frac{8\epsilon}{9\kappa}\right)^{2/3} k^{-5/3} [1 - (k_p/k)^{4/3}]^{2/3}, \tag{18}$$

where

$$k_p^{4/3} = \left(\frac{3}{8}\frac{\kappa'^3}{\kappa}\frac{1}{\epsilon^2}\right)^{1/3} U'^2 + \left(\frac{3}{8}\frac{\kappa'''}{\kappa}\frac{1}{\epsilon^3}\right)^{1/3} \frac{\partial}{\partial x_2}\left[\epsilon^{1/3}\frac{\partial}{\partial x_2}\left(\frac{1}{2}\overline{u_i^2}\right)\right],$$

and k_p/k is assumed to be small compared to unity. The spectrum

$$F = \left(\frac{8\epsilon}{9\kappa}\right)^{2/3} k^{-5/3}$$

of the homogeneous and isotropic turbulence is a particular case corresponding to $k_p = 0$.

For the reasons incorporated already in the conditions under which the respective laws k^{-1} and $k^{-5/3}$ are obtained, it is to be understood that the former law refers usually to larger eddies than does the latter one. Depending upon specific conditions, a spectrum may show clearly a portion representative of one of the laws and not the other, or may show clearly two portions representative of both laws successively. In the latter case, the primary motion possesses a pattern in resonance with the secondary motion. As the result of the resonance, the production function is first larger than the transfer function at small k, hence the spectrum shows a k^{-1} law. Afterwards, as k increases, the production function becomes smaller than the transfer function, while U' is not large enough to compensate, hence the spectrum changes over to a $k^{-5/3}$ law. The ranges of validity of the laws depend upon the ranges of predominance either by the production function or by the transfer function. For the viscous subrange, which we shall study in (c), the eddies are much smaller than the nonviscous subrange. Consider the case where we have a k^{-1} law, thus k is small and U' is large. Suppose that the Reynolds number is not sufficiently large, so that the viscous dissipation may become so important as to alter the tail portion of the k^{-1} spectrum. Under such circumstances, for increasing wave numbers, the k^{-1} law may pass over directly to the k^{-7} law, without a noticeable portion of the $k^{-5/3}$ law. For very small Reynolds numbers, a larger part of the tail portion or even the whole of the k^{-1} law may be affected, as could be observed in the turbulent flow in the close vicinity of a wall.

(c) In the viscous subrange, the turbulent friction of turbulent viscosity

$$\kappa \int_k^\infty dk'' \sqrt{F(k'')/k''^3}$$

is much smaller than the molecular friction. By differentiating (17) with respect to k, and by neglecting the turbulent viscosity compared to the molecular viscosity, we have

$$0 \simeq 2\nu k^2 F - \frac{\kappa\epsilon}{\nu}\sqrt{\frac{F}{k^3}}\left[1 + \frac{\kappa'}{\kappa}\frac{\nu}{\epsilon}U'^2\zeta_\infty + \frac{\kappa'''}{\kappa}\frac{\nu}{\epsilon}\frac{\partial^2}{\partial x_2^2}(\overline{u_i^2}/2)\right],$$

where ζ_∞ is obtained by putting $k = \infty$ in expression (17a).
The solution follows:

$$F = \left(\frac{\kappa\epsilon}{2\nu^2}\right)^2 k^{-7}\left[1 + \frac{\kappa'}{\kappa}\frac{\nu}{\epsilon}U'^2\zeta_\infty + \frac{\kappa'''}{\kappa}\frac{\nu}{\epsilon}\frac{\partial^2}{\partial x_2^2}(\overline{u_i^2}/2)\right].$$

For homogeneous and isotropic turbulence, the above formula degenerates to the Heisenberg formula [6]

$$F = \left(\frac{\kappa\epsilon}{2\nu^2}\right)^2 k^{-7}.$$

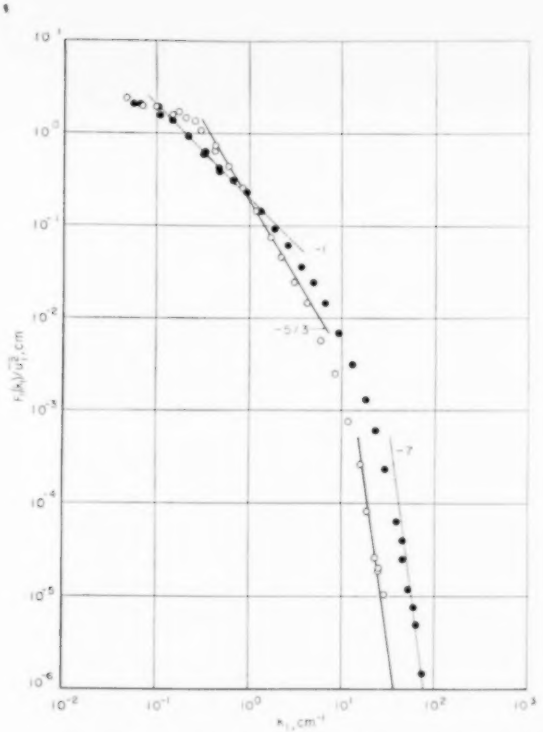

FIGURE 1. *Energy spectrum in a turbulent boundary layer.*

$F_1(k_1)$ is the spectrum of u_1^2 associated with the wave number k_1. The free stream velocity is 15 m/sec. The measurements are made at a distance of 320 cm downstream from the leading edge of the flat plate. The thickness of the boundary layer is 7.6 cm. The open circles are measurements at a distance of 6 cm. from the wall, and the crossed circles are measurements at a distance of 0.4 cm from the wall. The data are new measurements made by Klebanoff at the National Bureau of Standards. Some early results are published in reference [11].

The k^{-7} law follows from the assumption of the Heisenberg expression for the transfer function. We see that the eddies in the viscous subrange of the spectrum are not effected by any shear.

We shall compare (see fig. 1) the above results with the experimental investigations in a turbulent boundary layer made by P. S. Klebanoff and Z. W. Diehl [11]. It is to be remarked that the available measurements give the spectral function for $\overline{u_i^2}/2$ in the one-dimensional analysis of the wave-number space, while the spectral function in the theory refers to the energy $\overline{u_i^2}/2$ for the wave-number magnitude in the three dimensional analysis of the wave-number space. Assuming that the power laws for sufficiently large k remains unaltered by the transformation between the two kinds of spectral functions for the cases considered, we see that the laws k^{-1}, $k^{-5/3}$, k^{-7} agree with experiments respectively for the following cases:

(a) Near the wall where the average scale of the primary motion is small, there is strong resonance between the primary motion and the turbulent motion. If, moreover,

$$U'^2 \gg 2\int_0^k dk' k'^2 F(k')$$

in the nonviscous subrange, the production of turbulence predominates, and the spectral law is k^{-1}.

(b) Far away from the wall, and still not close to the rough edge of the boundary layer, the average scale of the primary motion is large, and the resonance is negligible. If, moreover,

$$U'^2 \ll 2\int_0^k dk' k'^2 F(k')$$

in the nonviscous subrange, the transfer of energy among the eddies predominates, and the spectral law is $k^{-5/3}$.

(c) In the viscous subrange, the eddies are under no circumstance effected by the shear. Therefore, everywhere in the boundary layer the power law k^{-7} of Heisenberg is reproduced, although this law is not expected to continue to infinite wave numbers.

If we consider as before a turbulent flow with a mean velocity in the x_1 direction, with a gradient $\partial U_1/\partial x_2$, and write energy equations of the type (7) and (7a), we notice that the production function will be absent in the energy equations for the u_2 and u_3 components. Therefore, the spectra of u_2 and u_3 will not show any k^{-1} law which is characteristic of the production function.

6. References

[1] Th. v. Kármán and L. Howarth, Proc. Roy. Soc. London A 164, 192 (1938); J. M. Burgers, Proc. Acad. Sci. Amsterdam **8,** 122, 248, 393, 718, 732 (1950).

[2] J. M. Burgers, Verhand. Kon. Nederl. Akademie v. Wetenschappen (le sect.) **17,** 18 (1939); Advances in Appl. Mech. **1,** 189 (1948).

[3] L. Onsager, Nuovo Cimento, Supplemento **6,** ser. 9, No. 2, 279 (1949); Phys. Rev. **68,** 286 (1945).

[4] A. M. Obukhoff, Bul. Acad. URSS, Ser. Geogr. Geophys. 453 (1941); Doklady **32,** 19 (1941).

[5] C. F. v. Weizsäcker, Z. Phys. **124,** 614 (1948).

[6] W. Heisenberg, Z. Phys. **124,** 628 (1948).

[7] A. N. Kolmogoroff, Doklady **30,** 301 (1941); **32,** 16 (1941).

[8] L. Prandtl, Z. Angew. Math. Mech. **5,** 136 (1925).

[9] J. J. Boussinesq, Théorie de l'écoulement tourbillonnant et tumultueux des liquides, Paris (1897).

[10] C. M. Tchen, J. Chem. Phys. **20,** 214 (1952).

[11] P. S. Klebanoff and Z. W. Diehl, NACA Tech. Notes 2475 (1951).

Washington, August 23, 1951.